

**Self-healing Al<sub>2</sub>O<sub>3</sub> ceramics  
Selection and testing of novel healing particles**

Boatema, Linda

**DOI**

[10.4233/uuid:f9bf1daf-a1f1-4b8a-b946-d23c22a106e5](https://doi.org/10.4233/uuid:f9bf1daf-a1f1-4b8a-b946-d23c22a106e5)

**Publication date**

2018

**Document Version**

Final published version

**Citation (APA)**

Boatema, L. (2018). *Self-healing Al<sub>2</sub>O<sub>3</sub> ceramics: Selection and testing of novel healing particles*. [Dissertation (TU Delft), Delft University<sup>3</sup> of Technology]. <https://doi.org/10.4233/uuid:f9bf1daf-a1f1-4b8a-b946-d23c22a106e5>

**Important note**

To cite this publication, please use the final published version (if applicable).  
Please check the document version above.

**Copyright**

Other than for strictly personal use, it is not permitted to download, forward or distribute the text or part of it, without the consent of the author(s) and/or copyright holder(s), unless the work is under an open content license such as Creative Commons.

**Takedown policy**

Please contact us and provide details if you believe this document breaches copyrights.  
We will remove access to the work immediately and investigate your claim.

**Self-Healing Al<sub>2</sub>O<sub>3</sub> ceramics:  
Selection and testing of novel healing particles**



**Self-Healing Al<sub>2</sub>O<sub>3</sub> ceramics:  
Selection and testing of novel healing particles**

Dissertation

for the purpose of obtaining the degree of doctor  
at Delft University of Technology  
by the authority of the Rector Magnificus Prof.dr.ir. T.H.J.J. van der Hagen  
chair of the Board for Doctorates  
to be defended publicly on  
Monday 7 May 2018 at 10:00 o'clock

by

**Linda BOATEMAA**

Master of Science Advanced Functional Materials  
Grenoble INP, France  
Born in Accra, Ghana



This dissertation has been approved by the promotors.

Composition of the doctoral committee:

Rector Magnificus	Chairperson
Dr. ir. W. G. Sloof	Delft University of Technology, promotor
Prof. dr. ir. S. van der Zwaag	Delft University of Technology, promotor

*Independent members:*

Prof. dr. D. Monceau	CIRIMAT, Toulouse, France
Prof. dr. ir. J. Vleugels	Catholic University of Leuven
Prof. dr. A.J.A. Winnubst	USTC/University of Twente
Prof. dr. E.H. Brück	Delft University of Technology
Prof. dr. ir. K. van Breugel	Delft University of Technology

*This work was funded by:*



*Keywords: Self-healing ceramics, Alumina, Oxidation kinetics, Spark plasma sintering*

*Front Image: SEM micrograph depicting self-healing in an Alumina-Ti composite*

Printed by: Delft Academic Press  
Copyright © 2018 by L. Boatemaa  
ISBN 9789065624215

All rights reserved. No part of the material protected by this copyright notice may be reproduced or utilized in any form or by any means, electronically or mechanically, including photocopying, recording or by any information storage or retrieval system, without written permission from the author.

Contact author at [lynboatemaa@gmail.com](mailto:lynboatemaa@gmail.com). An electronic version of this dissertation is available at <http://repository.tudelft.nl/>.



*To my husband, mother, sister and father<sup>†</sup>*





# Table of contents

<b>1 Introduction</b>	<b>1</b>
1.1 Background	2
1.2 Literature analysis and identification of remaining scientific questions	5
1.3 Outline of thesis	8
References	10
<b>2 Selection of healing agents for autonomous healing of alumina at high temperatures</b>	<b>13</b>
2.1 Introduction	15
2.2 Properties of the healing agent after its healing reaction	16
2.2.1 Melting point of the oxide formed	16
2.2.2 Adhesion between the healing oxide and the alumina matrix	18
2.2.3 Thermal mismatch stress in the healing oxide	19
2.3 Properties of the healing agent prior to the healing reaction	21
2.3.1 Melting point	21
2.3.2 Volume expansion	22
2.3.3 Thermal mismatch stresses	23
2.4 Conclusions	25
Acknowledgement	26
References	27
<b>3 The effect of the TiC particle size on the preferred oxidation temperature for self-healing of oxide ceramic matrix materials</b>	<b>33</b>
3.1 Introduction	35
3.2 Analysis of reactions	37
3.2.1 Activation energy	39
3.2.2 Reaction model	39
3.2.3 Arrhenius constant	40
3.2.4 Experimental procedure	41
3.3 Results	43
3.3.1 TiC powder oxidation	43
3.3.2 Effect of heating rate on oxidation	49
3.3.3 Evaluation of the activation energy	51
3.3.4 Reaction model for TiC oxidation	54
3.3.5 The Arrhenius pre-exponential factor	56
3.4 Conclusions	57
Acknowledgements	58
References	59

<b>4 Self-healing of Al<sub>2</sub>O<sub>3</sub> containing Ti microparticles</b>	<b>63</b>
4.1 Introduction	65
4.2 Crack gap filling model	67
4.2.1 Oxidation kinetics of the healing particles	69
4.2.2 Reaction model	70
4.2.3 Activation energy and Arrhenius constant	71
4.3 Experimental procedure	71
4.4 Results	74
4.4.1 Kinetics of Ti oxidation	74
4.4.2 Mechanical properties of the Al <sub>2</sub> O <sub>3</sub> -Ti composite	77
4.4.3 Evolution of crack filling	78
4.4.4 Strength-recovery	87
4.4.5 Application of the crack-gap filling model	89
4.5 Conclusions	92
Acknowledgements	93
References	94

<b>5 On the use of TiC as high-temperature healing particles in alumina based composites</b>	<b>97</b>
5.1 Introduction	99
5.2 Theoretical analysis of the healing potential of TiC in an alumina matrix	101
5.2.1 Thermodynamic stability of TiC	101
5.2.2 Relative volume expansion (RVE)	103
5.2.3 Work of adhesion	105
5.2.4 Comparison of the thermal expansion coefficients	106
5.2.5 Comparison of the elastic properties	107
5.3 Experimental	109
5.3.1 Sample preparation	109
5.3.2 Strength recovery tests	109
5.3.3 Structure characterization	111
5.4 Results and discussion	111
5.4.1 Strength recovery	111
5.4.2 Microstructural observations	112
5.5 Conclusions	115
Acknowledgements	116
References	117

<b>6 Autonomous high temperature healing of surface cracks in Al<sub>2</sub>O<sub>3</sub> containing Ti<sub>2</sub>AlC particles</b>	<b>123</b>
6.1 Introduction	125
6.2 Experimental procedure	127
6.3 Results and discussion	130
6.3.1 Synthesis of Ti <sub>2</sub> AlC particles and the alumina composite	130
6.3.2 Oxidation kinetics of the Ti <sub>2</sub> AlC particles	132
6.3.3 Mechanical properties of the Al <sub>2</sub> O <sub>3</sub> -Ti <sub>2</sub> AlC composite	135
6.4 Strength Recovery of the Al <sub>2</sub> O <sub>3</sub> -Ti <sub>2</sub> AlC composite	137
6.5 Stability of the dispersed MAX-phase in the Al <sub>2</sub> O <sub>3</sub> matrix	140
6.6 Conclusions	142
Acknowledgments	142
References	143

<b>7 Demonstrating the self-healing behaviour of some selected ceramics under combustion chamber conditions</b>	<b>147</b>
7.1 Introduction	149
7.2 Materials and methods	152
7.2.1 Synthesis	152
7.2.2 Characterization	153
7.2.3 Initiation of local crack damage	154
7.2.4 Crack healing in combustion chamber	157
7.3 Results	159
7.3.1 Materials characterization	159
7.3.2 Oxidation of TiC, Ti <sub>2</sub> AlC and Cr <sub>2</sub> AlC in air and combustion environments	159
7.4 Conclusions	164
Acknowledgements	164
References	165

<b>Summary</b>	<b>169</b>
<b>Samenvatting</b>	<b>173</b>
<b>Acknowledgements</b>	<b>177</b>
<b>List of publications</b>	<b>179</b>
<b>Curriculum Vitae</b>	<b>181</b>



# 1

## Introduction

### 1.1 Background

Ceramic materials are attractive for many applications in a wide range of fields ranging from aerospace, automotive, chemical, mechanical to medical because of their desirable properties [1]. For instance, zirconia and silicon carbide are used in crucial components for the automotive and aerospace industries because of their low thermal conductivity and high strength at high temperatures. Alumina and silicon nitride can be found in wear resistant parts and cutting tools because they exhibit high hardness and have a low friction. Hip and tooth implants can be made from alumina and zirconia because they bond well to tissues and are chemically inert [1].

In general, their desirable properties originate from the strong covalent and ionic bonds existing between their constituent atoms. However, these same strong and directional bonds are responsible for their inherent brittleness [2]. Due to this, a flaw the size of human hair can degrade the strength of a ceramic product by a factor 10 or even 100, whereas metallic products are generally more tolerant to the presence of micro-cracks [3]. Hence, a major goal of current research into ceramic materials is not to overcome this inherent brittleness but to modify its structure and composition such that the product is much less sensitive to initial defects or to defects which inevitably form during use.

Over the years, researchers have employed mechanical toughening of the ceramic matrix as a means of overcoming this damage sensitivity by turning the monolithic material into a composite. Ceramic Matrix Composites (CMC's) are key enabling technologies for efficient gas turbines for aerospace and maritime propulsion as well as land-based electric power generation and industrial processing applications [4]. General Electric global research indicated that CMC's will replace certain metal components in the hot section of the engine which reduces fuel consumption and subsequent emissions [5]. These composites are designed by adding discrete inclusions (particles, fibres or films) of metals [6], ceramics [7] or intermetallics [2] to the ceramic matrix in such fractions that the desirable properties of the ceramics are preserved and not overridden by those of the foreign entities. In general, the inclusions interact with a crack in such a way that the rate of crack propagation is reduced, leading to ceramic composites with an increased resistance to fracture [8].

The resulting increase in reliability will expand their current range of applications and make them competitive options for other emerging engineering applications.

Nonetheless, one clear drawback with this method is that reinforcement simply delays the time and/or increases the load for fracture to occur. Once a crack is initiated it always will have an increased probability to propagate leading to failure of the entire component or device. It might be argued that such failure can be prevented by frequent examination and replacement of weak and/or damaged parts, but, this could be infeasible or would be time and capital intensive anyway. Hence another method, explored in this thesis, focusses on exploring new approaches in which any micro-damage formed is autonomously ‘removed’ before it grows to catastrophic dimensions; i.e. the ceramic material becomes *self-healing*. As self-healing is the result of an intentional modification of the material, such materials are called ‘*engineered self-healing*’ materials. Such healing is realized by filling and closing up of any surface cracks without external intervention in order to restore a particular property (e.g., electrical conductivity, strength) and extend the lifetime of the component. Engineered self-healing materials have a much longer history, but the topic came to light with the landmark paper by White et al. in [9] who reported on the ability of a structural polymeric thermoset polymer to heal autonomously.

Catalyst and microencapsulated healing agents were incorporated in the polymeric matrix prior to its consolidation leading to a starting microstructure as shown in **Figure 1.1(a)**. When a crack forms in the matrix capsules in the wake of the crack are ruptured and the liquid healing agent flows into the gap as a result of capillary forces **Figure 1.1(b)**. When it comes into contact with the catalytic particles also incorporated in the matrix it polymerizes and chemically bonds the opposing crack faces **Figure 1.1(c)**. So, in a self-healing material, the crack is not only filled, but a desirable property or function is also restored.



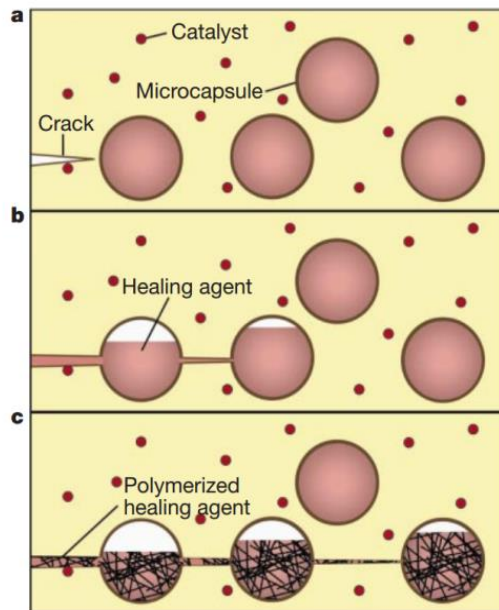


Figure 1.1: Self-healing of a polymeric material [9].

This approach of damage management has lately been named ‘*extrinsic self-healing*’ as healing is only made possible by the inclusion of discrete ‘foreign’ entities (in this case the encapsulated healing agents and the catalytic particles) to a non-self-healing matrix material. The other type of healing is termed ‘*intrinsic self-healing*’ and as the name suggests, in such materials the healing is due to physicochemical reactions linked to the (modified) matrix material itself. Over the years, self-healing has been developed and demonstrated for nearly all material types, i.e., metals [10], concrete [11], asphalt [12] and ceramics [13, 14].

In the currently known self-healing ceramics, micro-crack healing is achieved by an oxidative reaction at high temperatures and therefore requires (at least) the combined presence of a material which can be oxidized, oxygen and a high enough temperature. Based on this approach both intrinsic and extrinsic self-healing (high temperature) ceramics have been developed. The MAX phase ceramics (where M is a transition metal, A is an A group element, and X is either carbon or nitrogen) undergo intrinsic self-healing by selective oxidation of the A element autonomously [15] thereby locally filling any gap. Oxidic ceramics on the other hand, are already in their oxidized state and further oxidation is not possible. Hence for such ceramics

healing can only be realized with the help of an external agent leading to an extrinsic self-healing approach [14, 16-18].

In extrinsic self-healing for ceramic oxides, discrete healing particles (i.e., granular particles, fibers or whiskers) are added to the inert ceramic matrix before synthesis and in principle, they remain dormant during material use, until the moment of intersection by a neighboring crack. A local chemical (oxidative) reaction is then triggered at crack-particle interface leading to an expanding reaction product, which, if the reaction is to lead to self-healing behaviour, i.e. recovery of the mechanical strength, should also bond well to the neighbouring cracked matrix material as depicted in 1.2.

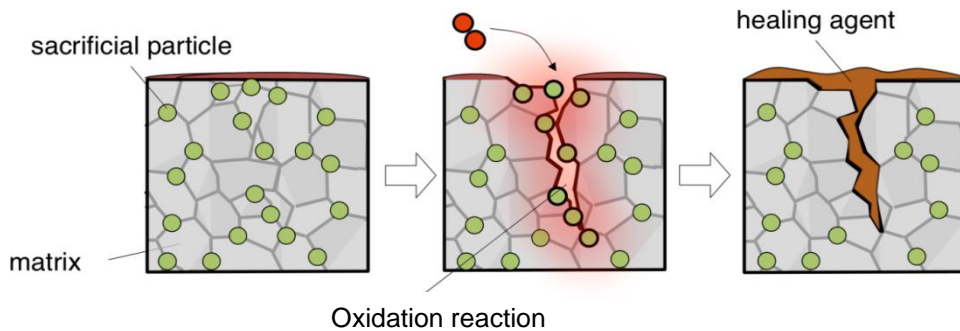


Figure 1.2: Schematic of extrinsic-self-healing of ceramic oxides [19].

## 1.2 Literature analysis and identification of remaining scientific questions

In recent years, the autonomous healing of oxidic ceramics as a result of high-temperature oxidation of second-phase inclusions has been studied by various researchers. A short analysis of the relevant literature leading to the identification of the remaining key scientific questions to be addressed in this thesis is presented here. More detailed literature reviews are presented at the beginnings of each of the following chapters.

When analysing the literature in the field of extrinsic self-healing ceramics, it becomes clear that the very great majority of the publications is rather descriptive in nature and reports the synthesis, testing and characterization of the materials in the initial, damaged and healed state as a function of the selected parameter(s), be it the chemical nature of the healing particle, the size of the healing particle, the type of initial damage or the temperature and time of the oxidative healing treatment.

The selection of the healing particle is generally made on sensible but unquantified physicochemical considerations mainly related to the tendency of the healing particle to form a well-defined oxidic reaction product, leading to the selection of either metallic or non-oxidic ceramics [17, 20-22]. In the selection process, other considerations such as the properties of the healing particle in its initial and reacted state do not seem to play any role.

The selection of the size of the healing particle is generally based on micromechanical and process engineering considerations which suggest that a smaller particle size will lead to higher mechanical strength values and that the healing particle should have a size not too different from the particle size used for the matrix material respectively [23, 24]. The implication of the choice of the size of the healing particle on the achievable degree of healing given the volume of the crack to be filled is invariably ignored, although an analytical study for liquid-based extrinsic healing systems has shown that the dependence is very strong [25].

The selection of the healing temperature seems to be generally based on an experience driven 'trial and error' basis and led to the selection of temperatures at which oxidation reactions take place at a rate such that the healing reaction can in principle be completed in less than 200 h. It is very clear that in the current literature the healing conditions are dictated by the selection of the healing particle [18, 22, 26]. The inverse approach, i.e. the prospective healing temperature in the intended application, is used as the selection criterion for the healing particle, have never been reported yet.

The nature of the crack filling process in the case of a solid-state oxidation reaction triggered at the intersected healing particle has been totally ignored. While in the case of liquid healing particles, the uniform spreading of the healing product over

the crack surface due to surface tension effects is very obvious, it is by no means clear how a local solid state oxidation reaction would lead to a complete and homogeneous filling of the crack. The only example of a detailed in-situ study of the crack filling process at high temperatures is the work by Sloof et al. [27], but that study concerned an intrinsic self-healing ceramic,  $Ti_2AlC$ , where the supply of the atoms involved in the healing reaction can take place everywhere along the crack surfaces.

Finally, all studies on self-healing high-temperature ceramics used typical laboratory experimental conditions, i.e. the atmosphere is (purified but otherwise unmodified) air flowing over the sample surface at a very low rate and the sample is kept at complete 'rest' at all times, i.e. the sample is not exposed to any vibration or stress state during the healing reaction. These conditions are very different from those encountered in the intended application, the hot section of a jet turbine. In the jet engine, the partial pressure of oxygen is very low and the structure is exposed to severe high-frequency vibrations.

Given the above analysis, the research as reported in this thesis aims to address the following questions, all related to self-healing high temperature extrinsic oxidic ceramic composites:

- I. Can we define objective selection criteria to select the best materials as healing agents?
- II. What effect does the size of a healing particle have on the self-healing process and the degree of healing?
- III. Can we tune healing temperature by changing the particle size?
- IV. How does crack filling evolve or progress and which parameters are paramount in crack healing
- V. Can we use an intrinsic healing material as the healing agent in an extrinsic healing system?
- VI. Can self-healing be realized under realistic engineering conditions such as a low  $pO_2$  level and the presence of mechanical vibrations?

### 1.3 Outline of thesis

The chapters can be grouped into two sets: Chapters 2 to 4 focus on formulating and elaborating a concept-driven design of extrinsic self-healing ceramic composites while chapters 5 to 7 are concerned with testing the self-healing behaviour of novel healing systems as a function of temperature and time not only under laboratory conditions (chapters 5 and 6) but also under conditions resembling those in a jet-turbine engine (chapter 7) application conditions.

Chapter 2 presents an unbiased multi-criteria selection procedure to determine which materials could serve as effective healing agents for the healing of alumina at high temperatures. The selection process is based on an analysis of the requested characteristics of the oxide to fill the crack as well as those of the healing agent prior to being activated. Application of all selection criteria and taking alumina as the matrix material yields a list of (known but also unexplored) candidate materials.

In Chapter 3, the effect of particle size on the kinetics of self-crack-healing is investigated using TiC powder. Different sizes of TiC powder ranging from nanometer to sub-millimeter are studied. The Kissinger analysis for non-isothermal oxidation is employed in determining the energy needed to activate the particles and the active temperature window available for healing due to increase/ decrease in surface area.

Chapter 4 addresses three different issues; first, the capability of metallic Ti particles to heal surface cracks in  $\text{Al}_2\text{O}_3$  is assessed at different temperatures and times. It follows from chapter 2, which predicts Ti as a viable healing agent. Secondly, the evolution of crack filling is explored as the formed healing agent is in the solid state. The ability of  $\text{TiO}_2$  to '*spread*' into, fill the gap and bond with the crack faces is investigated. Finally, the parameters which influence the filling up of a crack is analyzed and presented in a simple model which is used to predict the degree of filling a unit area of crack.

Chapter 5 reports the use of TiC as a healing particle in alumina-based composites. As for chapter 4, the choice of TiC also follows from chapter 2. Crack healing was studied as a function of temperature and time for Alumina samples containing 15 or

30 vol. % of TiC. Composites were made by spark plasma sintering and damage was introduced by Vicker's indentations. Strength tests were performed on a 4 point bending stage with self-aligning capability.

In Chapter 6, the ability of intrinsically healing  $\text{Ti}_2\text{AlC}$  MAX phase ceramic particles to heal indentation induced cracks in Alumina is explored. Healing is studied as a function of temperature and time in an  $\text{Al}_2\text{O}_3$  matrix containing 20 vol. %  $\text{Ti}_2\text{AlC}$  particles.

In Chapter 7, healing of one extrinsic and two intrinsic self-healing ceramics under quasi-realistic jet engine combustion chamber conditions is presented. For the extrinsic material,  $\text{Al}_2\text{O}_3$  containing 20 vol. % of TiC is used while the  $\text{Ti}_2\text{AlC}$  and  $\text{Cr}_2\text{AlC}$  systems are selected as the most relevant intrinsic healing materials. This chapter assesses self-healing under real-life conditions and the results are compared with healing experiments under quasi-static gas flow laboratory conditions.

## References

- [1] US-Congress, *Office of technology assessment-Advanced, materials by design*, OTA-E-351. 1988, U.S. Government Printing Office: Washington DC. p. 38 and 43.
- [2] Huang, M., Li, Z., Wu, J., Khor, K.A., Huo, F., Duan, F., Lim, S.C., Yip, M.S., and Yang, J., *Multifunctional alumina composites with toughening and crack-healing features via incorporation of NiAl particles*. Journal of the American Ceramic Society, 2015. 98(5): p. 1618-1625.
- [3] National-Research-Council, *A review of United States air force and department of defense aerospace propulsion needs* committee on air force and department of defense aerospace propulsion needs. 2007, United states of America: National Academies Press. 289.
- [4] Glen, M. and Doug, F. *A primer on CMC's*. American Composites Manufacturing Association, 2015.
- [5] Liverani, S. *The spin on state of the art ceramics—coming to a turbine near you*. American Ceramic Society Bulletin, 2015.
- [6] Fahrenholtz, W.G., Ellerby, D.T., and Loehman, R.E., *Al<sub>2</sub>O<sub>3</sub>-Ni Composites with high strength and fracture toughness*. Journal of the American Ceramic Society, 2000. 83(5): p. 1279-1280.
- [7] Wei, G.C. and Becher, P.F., *Development of SiC whisker reinforced ceramics*. American Ceramic Society Bulletin, 1985. 64(2): p. 298-304.
- [8] Gutierrez-Gonzalez, C.F., Fernandez-Garcia, E., Fernandez, A., Torrecillas, R., and Lopez-Esteban, S., *Processing, spark plasma sintering, and mechanical behavior of alumina/titanium composites*. Journal of Materials Science, 2014. 49(10): p. 3823-3830.
- [9] White, S.R., Sottos, N.R., Geubelle, P.H., Moore, J.S., Kessler, M.R., Sriram, S.R., Brown, E.N., and Viswanathan, S., *Autonomic healing of polymer composites*. Nature, 2001. 409(6822): p. 794-797.
- [10] Zhang, S., Kwakernaak, C., Sloof, W.G., Brück, E., van der Zwaag, S., and van Dijk, N., *Self healing of creep damage by gold precipitation in iron alloys*. Advanced Engineering Materials, 2015. 17(5): p. 598-603.
- [11] Dry, C., *Matrix cracking repair and filling using active and passive modes for smart timed release of chemicals from fibers into cement matrices*. Smart Materials and Structures, 1994. 3(2): p. 118-123.

- [12] García, Á., Schlangen, E., van de Ven, M., and Liu, Q., *Electrical conductivity of asphalt mortar containing conductive fibers and fillers*. Construction and Building Materials, 2009. 23(10): p. 3175-3181.
- [13] Song, M.G., Pei, Y.T., Sloof, G.W., Li, B.S., De Hosson, T.M.J., and van der Zwaag, S., *Oxidation-induced crack healing in  $Ti_3AlC_2$  ceramics*. Scripta Materialia 2008. 58: p. 13-16.
- [14] Ando, K., Kim, B.S., Chu, M.C., Saito, S., and Takahashi, K., *Crack-healing and mechanical behaviour of  $Al_2O_3/SiC$  composites at elevated temperature*. Fatigue & Fracture of Engineering Materials & Structures, 2004. 27(7): p. 533-541.
- [15] Farle, A., Boatemaa, L., Shen, L., Gövert, S., Kok, J.B.W., Bosch, M., Yoshioka, S., van der Zwaag, S., and Sloof, W.G., *Demonstrating the self-healing behaviour of some selected ceramics under combustion chamber conditions*. Smart Materials and Structures, 2016. 25(8): p. 084019.
- [16] Takahashi, K., Uchiide, K., Kimura, Y., Nakao, W., Ando, K., and Yokouchi, M., *Threshold stress for crack healing of mullite reinforced by SiC whiskers and SiC particles and resultant fatigue strength at the healing temperature*. Journal of the American Ceramic Society, 2007. 90(7): p. 2159-2164.
- [17] Salas-Villaseñor, A.L., Lemus-Ruiz, J., Nanko, M., and D., M., *Crack disappearance by high-temperature oxidation of alumina toughened by Ni nanoparticles*. Advanced Materials Research, 2009. 68: p. 34-43.
- [18] Houjou, K., Ando, K., and Takahashi, K., *Crack-healing behaviour of  $ZrO_2/SiC$  composite ceramics*. International Journal of Structural Integrity, 2010. 1(1): p. 73-84.
- [19] Yoshioka, S. and Nakao, W., *Methodology for evaluating self-healing agent of structural ceramics*. Journal of Intelligent Material Systems and Structures, 2015. 26(11): p. 1395-1403.
- [20] Petrovic, J.J. and Jacobson, L.A., *Controlled surface flaws in hot-pressed SiC*. Journal of the American Ceramic Society, 1976. 59(1-2): p. 34-37.
- [21] Choi, S.R. and Tikare, V., *Crack healing behavior of hot pressed silicon nitride due to oxidation*. Scripta Metallurgica et Materialia, 1992. 26(8): p. 1263-1268.
- [22] Yao, F., Ando, K., Chu, M.C., and Sato, S., *Crack-healing behavior, high temperature and fatigue strength of SiC-reinforced silicon nitride composite*. Journal of Materials Science Letters, 2000. 19(12): p. 1081-1083.



- [23] Chu, M.C., Sato, S., Kobayashi, Y., and Ando, K., *Damage healing and strengthening behaviour in intelligent mullite/SiC ceramics*. Fatigue & Fracture of Engineering Materials & Structures, 1995. 18(9): p. 1019-1029.
- [24] Nakao, W., Tsutagawa, Y., and Ando, K., *Enhancement of In situ self-crack-healing efficient temperature region by SiC nanosizing*. Journal of Intelligent Material Systems and Structures, 2008. 19(3): p. 407-410.
- [25] Mookhoek, S.D., Fischer, H.R., and van der Zwaag, S., *A numerical study into the effects of elongated capsules on the healing efficiency of liquid-based systems*. Computational Materials Science, 2009. 47(2): p. 506-511.
- [26] Sugiyama, R., Yamane, K., Nakao, W., Takahashi, K., and Ando, K., *Effect of difference in crack-healing ability on fatigue behavior of alumina/silicon carbide composites*. Journal of Intelligent Material Systems and Structures, 2008. 19(3): p. 411-415.
- [27] Sloof, W.G., Pei, R., McDonald, S.A., Fife, J.L., Shen, L., Boatemaa, L., Farle, A.-S., Yan, K., Zhang, X., van der Zwaag, S., Lee, P.D., and Withers, P.J., *Repeated crack healing in MAX-phase ceramics revealed by 4D in situ synchrotron X-ray tomographic microscopy*. Scientific Reports, 2016. 6: p.23040.

# 2

## **Selection of healing agents for autonomous healing of alumina at high temperatures**

---

This chapter has been published in the Journal of the European Ceramic Society 36 (16) 2016 p 4141-4145. Authors: Boatemaa, L., Kwakernaak, C., van der Zwaag, S. and Sloof, W. G.

To date, the research aimed at creating a high-temperature alumina ( $Al_2O_3$ ) grade capable of autonomously repairing crack damage focussed on the use of SiC particles which turns to  $SiO_2$  as the healing agent. The present work presents an unbiased selection procedure to determine other attractive substances and phases which could serve as an effective healing agent for healing at high temperatures. The selection process is based on an analysis of the requested characteristics of the oxide to fill the crack (melting point, adhesion to the alumina matrix and thermal mismatch) as well as those of the healing agent prior to being activated (melting point, volume expansion upon oxidation and thermal mismatch). Application of all selection criteria resulted in identifying granular Ti, Cr, Zr, Nb, Hf, TiC, TiN,  $Cr_3C_2$ ,  $Cr_2N$ , ZrN, NbC and NbN as promising agents for autonomous healing of alumina when used in air at high temperatures.

## 2.1 Introduction

Alumina ( $\text{Al}_2\text{O}_3$ ) is an attractive ceramic for engineering applications operating at elevated or high temperatures because of its good thermal and chemical resistance. It also maintains a high strength and hardness at high temperatures [1]. These desirable properties are due to the strong covalent and ionic bonds existing between its atoms [2]. However, the same strong and directional bonds are the origin of its inherent brittleness [3]. One way to minimise the consequences of the inherent brittleness for real life applications is to delay the time to fracture by reinforcing the matrix with metallic or ceramics inclusions (particles or whiskers), which reduce the maximum local tensile strength for a given external load [4, 5]. Another way is to modify the material by the inclusion of discrete healing ‘particles’, which upon the occurrence of a non-catastrophic crack initiate a chemical reaction leading to crack filling and restoration of its load bearing capability, a concept known as ‘extrinsic self-healing’ [6].

The concept of *extrinsic* ‘self-engineered-healing’ was first demonstrated for concrete [7] but only became widely known since its application to brittle polymer matrices [8]. The concept is based on the inclusion of discrete entities (granular particles, fibres or vascular networks) containing a healing agent in an otherwise inert matrix material. The healing particles remain dormant in the matrix but become active when intersected by a (micro- or meso-) crack in the matrix. Upon intersection of the healing particle a chemical reaction is triggered which leads to local filling of the crack and adhesion between the reaction product and the crack faces in such a manner that the load bearing capabilities of the material is restored. The concept of extrinsic healing, i.e. making use of discrete ‘foreign’ particles in an otherwise unreactive matrix material, has since been applied to other material classes such as concrete [9, 10], asphalt [11, 12], metals [13] and ceramics [14-16]. The alternative approach, *intrinsic* self-healing, in which the healing action is due to a controlled reaction or decomposition of the matrix itself has been demonstrated for polymers [17, 18], metals [19, 20], and MAX phase ceramics [16, 21]. However, this approach cannot be used for alumina or other oxidic materials as the material is already in its lowest energetic state. Hence healing in alumina or other oxidic ceramics can only be achieved via *extrinsic* self-healing routes [22-25].

To date the research into self-healing alumina has concentrated on the use of SiC as the healing particle [24, 26-31]. The choice for SiC is based on the fact that a) SiC is relatively stable up to 2270 °C; b) will decompose into SiO<sub>2</sub> which has a specific volume 113 % larger than its parent phase when exposed to air at higher temperatures and c) the reaction products SiO<sub>2</sub> bonds well to the alumina matrix [25]. Other materials such as Al, Al<sub>4</sub>C<sub>3</sub> or AlN will fail as healing particles respectively due to too low a melting point [32], early decomposition due to hydrophobicity [33], or too low a relative volume expansion (RVE of 22%) leading to incomplete crack filling and modest strength recovery [34].

It is unlikely that a random or quasi-systematic exploration of the phases potentially functioning as healing agents for the autonomous repair or (micro-) cracked alumina will lead to optimal results. Hence, the present work presents a unbiased selection procedure to determine attractive substances and phases which could serve as effective healing agents to autonomously heal alumina (Al<sub>2</sub>O<sub>3</sub>) when exposed to air at temperatures in excess of 1500 K. The scope of this study comprises the oxides of the following transition metals; Ti, V, Cr, Mn, Fe, Co, Ni, Cu, Zn, Y, Zr, Nb, Mo, Hf, Ta and W. A stepwise selection process is presented which is based on an analysis of the requested characteristics of the oxide to fill the crack (melting point, adhesion to the alumina matrix and thermal mismatch) as well as the characteristics of the healing agent prior to being activated (melting point, volume expansion upon oxidation and thermal mismatch). Here, the analysis is applied for an alumina matrix but the concept can easily be expanded for other high temperature stable oxidic ceramics. The approach presented here conceptually mimics the approach used to determine MAX phase materials with attractive yet unexplored high temperature self-healing characteristics [21].

## **2.2 Properties of the healing agent after its healing reaction**

### **2.2.1 Melting point of the oxide formed**

A crucial requirement for any product filling a crack in a self-healing alumina matrix is that it is in the solid state as liquids have no (tensile) load bearing capability. Arbitrarily setting the use temperature of the alumina composite at 1500 K, we should first evaluate the stability of the above mentioned transition metal and other

appropriate oxides. In **Figure 2.1**, the Gibb's free energy of formation ( $\Delta^\circ G_f$ ) of the oxides as a function of their melting temperature ( $T_m$ ) is presented. Oxides that melt or evaporate below the operational limit of 1500 K are excluded. For example,  $V_2O_5$  melts at 943 K while  $MoO_3$  becomes volatile at 1074 K and both are therefore expelled. Having a melting temperature of about 44 K above the set temperature limit  $Cu_2O$  is also not attractive and is therefore also not considered further.

All remaining oxides are possible options and are moved up to the next selection step. These oxides can be divided into 3 groups. The first group comprises very stable oxides with a Gibbs free energy of formation less than -400 kJ per mol  $O_2$ , viz. :  $Nb_2O_5$ ,  $Ta_2O_5$ ,  $MnO$ ,  $SiO_2$ ,  $TiO_2$ ,  $ZrO_2$ ,  $HfO_2$  and  $Y_2O_3$ . The second group encompass moderate stable oxides with a Gibbs free energy of formation between -400 to -200 kJ per mol  $O_2$ , which are:  $WO_3$ ,  $FeO$  and  $Cr_2O_3$ . Finally, the less stable oxides corresponding with Gibbs free energy of formation of more than -200 kJ per mol  $O_2$ , namely:  $ZnO$ ,  $NiO$  and  $CoO$ .

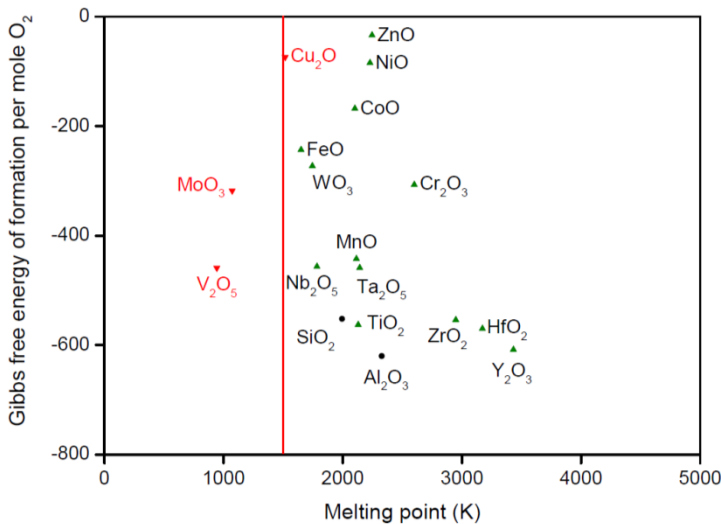


*Figure 2.1: Representation of the healing oxides by the Gibb's free energy of formation ( $\Delta^\circ G_f$ ) and melting point ( $T_m$ ).*

## 2.2.2 Adhesion between the healing oxide and the alumina matrix

The second criterion applied to the oxides passing the first screening test considers the adhesion of the healing oxide to the alumina matrix. A strong adhesion between the oxide and matrix is a key requisite because it is a 'condicio sine qua non' for strength recovery for the healed ceramic. The energy required to separate the healing oxide from the matrix should be comparable or preferably larger than the cohesive energy of the matrix. This adhesion energy is known as the work of adhesion and is defined as [35]:

$$W_{ad} = -(\gamma_{Alumina}^{surf} + \gamma_{Oxide}^{surf}) + \gamma_{Alumina}^{interface} \quad (2.1)$$

The work of adhesion can be estimated using the macroscopic atom model [36], the surface energy of Alumina ( $\gamma_{Alumina}^{surf}$ ) and the oxide ( $\gamma_{oxide}^{surf}$ ) are estimated from the surface enthalpy of each element which constitutes the interface weighted by the molar surface density. The interface energy ( $\gamma_{Alumina}^{interface}$ ) is determined by the interaction energies of the atoms on either side of the interface. This interaction energy is further estimated from enthalpy of solutions using a semi-empirical macroscopic atom model [37].

The evaluated works of adhesion are graphically presented in **Figure 2.2**, it shows that all oxides have sufficiently high surface and interaction energy and hence will adhere strongly to alumina. The cohesive energy of alumina, which equals  $4.0 \text{ J/m}^2$ , is taken as the lower limit for the adhesion between the alumina matrix and the healing oxide. Separating ZnO from Alumina will require  $3.9 \text{ J/m}^2$ , which is slightly lower than the set limit, nonetheless, the adhesion is considered strong enough. Hence, all the oxides considered here are moved up to the next selection stage. The oxides that promise the strongest adherence to alumina are:  $\text{WO}_3$ ,  $\text{Ta}_2\text{O}_5$ ,  $\text{Nb}_2\text{O}_5$ ,  $\text{ZrO}_2$ ,  $\text{HfO}_2$  and  $\text{TiO}_2$ .

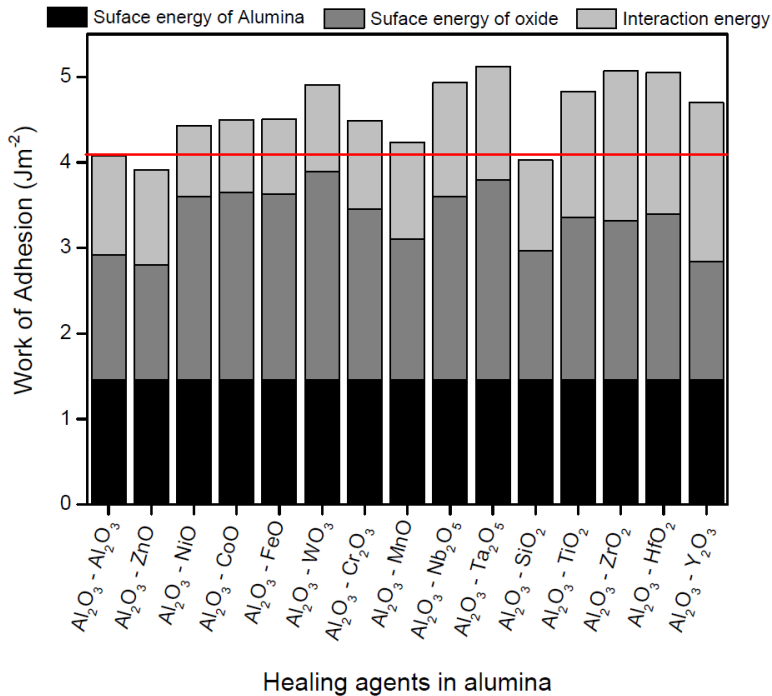


Figure 2.2: Work of adhesion between alumina (Al<sub>2</sub>O<sub>3</sub>) and the various healing oxides.

### 2.2.3 Thermal mismatch stress in the healing oxide

Residual stresses may be generated upon cooling down an autonomously healed alumina from its operational temperature (1500 K) to room temperature (300 K) because of a mismatch between the coefficient of thermal expansion (CTE) of the alumina matrix and that of the oxide of the healing agent. Such stresses may affect the mechanical properties and even impair the integrity of the composite, i.e. alumina matrix and healed crack. The magnitude of the residual stresses depend on the coefficient of thermal expansion and the elastic modulus of the matrix and healing oxide [38]. To estimate the residual stresses generated in the healed material upon cooling a thin film approach is employed [39]. In the very simplified model it is assumed that the mismatch strain is fully accommodated by the oxide layer covering the fracture surfaces in the crack gap. A rotational symmetric bi-axial state



of stress (plane stress) is considered in the healing oxide. Then the thermal stress generated in the healing oxide ( $\sigma_{ox}$ ) is obtained from:

$$\sigma_{ox} = \frac{E_{ox}}{1-\nu_{ox}}(\alpha_{ox} - \alpha_m)\Delta T \quad (2.2)$$

Where  $E_{ox}$  and  $\nu_{ox}$  are the elastic modulus and poisson's ratios of the oxide,  $\alpha_{ox}$  and  $\alpha_m$  are the CTE of the oxide and matrix respectively, and  $\Delta T$  is the change in temperature.

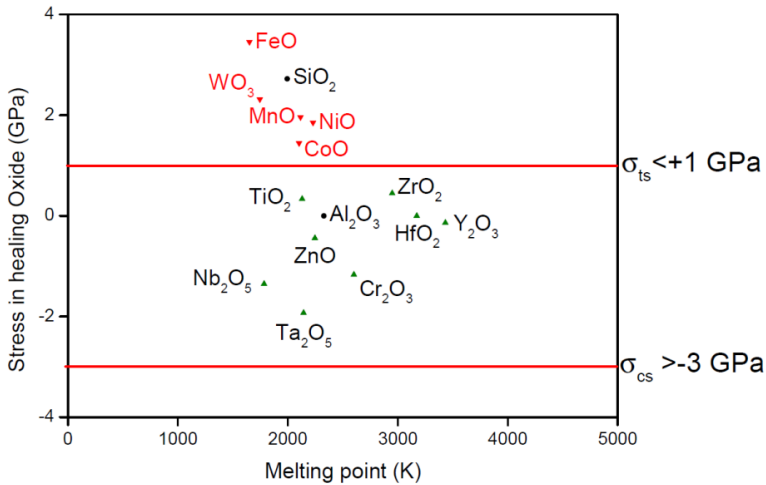


Figure 2.3: Thermal mismatch stress in the healing oxide in alumina when cooled from 1500 K to 300 K as a function of the healing oxide melting points. Oxides represented with a green symbol are further considered, those in red are discarded.

The maximum allowable stress depends on the nature of the stress field (tensile or compressive) and the room temperature strength of the healing oxide. The compressive and tensile strength of alumina is used as an estimation of the limit for the allowable thermal stresses generated in the formed oxides. The strength of alumina ranges from -3 GPa under compression to + 1 GPa under tensile loading. [40]. The stress calculated according Eq. (2.2) to for the healing oxides can be

directly compared with the aforementioned strength values and the result is shown in **Figure 2.3**.

It is evident that in FeO, WO<sub>3</sub>, MnO, NiO or CoO tensile stresses greater than 1 GPa are generated, which over time could be detrimental to the mechanical stability of the composite and hence these compounds are considered not suitable. On the other hand in Nb<sub>2</sub>O<sub>5</sub> and Ta<sub>2</sub>O<sub>5</sub> the greatest compressive stresses are generated, yet they are suitable since these compressive stresses are less than the limit of -3 GPa. The healing oxides that meet the requirement are: TiO<sub>2</sub>, ZrO<sub>2</sub>, ZnO, HfO<sub>2</sub>, Y<sub>2</sub>O<sub>3</sub>, Nb<sub>2</sub>O<sub>5</sub>, Cr<sub>2</sub>O<sub>3</sub> and Ta<sub>2</sub>O<sub>5</sub>. Although SiO<sub>2</sub> induces tensile stresses larger than 1 GPa, it is still considered a viable healing oxide because before crystallization SiO<sub>2</sub> is amorphous with fluidity and thereby relaxing part of the thermal stress [41], hence it is moved up to the next selection stage.

## **2.3 Properties of the healing agent prior to the healing reaction**

### **2.3.1 Melting point**

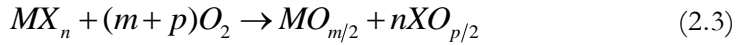
With the oxides potentially suitable to heal cracks in alumina being identified, the properties of the elements and compounds (carbides and nitrides) from which the oxides are formed will be considered; see **Table 2.1**. The elements and compounds to be used as healing particles should be able to withstand the very high sintering temperatures. Alumina composites can be sintered to very high densities at 1700 K by spark plasma sintering [42,43] or by hot pressing [44]. Therefore a suitable particle should have a substantially higher melting point or decomposition temperature. Of all the materials presented in **Table 2.1**, Zn and Si are omitted having melting temperatures of 692 and 1687 K, respectively. Melting points for ZnC, Zn<sub>3</sub>N<sub>2</sub> and YN are not available, so they are not further considered. The melting points of suitable materials are presented as a function of thermal stresses generated upon sintering in Section 2.3.3.

Table 2.1: Evaluated elements, carbides and nitrides as healing particles forming healing oxides.

Healing oxide	TiO <sub>2</sub>	Cr <sub>2</sub> O <sub>3</sub>	ZnO	Y <sub>2</sub> O <sub>3</sub>	ZrO <sub>2</sub>	Nb <sub>2</sub> O <sub>5</sub>	HfO <sub>2</sub>	Ta <sub>2</sub> O <sub>5</sub>	SiO <sub>2</sub>
Element	Ti	Cr	Zn	Y	Zr	Nb	Hf	Ta	Si
Carbide	TiC	Cr <sub>3</sub> C <sub>2</sub>	ZnC	YC <sub>2</sub>	ZrC	NbC	HfC	TaC	SiC
Nitride	TiN	Cr <sub>2</sub> N	Zn <sub>3</sub> N <sub>2</sub>	YN	ZrN	NbN	HfN	TaN	Si <sub>3</sub> N <sub>4</sub>

### 2.3.2 Volume expansion

In order to fill a crack gap with the healing agent, it is required that an adequate volume expansion occurs upon oxidation of the healing particles such that the oxide formed can fill the new free volume within the material created by the crack. This volume expansion can be estimated by considering the oxidation reaction:



where  $MX_n$  is a carbide or nitride, and  $MO_{m/2}$  and  $XO_{p/2}$  the oxidation products. The oxidation product of carbon (CO or CO<sub>2</sub>) and nitrogen (NO<sub>x</sub>) will be volatile and thus does not contribute to filling of the crack gap. Hence,

$$RVE = \left( \frac{V_{MO_{m/2}}}{V_{MX_n}} - 1 \right) * 100 \quad (2.4)$$

where  $V$  is the molar volume of the healing particle  $MX_n$  and the healing oxide  $MO_{m/2}$ , respectively.

To ensure that fractured surfaces are completely bridged with the healing oxide a limit of + 50 % is set as the minimally required increase in specific volume. Then based on a simple model for crack gap filling [34] the volume fraction of healing particles (with size between 1 to 10 μm) necessary to fill a crack of about 1 μm in width is less than 30 %. All healing materials passing the previous selection steps

exhibit a positive volume expansion upon oxidation see **Figure 2.4**, with the exception of  $YC_2$ . Those with the highest volume expansion (RVE > 100 %) are: Cr, Nb, Ta, NbC, NbN, and SiC. Next are those which expand appreciably with a net volume gain above 50% but less than 100 %, they are: Ti, Zr, Hf, TiC,  $Cr_3C_2$ , TaC, TiN,  $Cr_2N$ , ZrN, TaN and  $Si_3N_4$ . Lastly, those elements or phases having a positive RVE may not be able to fully fill the cracks (however dependent on the volume fraction and size of the healing particles and the dimensions of the crack to be filled) and therefore are not further considered: Y, ZrC, HfC, and HfN.

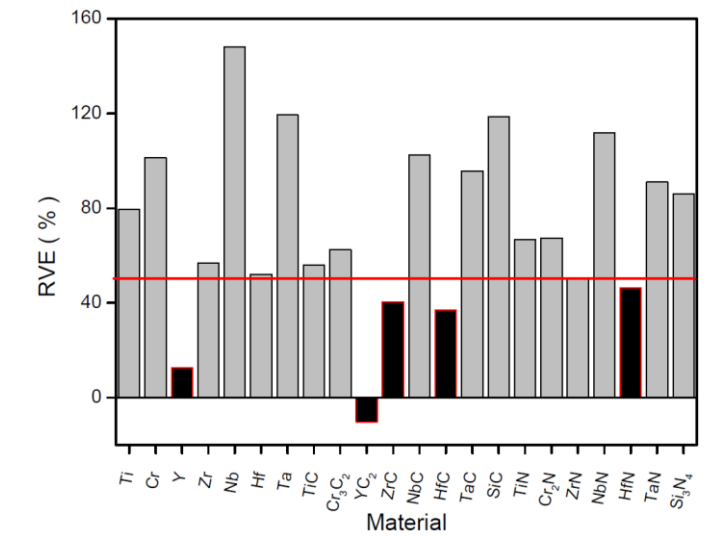


Figure 2.4: Relative volume expansion upon oxidation of viable healing particles.

### 2.3.3 Thermal mismatch stresses

The last criterion to be discussed is the stress generated in the alumina matrix upon cooling after sintering due to the difference in thermal expansion between the alumina matrix and healing particle which may lead to local fracture. To determine the magnitude of these stresses a 3-D spherical inclusion model is used to estimate the radial and tangential thermal stress in the matrix at the interface with the healing particle [45] denoted as  $\sigma_r$  and  $\sigma_t$ , respectively. Assuming that the healing particle

has a quasi- spherical shape and that both the matrix and the particle are elastically isotropic the stresses equals:

$$\sigma_r = \frac{\Delta\alpha\Delta T}{\left(\frac{1+\nu^m}{2E^m}\right) + \left(\frac{1-2\nu^p}{E^p}\right)} \quad (2.5)$$

$$\sigma_t = -\frac{\sigma_r}{2} \quad (2.6)$$

where  $\Delta\alpha$  is the difference between the CTE of the particle and matrix, and  $\Delta T$  is the change in temperature.  $E$  and  $\nu$  are the Young's modulus and Poisson ratio of the matrix ( $m$ ) and particle ( $p$ ), respectively. The value of stresses due to cooling from the assumed sintering temperature (1700 K) to room temperature (about 300 K) is calculated for the different healing particles passing all imposed selection criteria.

Since a tri-axial state of principle stresses (i.e.  $\sigma_1 = \sigma_2 = \sigma_t$  and  $\sigma_3 = \sigma_r$ ) exist in the matrix near the interface with the particle the von Misses yield criterion [46] is

adopted, hence:  $\sigma_{vM} = -\frac{3}{2}\sigma_r$ .

For large particle contraction (i.e.,  $\alpha_p > \alpha_m$ ), the interface will be under compression. Then, the criterion for fracture is defined by the compressive strength of alumina (-3 GPa). While for large matrix contraction (i.e.,  $\alpha_m > \alpha_p$ ) the interface will be under tension then the criterion for fracture is given by the tensile strength of alumina (+1 GPa).

The estimated Von Misses stresses in the alumina matrix due to the thermal mismatch with the healing particles as a function of their melting temperatures are presented in **Figure 2.5**. According to the set criteria and definitions, SiC, Si<sub>3</sub>N<sub>4</sub>, Ta, TaN and TaC are not suitable. However it should be noted that the limits of this criterion are rather stringent and for instance the effect of large tensile stresses as defined here would only be detrimental over really long cycles. In particular, the fact that SiC is a healing agent with demonstrated healing ability for an alumina matrix suggests that the maximum tolerable stress level is possibly set at too low a value. The materials which satisfy the final and all previous selection criteria and therefore are potentially optimally suitable materials to heal alumina are: Ti, Zr, NbN, TiN, TiC,

Cr and  $\text{Cr}_3\text{C}_2$ . Hf, Nb, and NbC are also considered suitable since they lie very close to the tensile limit. We anticipate that their identification via this un-biased analysis will lead to dedicated experimental research confirming their suitability as healing agent.

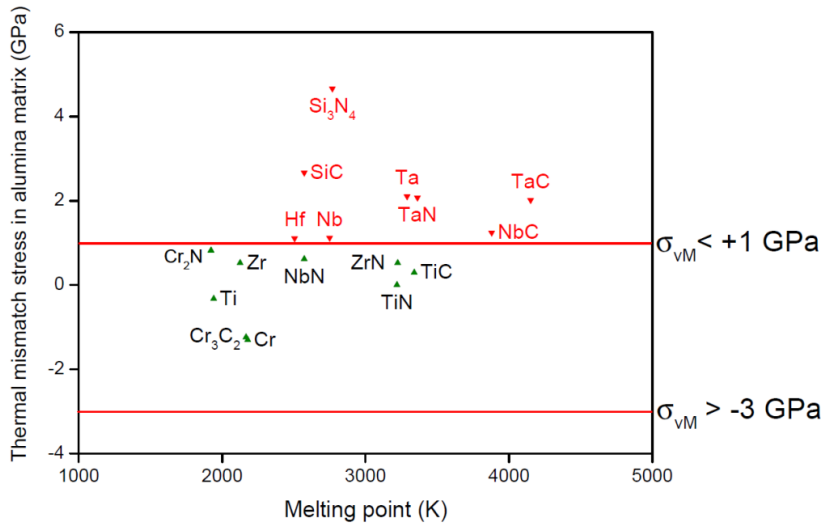


*Figure 2.5: Thermal mismatch stress in alumina matrix according to von Misses yield criterion due to difference in thermal expansion between the matrix and healing particle when cooling from sintering temperature of 1700 K to room temperature (300 K) vs melting point ( $T_m$ ) of the healing particles.*

## 2.4 Conclusions

Viable healing particles composed of transition metals and their carbides and nitrides were selected to repair crack damage in alumina ceramic components used in high temperature applications. The healing is based oxidation of the particle by filling the crack gap with the transition metal oxide. The healing particle and oxide should be stable at 1700 and 1500 K, respectively. Volume expansion should occur upon oxidation preferably 50 % or more. Thermal stresses should not exceed -3.0 and 1.0 GPa. The promising oxides selected were  $\text{TiO}_2$ ,  $\text{ZrO}_2$ ,  $\text{ZnO}$ ,  $\text{HfO}_2$ ,  $\text{Nb}_2\text{O}_5$ ,  $\text{Cr}_2\text{O}_3$  and  $\text{Y}_2\text{O}_3$ . Ultimately, application of all selection criteria resulted in as Ti, Cr,

Zr, Nb, Hf, TiC, TiN, Cr<sub>3</sub>C<sub>2</sub>, Cr<sub>2</sub>N, ZrN, NbC and NbN promising materials for efficient healing. However, further oxidation studies and extensive crack healing tests are required to fully evaluate their self-healing capabilities.

### **Acknowledgement**

This research was sponsored by the People Program (Marie Curie ITN) of the European Union's seventh framework program, FP7, grant number 290308 (SHeMat).

## References

- [1] Ono, M., Nakao, W., Takahashi, K., Nakatani, M., and Ando, K., *A new methodology to guarantee the structural integrity of Al<sub>2</sub>O<sub>3</sub>/SiC composite using crack healing and a proof test*. *Fatigue & Fracture of Engineering Materials & Structures*, 2007. 30(7): p. 599-607.
- [2] Huang, M., Li, Z., Wu, J., Khor, K.A., Huo, F., Duan, F., Lim, S.C., Yip, M.S., and Yang, J., *Multifunctional alumina composites with toughening and crack-healing features via incorporation of NiAl particles*. *Journal of the American Ceramic Society*, 2015. 98(5): p. 1618-1625.
- [3] Nakao, W., Takahashi, K., and Ando, K., *Threshold stress during crack-healing treatment of structural ceramics having the crack-healing ability*. *Materials Letters*, 2007. 61(13): p. 2711-2713.
- [4] Chou, W.B. and Tuan, W.H., *Toughening and strengthening of alumina with silver inclusions*. *Journal of the European Ceramic Society*, 1995. 15(4): p. 291-295.
- [5] Wei, G.C. and Becher, P.F., *Development of SiC whisker reinforced Ceramics*. *American Ceramic Society Bulletin*, 1985. 64(2): p. 298-304.
- [6] Nakao, W., Tsutagawa, Y., and Ando, K., *Enhancement of in situ self-crack-healing efficient temperature region by SiC nanosizing*. *Journal of Intelligent Material Systems and Structures*, 2008. 19(3): p. 407-410.
- [7] Dry, C., *Matrix cracking repair and filling using active and passive modes for smart timed release of chemicals from fibers into cement matrices*. *Smart Materials and Structures*, 1994. 3(2): p. 118-123.
- [8] White, S.R., Sottos, N.R., Geubelle, P.H., Moore, J.S., Kessler, M.R., Sriram, S.R., Brown, E.N., and Viswanathan, S., *Autonomic healing of polymer composites*. *Nature*, 2001. 409(6822): p. 794-797.
- [9] Jonkers, M.H., *Self-healing concrete: a biological approach*. *Self healing materials: an alternative approach to 20 centuries of materials science*, Ed. van der Zwaag, S. 2007, The Netherlands: Springer. p. 195-204.
- [10] Dry, M.C., *Three designs for the internal release of sealants, adhesives, and waterproofing chemicals into concrete to reduce permeability*. *Cement and Concrete Research* 2000. 30: p. 1969-1977.



- [11] García, Á., Schlangen, E., van de Ven, M., and Liu, Q., *Electrical conductivity of asphalt mortar containing conductive fibers and fillers*. Construction and Building Materials, 2009. 23(10): p. 3175-3181.
- [12] Tuan, C.Y., *Electrical resistance heating of conductive concrete containing steel fibers and shavings*. ACI Materials Journal, 2004. 101(1): p. 65-71.
- [13] Bernikowicz, P., *Design of tin based biomimetic self healing alloy tensile specimens*. in TMS outstanding student paper contest. 1994.
- [14] Yao, F., Ando, K., Chu, M.C., and Sato, S., *Static and cyclic fatigue behaviour of crack-healed Si<sub>3</sub>N<sub>4</sub>/SiC composite ceramics*. Journal of the European Ceramic Society, 2001. 21(7): p. 991-997.
- [15] Lee, S.K., Ono, M., Nakao, W., Takahashi, K., and Ando, K., *Crack-healing behaviour of mullite/SiC/Y<sub>2</sub>O<sub>3</sub> composites and its application to the structural integrity of machined components*. Journal of the European Ceramic Society, 2005. 25(15): p. 3495-3502.
- [16] Song, M.G., Pei, Y.T., Sloof, G.W., Li, B.S., De Hosson, T.M.J., and van der Zwaag, S., *Oxidation-induced crack healing in Ti<sub>3</sub>AlC<sub>2</sub> ceramics*. Scripta Materialia 2008. 58: p. 13-16.
- [17] Blaiszik, B.J., Kramer, S.L.B., Olugebefola, S.C., Moore, J.S., Sottos, N.R., and White, S.R., *Self-healing polymers and composites*. Annual Review of Materials Research, 2010. 40(1): p. 179-211.
- [18] Wu, D.Y., Meure, S., and Solomon, D., *Self-healing polymeric materials: A review of recent developments*. Progress in Polymer Science, 2008. 33(5): p. 479-522.
- [19] Lumley, R., *Self Healing in aluminium alloys*. Self Healing Materials, 2007. 100: p. 219.
- [20] Zhang, S., Kwakernaak, C., Sloof, W., Brück, E., van der Zwaag, S., and van Dijk, N., *Self Healing of creep damage by gold precipitation in iron alloys*. Advanced Engineering Materials, 2015. 17(5): p. 598-603.
- [21] Farle, A.-S., Kwakernaak, C., van der Zwaag, S., and Sloof, W.G., *A conceptual study into the potential of M<sub>n+1</sub>AX<sub>n</sub>-phase ceramics for self-healing of crack damage*. Journal of the European Ceramic Society, 2015. 35(1): p. 37-45.
- [22] Ando, K., Chu, M.C., Tsuji, K., Hirasawa, T., Kobayashi, Y., and Sato, S., *Crack healing behaviour and high-temperature strength of mullite/SiC composite*

- ceramics. *Journal of the European Ceramic Society*, 2002. 22(8): p. 1313-1319.
- [23] Houjou, K., Ando, K., and Takahashi, K., *Crack-healing behaviour of ZrO<sub>2</sub>/SiC composite ceramics*. *International Journal of Structural Integrity*, 2010. 1(1): p. 73-84.
- [24] Nakao, W., Tsutagawa, Y., Takahashi, K., and Ando, K. *Self-crack-healing ability of alumina/ SiC nanocomposite fabricated by self-propagating high-temperature synthesis*. in *31st International Conference on Advanced Ceramics and Composites*. 2008. Daytona Beach, FL.
- [25] Nakao, W., Takahashi, K., and Ando, K., *Self-Healing materials: Fundamentals, design strategies and applications*. *Self-healing of Surface Cracks in Structural Ceramics*, ed. Ghosh, S.K. 2009: WILEY-VCH Verlag GmbH & Co. KGaA, Weinheim.
- [26] Kim, B.S., Ando, K., Chu, M.C., and Saito, S., *Crack-healing behavior of monolithic alumina and strength of crack-healed member*. *Zairyo/Journal of the Society of Materials Science, Japan*, 2003. 52(6): p. 667-673.
- [27] Houjou, K., Ando, K., Liu, S.P., and Sato, S., *Crack-healing and oxidation behavior of silicon nitride ceramics*. *Journal of the European Ceramic Society*, 2004. 24(8): p. 2329-2338.
- [28] Sugiyama, R., Yamane, K., Nakao, W., Takahashi, K., and Ando, K., *Effect of difference in crack-healing ability on fatigue behavior of alumina/silicon carbide composites*. *Journal of Intelligent Material Systems and Structures*, 2008. 19(3): p. 411-415.
- [29] Ando, K., Ono, M., Nakao, W., Takahashi, K., and Saito, S., *Increase of structural integrity machined alumina/SiC using crack-healing*, in *6th Pacific Rim Conference on Ceramic and Glass Technology, PacRim6*. 2006: Maui, HI. p. 155-162.
- [30] Korouš, J., Chu, M.C., Nakatani, M., and Ando, K., *Crack healing behavior of silicon carbide ceramics*. *Journal of the American Ceramic Society*, 2000. 83(11): p. 2788-2792.
- [31] Ando, K., Ikeda, T., Sato, S., Yao, F., and Kobayasi, Y., *A preliminary study on crack healing behaviour of Si<sub>3</sub>N<sub>4</sub>/SiC composite ceramics*. *Fatigue and Fracture of Engineering Materials and Structures*, 1998. 21(1): p. 119-122.
- [32] Mei, J. and Davenport, J.W., *Free-energy calculations and the melting point of Al*. *Physical Review B*, 1992. 46(1): p. 21-25.

- [33] Etter, T., Schulz, P., Weber, M., Metz, J., Wimmmler, M., Löffler, J.F., and Uggowitzer, P.J., *Aluminium carbide formation in interpenetrating graphite/aluminium composites*. *Materials Science and Engineering: A*, 2007. 448(1-2): p. 1-6.
- [34] Mookhoek, S.D., Fischer, H.R., and van der Zwaag, S., *A numerical study into the effects of elongated capsules on the healing efficiency of liquid-based systems*. *Computational Materials Science*, 2009. 47(2): p. 506-511.
- [35] Howe, J.M., *Bonding, structure, and properties of metal/ceramic interfaces: Part 2 Interface fracture behaviour and property measurement*. *International Materials Reviews*, 1993. 38(5): p. 257-271.
- [36] Bennett, I.J., Kranenburg, J.M., and Sloof, W.G., *Modeling the influence of reactive elements on the work of adhesion between oxides and metal alloys*. *Journal of the American Ceramic Society*, 2005. 88(8): p. 2209-2216.
- [37] de Boer, F.R., Boom, R., Mattens, W.C.M., Miedema, A.R., and Niessen, A.K., *Cohesion in metals: transition metal alloys (Cohesion and Structure)*. Vol. 1. 1989, Amsterdam, North Holland: Elsevier Science Publishers B.V.
- [38] Wu, H., *10 - Understanding residual stresses and fracture toughness in ceramic nanocomposites*, in *Residual Stresses in Composite Materials*, Shokrieh, M.M., Editor. 2014, Woodhead Publishing. p. 256-292.
- [39] Laconte, J., Flandre, D., and Raskin, J.-P., *Thin dielectric films stress extraction*, in *Micromachined Thin-Film Sensors for SOI-CMOS Co-Integration*. 2006, Springer US. p. 47-103.
- [40] Warlimont, H., *Springer handbook of condensed matter and materials data*, ed. Martienssen, W. and Warlimont, H. 2005, Heidelberg, Germany: Springer. 431-471.
- [41] Ojovan, M.I., *Glass formation in amorphous SiO<sub>2</sub> as a percolation phase transition in a system of network defects*. *Journal of Experimental and Theoretical Physics Letters*, 2004. 79(12): p. 632-634.
- [42] Shen, Z., Johnsson, M., Zhao, Z., and Nygren, M., *Spark Plasma Sintering of alumina*. *Journal of the American Ceramic Society*, 2002. 85(8): p. 1921-1927.
- [43] Chen, W.-H., Lin, H.-T., Nayak, P.K., and Huang, J.-L., *Material properties of tungsten carbide–alumina composites fabricated by spark plasma sintering*. *Ceramics International*, 2014. 40(9, Part B): p. 15007-15012.

- [44] Fu, C.-T., Li, A.-K., and Wu, J.-M., *Effects of oxidation of Cr<sub>3</sub>C<sub>2</sub> particulate-reinforced alumina composites on microstructure and mechanical properties*. Journal of Materials Science, 1993. 28(23): p. 6285-6294.
- [45] Li, Z. and Bradt, R.C., *Micromechanical stresses in SiC-reinforced Al<sub>2</sub>O<sub>3</sub> composites*. Journal of the American Ceramic Society, 1989. 72(1): p. 70-77.
- [46] Hosford, W.F., *A generalized isotropic yield criterion*. Journal of Applied Mechanics, 1972. 39(2): p. 607-609.



# 3

## **The effect of the TiC particle size on the preferred oxidation temperature for self-healing of oxide ceramic matrix materials**

---

This chapter has been published in the Journal of Materials Science, 53 (8) 2018 p 5973-5986. Authors: Boatemaa, L., Brouwer, J. C., van der Zwaag, S. and Sloof, W. G.

*The effect of particle size on the oxidation kinetics of TiC powders is studied. Different sizes of TiC powder ranging from nanometer to sub-millimetre sizes are investigated. The samples are heated at different heating rates from room temperature up to 1200 °C in dry synthetic air. The Kissinger method for analysis of non-isothermal oxidation is used to estimate the activation energy for oxidation of the powders and to identify the active temperature window for efficient self-healing. The master curve plotting method is used to identify the model which best describes the oxidation of TiC powders and the Senum & Yang method is used to approximate the value for the Arrhenius constant. The oxidation of TiC proceeds via the formation of oxycarbides, anatase and then finally the most stable form: rutile. The activation energy is found to be a strong function of the particle size for particle sizes between 50 nm and 11 μm and becomes constant at larger particle sizes. The data demonstrate how the minimal healing temperature for oxide ceramics containing TiC as healing particles can be tailored between 400 and 1000 °C by selecting the right average TiC particle size.*

### 3.1 Introduction

Embedded Titanium carbide (TiC) particles are being considered as a potential healing agent to autonomously repair crack damage in oxide ceramics used in high temperature applications [1]. For such (extrinsic) self-healing ceramics, microscopic cracks in the material will also intersect the sacrificial healing particle and allow atmospheric oxygen to reach it. The local supply of oxygen via the open cracks to the intersected TiC particles will cause them to oxidize, leading to the formation of  $\text{TiO}_2$  which both fills the crack and adheres strongly to the faces of the crack [2]. Hence, the so-called healing reaction leads to a partial or complete recovery of the mechanical properties of the material and an extension of the life time of the component. To be a successful strategy, it is important that the oxidation reaction takes place at the prevailing conditions (in particular the right temperature) and with the right kinetics. A general analysis of the required properties of the healing particles leading to autonomous self-healing at high temperature can be found in [2].

However, the cited analysis did not specify the minimal temperature window required to trigger the healing reaction. Of course, the required minimal temperature to trigger the healing reaction depends primarily on the chemical stability of the healing material in an oxygen containing environment. This dependence has already been demonstrated (but apparently not been appreciated) in the combined first-generation studies on self-healing of  $\text{Al}_2\text{O}_3$  or  $\text{Si}_3\text{N}_4$  filled with SiC or Ni particles [3-7]. In these studies the crack healing ability was studied as a function of both temperature (from 900 to 1400 °C) and time (between 1 to 300 h) and widely different values were obtained for different particle sizes.

While the optimal healing temperature has been shown to vary significantly with the chemical composition of the healing particle and to a lesser degree of that of the matrix material, very few studies, with the exception of [8], performed a systematic study on the effect of particle size on the healing kinetics given a fixed composition for both the particle and the matrix. In their study, Nakao and Abe [8] measured the strength recovered by high temperature oxidation of alumina containing 18 vol. % SiC particles of size 270, 30 and 10 nm. They reported that reducing the size of SiC reduced the oxidation/healing temperature from 1200 to 950 °C, due to the faster oxidation kinetics at lower particle sizes.



Recently, the ability of 2  $\mu\text{m}$  sized TiC particles to heal surface cracks in alumina has been studied by Yoshioka et al. [1]. Healing of two different composites containing 15 and 30 vol. % of TiC was studied as a function of temperature ranging from 400 to 800 °C in air and a fixed time of 1 h. Full strength was obtained for a composite containing 30 vol. % of TiC upon annealing in air at 800 °C for 1 hr. Also, in-situ healing of these alumina composites was demonstrated [9]. Surface cracks were healed when the material was exposed in a combustion chamber with a high velocity exhaust gas mixture at approx. 1000 °C and a low oxygen partial pressure.

The oxidation behaviour of bulk TiC has already been investigated as a function of temperature (from 600 to 1200 °C) and oxygen partial pressure (13 Pa to 100 kPa) [10, 11]. The observable trend in these studies is that oxidation proceeds parabolically from 600 to 800 °C and switches to linear kinetics at higher temperatures and higher oxygen partial pressures. Four steps were identified during the transformation of TiC powders to  $\text{TiO}_2$  [12, 13]. The first step involves the substitution of atomic oxygen for the carbon present at the interstitial vacancies of the TiC lattice leading to the formation of the oxycarbides/titanium suboxide layer. In the next step, the titanium suboxides oxidise into amorphous titanium dioxide and further crystallize to anatase. In third stage, the crystallization of anatase continues and the resulting volume expansion leads to the cracking of the oxide layers, and this provides fast short circuit diffusion paths oxidation. In the fourth and final step, anatase is formed continuously and rather rapidly transformed into rutile. The rate determining step is the diffusion of oxygen through the already formed oxide layers.

With TiC having been identified as a potential healing agent for alumina [2], the current work focusses on the determination of the effect of TiC particle size on its oxidation kinetics in order to explore the possibility to lower the minimal healing temperature of alumina containing TiC to temperatures below 1000 °C. To this aim, differential thermal and thermogravimetric analyses are performed for TiC powders of different particle sizes over the temperature range from room temperature to 1200 °C. The kinetic triplet, i.e., the activation energy, the reaction model and the Arrhenius constant are determined for all powders and such information, in principle, allows the prediction of the optimal healing temperature for any inert ceramic containing TiC particles as the discrete, extrinsic healing agent.

### 3.2 Analysis of reactions

In solid-gas reactions the solid phase is usually a granular medium through which the gaseous reactant circulate and react at the solid interface [14]. Due to the reactions occurring at a microscopic level, the solid material undergoes chemical and structural change as the reaction proceeds. Several reaction models are used in describing gas-solid reactions [15]. The unreacted shrinking core model is commonly used. In this model the reaction product forms a solid layer that allows diffusion of reactant gas toward the interface between the product layer and unreacted core. A continuous reaction leads to the advancing of a reaction front, or equivalently, a shrinking core. The entire reaction kinetics involves three steps; transport and dissolution of the gas reactant at the solid surface, diffusion of the gas reactant through the product layer towards the unreacted core, and finally, chemical reaction of the gas with the solid reactant at the product-core interface [16].

Thermal analysis is employed to study the heterogeneous reactions. In (simultaneous) differential thermal analysis (DTA) the heat flow and in thermogravimetric analysis (TGA), the mass change is measured while the material is heated at a constant heating rate [17]. From the measured data the kinetic triplet which describes the conversion of a material ( $\alpha$ ) as a function of temperature ( $T$ ) and time ( $t$ ), is derived. The kinetic triplet parameters are the activation energy  $E_A$ , the Arrhenius or frequency constant  $A$  and the reaction model  $f(\alpha)$  [18]. For non-isothermal experiments the rate of transformation of any material is given by:

$$\frac{d\alpha}{dT} = \frac{d\alpha}{dt} \cdot \frac{dt}{dT} \quad (3.1)$$

where the fraction converted at any time is given by:

$$\alpha = \frac{m_t - m_0}{m_\infty - m_0} \quad (3.2)$$

in which  $m_0$ ,  $m_t$  and  $m_\infty$  denote the mass at time  $t$  is 0,  $t$  and  $\infty$  (i.e. after full conversion), respectively.  $dT/dt$  is the heating rate denoted as  $\beta$ , and  $d\alpha/dt$  is the isothermal conversion rate and expressed as:

$$\frac{d\alpha}{dt} = A e^{\frac{-E_A}{RT}} f(\alpha) \quad (3.3)$$

Combining Eqs. (3.1) and (3.3) leads to the non-isothermal conversion rate:

$$\frac{d\alpha}{dT} = \frac{A}{\beta} e^{\frac{-E_A}{RT}} f(\alpha) \quad (3.4)$$

Integration results in the non-isothermal transformation rate law given by:

$$g(\alpha) = \frac{A}{\beta} \int_0^T e^{\frac{-E_A}{RT}} dT \quad (3.5)$$

This temperature integral has no analytical solution [17, 19], but is usually approximated by a series expansion or converted in an approximate form that can be integrated. A frequently used approximation is that by Senum and Yang [20]. Consider  $x = E_A/RT$ , then:

$$\int_0^T e^{\frac{-E_A}{RT}} dT = \frac{E_A}{R} \int_x^\infty \frac{e^{-x}}{x^2} dx \quad (3.6)$$

with  $p(x) = \int_x^\infty \frac{e^{-x}}{x^2} dx$ , Eq. (3.6) is approximated with the fourth rational of Senum and Yang [20], i.e.:

$$p(x) = \frac{e^{-x}}{x} \left( \frac{x^3 + 18x^2 + 86x + 96}{x^4 + 20x^3 + 120x^2 + 240x + 120} \right) \quad (3.7)$$

Successively, the activation energy, the reaction model and finally the Arrhenius constant will be determined from non-isothermal experimental data. In the above analysis, the kinetic parameters are considered to be independent of temperature and fraction converted.

### 3.2.1 Activation energy

Regardless of the reaction order the activation energy of the conversion reaction  $E_A$  can be obtained directly from non-isothermal TGA or DTA data using the so-called Kissinger method [21, 22]. If the temperature rises during the reaction, the reaction rate will rise to a maximum value, but return to zero as the reactant is exhausted. The maximum rate is associated with either a maximum mass change or heat evolution, which occurs at the peak temperature. Then, the governing equation for the determination of the activation energy reads:

$$\ln\left(\frac{\beta}{T_p^2}\right) + \frac{E_A}{RT_p} = C \quad (3.8)$$

Where  $T_p$  is the peak temperature, corresponding to the temperature at which the reaction rate is at maximum. Then, the highest heat flux or mass change rate is recorded.  $R$  is the gas constant and  $C$  is a constant. Thus, the activation energy ( $E_A$ ) is obtained by plotting  $\ln(\beta/T_p^2)$  versus  $1/T_p$  for a series of measurements at different heating rates  $\beta$ .

### 3.2.2 Reaction model

The reaction model mathematically describes the conversion process of a material as a result of an occurring chemical or physical reaction. Different models have been derived for solid state reactions [18], which comprises nucleation, geometrical contraction, diffusion and reaction-order models. To determine the appropriate model to analyse the experimental data the so-called ‘master curve plotting’ method is used. This method is based on the concept of generalized time  $\theta$  [23], which is defined by Eq. (3.9) for isothermal or non-isothermal reactions respectively as:

$$\theta = \int_0^t e^{\frac{-E_A}{RT}} dt \quad \text{or} \quad \theta = \frac{1}{\beta} \int_0^T e^{\frac{-E_A}{RT}} dT \quad (3.9)$$

$\theta$  denotes the reaction time taken to attain a particular fraction converted at infinite temperature. Now, **Eqs. (3.3)** and **(3.5)** can be rewritten in terms of generalized time respectively as:

$$\frac{d\alpha}{d\theta} = Af(\alpha) \quad (3.10)$$

$$g(\alpha) = A\theta \quad (3.11)$$

As a reference point for the master-curve plotting analysis generally the level  $\alpha = 0.5$  is chosen and using **Eq. (3.10)** it can be derived that:

$$\frac{d\alpha/d\theta}{(d\alpha/d\theta)_{\alpha=0.5}} = \frac{f(\alpha)}{f(0.5)} \quad (3.12)$$

From the experimentally determined conversion rate, with respect to the generalized time, as a function of fraction converted,  $f(\alpha)/f(0.5)$  versus  $\alpha$  can be obtained, since:

$$\frac{d\alpha}{d\theta} = \frac{d\alpha}{dt} \exp\left(\frac{E_A}{RT}\right) \quad \text{or} \quad \frac{d\alpha}{d\theta} = \beta \frac{d\alpha}{dT} \exp\left(\frac{E_A}{RT}\right) \quad (3.13)$$

By comparing the experimental result with theoretical reaction models [23], the reaction model that best fits the measured data can be determined. From this, the key reaction mechanisms can be determined and this knowledge can be used to optimise the material performance.

### 3.2.3 Arrhenius constant

The last of the kinetic triplet, i.e., the pre-exponential factor ( $A$ ) can be evaluated from **Eq. (3.11)**, once the reaction model is determined; cf. Section 2.2. The generalized time  $\theta$  for non-isothermal reactions **Eq. (3.9)** resembles **Eq. (3.6)** and hence can be written as:

$$\theta = \frac{E_A}{\beta R} p(x) \quad (3.14)$$

while  $p(x)$  is approximated using Eq. (3.7).

### 3.2.4 Experimental procedure

The five TiC powders used in this study are all commercially available and their main features are summarized in Table 3.1. The first and second powders, having an average particle size of 140 and 48  $\mu\text{m}$ , respectively, were obtained by sieving a TiC powder with a broad size distribution (Goodfellow, UK; product number TI546030). The third TiC powder with an average particle size of 5  $\mu\text{m}$  was supplied by Alfa Aesar, Germany (product number TiC 40178). The fourth TiC powder with an average particle size of 0.8  $\mu\text{m}$  was supplied by American Elements, USA (product number TI-C-03M-NP.800NS). Finally, the fifth TiC powder with an average particle size of 50 nm was supplied by Chempur, Germany (product number CFF-NP059).

The purity of the powders studied was determined with X-ray fluorescence spectroscopy (XRF) using an Axios Max WD-XRF instrument (PANalytical, The Netherlands) and the data were evaluated with SuperQ5.0i/Omnian software. The size distribution of the TiC particles was determined by laser diffraction using the Microtrac 3500 (Microtrac Inc. USA) equipped with a tri-laser diode detection system. The particle morphology of each TiC powder was recorded with scanning electron microscopy (SEM) using a JSM 6500F (JEOL, Japan). The instrument used was equipped with an energy dispersive spectrometer (EDS; Ultra Dry 30  $\text{mm}^2$  detector, Thermo Fisher Scientific, USA) for X-ray microanalysis (XMA).

The oxidation kinetics of the TiC powders was studied non-isothermally using simultaneous thermogravimetric (TG) and differential thermal analysis (DTA) using a high performance symmetrical double furnace balance (TAG 16/18, Setaram, France).  $20 \pm 1$  mg of the powder was put into a 100  $\mu\text{L}$   $\text{Al}_2\text{O}_3$  crucible and placed onto a TG-DTA rod with an S-type thermocouple. A similar rod but without crucibles was placed as a counter weight on the other side of the balance to aid automatic correction of buoyancy effects. Then, the dual furnaces were heated up

from room temperature to 1200 °C with various heating rates (between 1-10 °C/min). In each measurement, both furnaces were purged with dry synthetic air ( $N_2$  + 20 vol. %  $O_2$  and  $H_2O < 10$  ppm) at a total flow rate of 50 sccm. The evolved gas at the sample location was collected and analysed with an Omnistar GSD 301 system having a quadrupole mass spectrometer (QMS 200 M3 from Pfeiffer Omnistar, Germany) in order to observe the evolution of  $CO_2$ .

*Table 3.1: Size and composition of TiC powders with  $d_{50}$  as the average particle size and  $D_{10}$  and  $D_{90}$  as the particle size at 10 and 90 % cut-off respectively in the size distribution.*

Powder	$D_{50}$ ( $\mu m$ )	$D_{10}$ - $D_{90}$ ( $\mu m$ )	TiC (wt %)	Main impurities (wt %)	
1	140	100 – 150	99.75	Fe	0.089
				Si	0.04
2	48	40 – 50	99.75	Fe	0.089
				Si	0.04
3	5	2 – 15	98.17	WC	1.552
				Fe	0.105
4	0.8	0.6 – 1	90.8	W	7.25
				Co	0.68
5	0.05	0.04-0.07	99.966	Si	0.017
				Cl	0.008

The thermal analysis system used was equipped with Calisto acquisition and processing software (v1.43 DB v1.44, Setaram, France) which records both the furnace and the sample temperature. For accurate results the temperature measured by the thermocouples at the sample position is used for the analysis as this represents the true sample temperature. Prior to admitting the gases to the furnaces, each gas, i.e. Ar,  $N_2$ , and  $O_2$  (all with 5N vol. % purity), was filtered to remove any residual hydrocarbons, moisture and oxygen (for  $N_2$  and Ar). The Accosorb (< 10 ppb hydrocarbons), Hydrosorb (<10 ppb  $H_2O$ ) and Oxysorb (< 5 ppb  $O_2$ ) filters (Messer Griesheim, Germany) were used. The flow of each gas was regulated and monitored with LabView (version 12, National Instruments, USA) using calibrated mass flow controllers (Bronkhorst, The Netherlands).

The oxidation products and lattice parameter were identified and measured by X-ray diffraction using a Bruker D8 Advance diffractometer (Bruker, Germany) equipped

with a graphite monochromator. Diffractograms were recorded with Co  $K\alpha$  radiation in the  $2\theta$  range of 10 to 130° and a step size of 0.034°. The data were processed with the Diffrac EVA 4.1 Bruker software.

### 3.3 Results

#### 3.3.1 TiC powder oxidation

Oxidation of the 5  $\mu\text{m}$  powder was studied first by heating from room temperature to 1200 °C at 5 °C/min in air, the heat flow and the conversion curves are presented in **Figure 3.1**. Transformation starts just before 400 °C and ends around 900 °C via two exothermic peaks at about 470 and 710 °C. Therefore, to fully describe the oxidation of TiC, two separate experiments are performed on the same powder under the same conditions till the end of each peak (i.e. till 530 and 900 °C) and the oxidation products analysed.

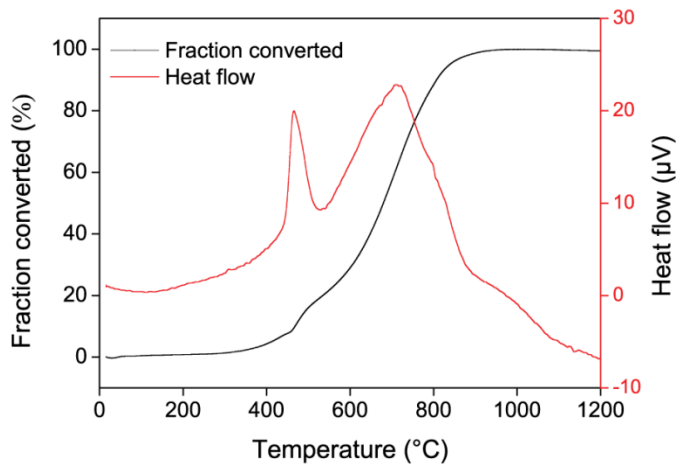


*Figure 3.1: Heat flow and mass gained signals for the 5  $\mu\text{m}$  powder oxidized at 5 °C/min in dry synthetic air.*

XRD confirms that part of the TiC powder is converted into anatase and rutile in the ratio of about 3:2 in the first peak and the remaining TiC, oxycarbide and anatase are converted into rutile in the second peak. The morphology of the 5  $\mu\text{m}$



TiC powder at different stages of non-isothermal oxidation with a heating rate of 5 °C/min in dry synthetic air is shown in **Figure 3.2**.

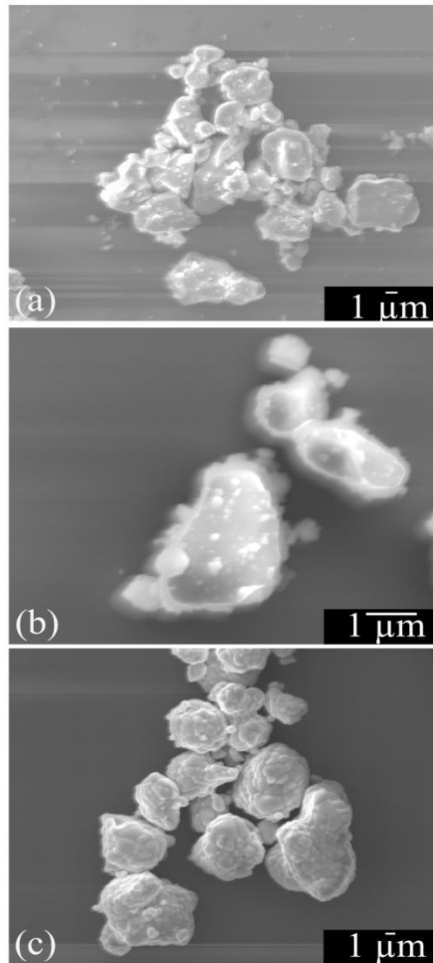


*Figure 3.2: SEM images of TiC powder with an average particle size of 5 μm after non-isothermal oxidation in synthetic dry air with a heating rate of 5 °C/min; cf. Figure 3.1(a) the raw powder, (b) oxidized up to 530 °C (formation of anatase) and (c) oxidised up to 1200 °C (fully transformed into rutile).*

The starting TiC particles are irregularly shaped with sharp edges; see **Figure 3.2(a)**. After oxidation up to 530 °C some Anatase was formed at the surfaces; see **Figure 3.2 (b)**. Finally, after full transformation into rutile the particles became more rounded at the edges as can be seen in **Figure 3.2(c)**.

As the experiment in **Figure 3.1** proceeded, the gases evolved were collected and analyzed. CO<sub>2</sub> was the only gas detected and the recorded pressure is presented in **Figure 3.3**. It is noticeable that the removal of C via CO<sub>2</sub> release and the precipitation of TiO<sub>2</sub> occurs simultaneously as the heat flow peaks in **Figure 3.1** and the CO<sub>2</sub> signal in **Figure 3.3** closely overlap at the same temperatures.

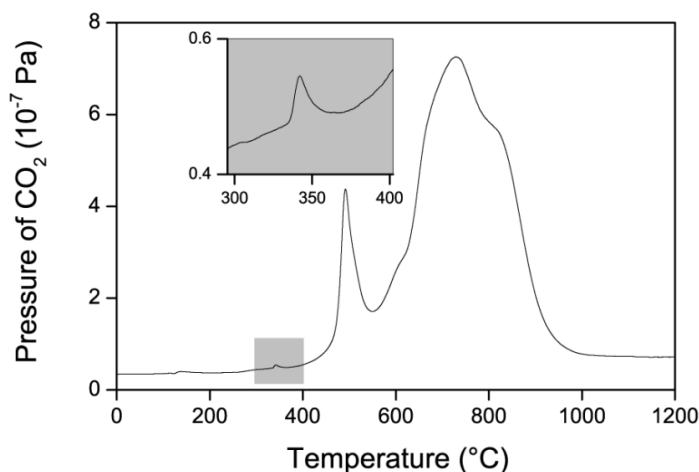


*Figure 3.3: Evolution of CO<sub>2</sub> during oxidation of TiC powder with average particle size of 5  $\mu\text{m}$  in dry synthetic air recorded with 5  $^{\circ}\text{C}/\text{min}$ , insert confirms the release of CO<sub>2</sub> during oxycarbide formation.*

A zoom in at about 320  $^{\circ}\text{C}$  of **Figure 3.3**, shows a small peak (insert of **Figure 3.3**) which is not immediately identified in the heat flow signal in **Figure 3.1**. Hence, the mass change signal in **Figure 3.1** is further differentiated in **Figure 3.4**, then, a kink coinciding with the peak at 320  $^{\circ}\text{C}$  in **Figure 3.3** is identified.

Another experiment using a fresh sample was run under the same conditions until 360  $^{\circ}\text{C}$  to determine the reaction occurring around 320  $^{\circ}\text{C}$ . No oxide was identified by XRD after controlled cooling of the reaction product obtained although the sample weight had increased and CO<sub>2</sub> had been released. The combination of observations shows that the low temperature peak is due to the substitution of atomic oxygen at carbon sites of the TiC lattice [12], leading to the formation of TiC<sub>y</sub>O<sub>1-y</sub>, which is evidenced by the reduction in the lattice parameter of TiC [24]. In this specific case, the lattice parameter of the starting material reduced from  $4.3275 \pm 0.0001$  to  $4.3260 \pm 0.00005$   $\text{\AA}$  after heating up to 360  $^{\circ}\text{C}$ . This oxycarbide phase

exists throughout the oxidation process [12, 25], and thus may act as a precursor for the formation of anatase and rutile.

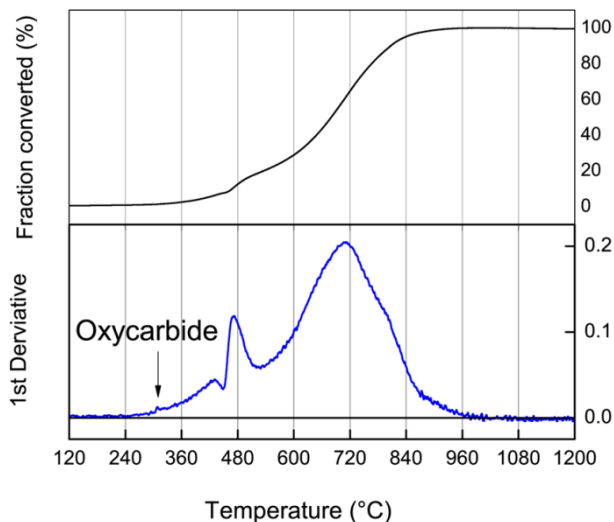


*Figure 3.4: Differentiated mass gain signal ( $d\Delta m/dt$ ) of 5  $\mu\text{m}$  TiC powder recorded with 5  $^{\circ}\text{C}/\text{min}$  when oxidizing in dry synthetic air.*

The oxidation of the 5  $\mu\text{m}$  powder can be summarized as follows. A first oxycarbide formation stage takes place over the interval from about 300 to 360  $^{\circ}\text{C}$ . A second oxidation stage which leads to the formation of both rutile and anatase sets in after the first reaction and peaks around 470  $^{\circ}\text{C}$  and ends just before 530  $^{\circ}\text{C}$ ; see **Figure 3.1** (this stage is hereafter referred to as the anatase formation stage). Although a single peak in the heat flow signal characterizes this step, the mass change signal clearly shows two consecutive stages. The first of these two stages start from 430 to 470  $^{\circ}\text{C}$ , this proceeds relatively fast showing a very steep conversion versus temperature curve. The second stage which proceeds at a relatively slower rate continues from 470  $^{\circ}\text{C}$  and ends at about 520  $^{\circ}\text{C}$ . A last oxidation stage starts from 530  $^{\circ}\text{C}$  and ends at around 960  $^{\circ}\text{C}$ , where the remaining TiC, oxycarbide and anatase are converted into rutile. A similar reaction scheme was observed and reported earlier by [12] when studying the oxidation behaviour of TiC powder at various oxygen partial pressures. However, in that study the second stage was split up

into the formation of anatase and rutile, in addition, it was mentioned that these two stages may overlap and cannot be clearly distinguished from each other.

To continue, the other powders were all heated at 5 °C/min in air in separate experiments. The results are presented in **Figure 3.5**. As observed for the 5  $\mu\text{m}$  powder, multiple peaks are identified for the different particle sizes. The stages of oxidation were resolved by running separate experiments up to each identified peak in the heat flow or the differentiated mass change signal, then the products were analysed by XRD and/or XMA.

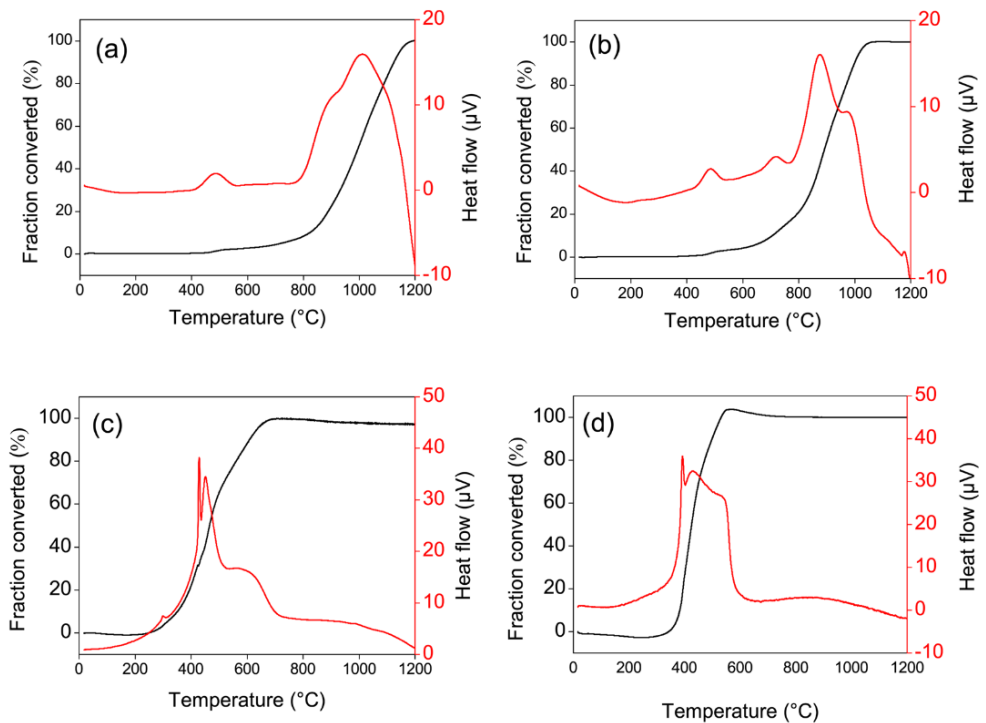


**Figure 3.5:** Heat flow and mass change in terms of converted fraction TiC (in %) as a function of temperature recorded at 5 °C.min in dry synthetic air of TiC powders with average size of: (a) 140  $\mu\text{m}$ , (b) 48  $\mu\text{m}$ , (c) 0.8  $\mu\text{m}$  and (d) 0.05  $\mu\text{m}$ .

For the coarsest powders having an average particle size of 140 and 48  $\mu\text{m}$  only the peaks pertaining to the formation of anatase and rutile can be identified in the heat flow and mass change signals (see **Figure 3.5(a)** and **(b)**, respectively). The stage of

oxy-carbide formation appears to be overshadowed. For both powders, the peak occurring between 400 to 600 °C corresponds to the formation of anatase. The formation of rutile sets in at 800 °C and ends at 1195 °C for the 140 μm powder and for the 48 μm powder it starts from 700 °C and ends around 1050 °C. It is noteworthy that the transformation into rutile of both coarse powders occurs via multiple steps while the mass gain signal for this range reflects a single peak event (i.e. a non-changing slope).

For the 0.8 μm TiC powder all 3 stages observed for the 5 μm powder can be identified in the heat flow signal. The formation of the oxycarbide can be seen in **Figure 3.5(c)** peaking at about 310 °C, as well as in the differentiated mass gain signals shown in **Figure 3.6**. Anatase is formed in the sharp peak around 420 °C followed immediately by conversion into rutile which also occurs via two peaks.

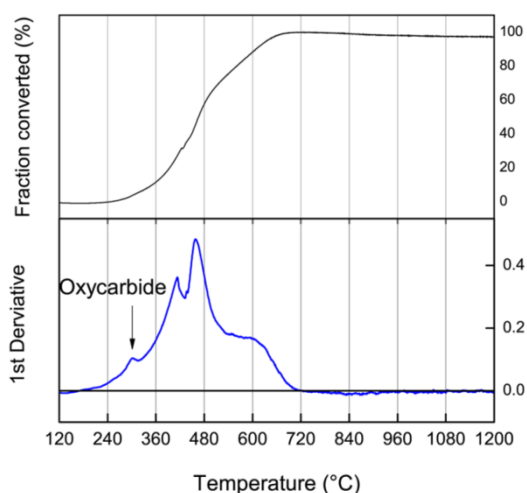


*Figure 3.6: Differentiated mass gain signal ( $d\Delta m/dt$ ) of 0.8 μm TiC powder recorded with 5 °C/min in dry synthetic air.*

For the nano-powder the mechanism somewhat reverses to that of the coarser powders as no trace of the oxycarbide formation can be detected. A peak corresponding with the formation of anatase can be identified at 400 °C and two peaks associated with the formation of rutile can be identified at about 430 and 550 °C, respectively in **Figure 3.5(d)**. The various stages of oxidation, as identified for the different particle sizes, are summarized as a function of temperature in **Figure 3.7**.

Depending on the particle size some stages may overlap or is overshadowed and hence not always clearly resolved in the mass gain and heat flow signals as a function of temperature.

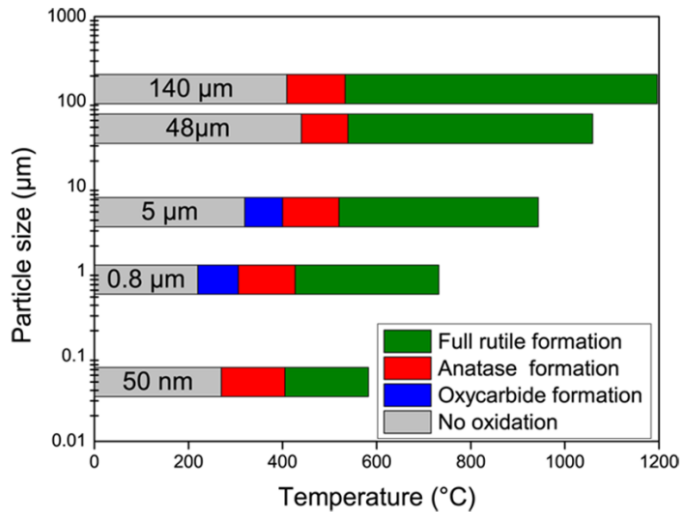


Figure 3.7: Chart showing the various stages of oxidation in dry synthetic air of TiC particles with different average particle sizes.

### 3.3.2 Effect of heating rate on oxidation

As the heating rate is increased, the amount of TiC transformed into anatase is reduced. For example, for the 140 μm powder the amount of TiC transformed decreases from 4 to 1 % as heating rate is increased from 1 to 10 °C/min. Similarly, there was a decrease of about 5 to 1.5 % and 40 to 15 % for the 48 and 5 μm powders respectively, during the same stage, see **Figure 3.8**.

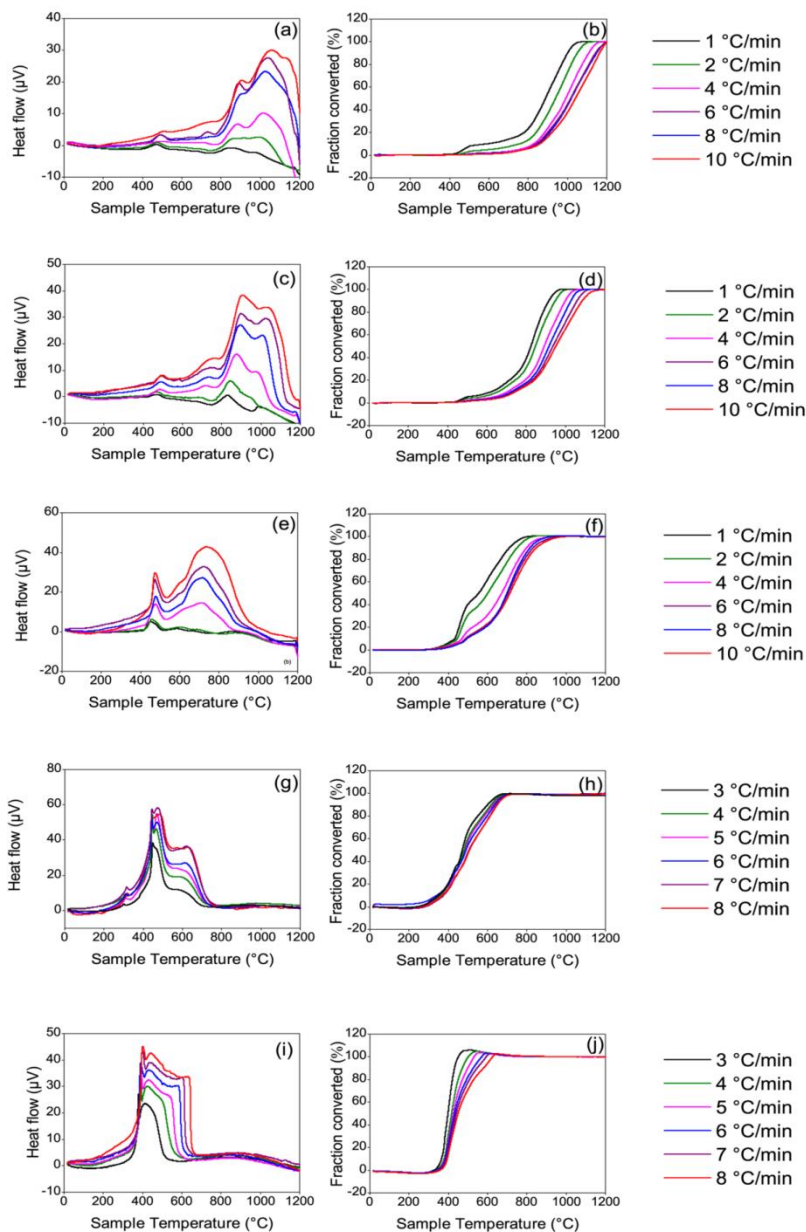


Figure 3.8: Heat flow and mass change in terms of converted fraction TiC (in %) as a function of temperature recorded at different heating rates in dry synthetic air of TiC powders with average particle size of: (a,b) 140  $\mu\text{m}$ , (c,d) 48  $\mu\text{m}$ , (e,f) 5  $\mu\text{m}$ , (g,h) 0.8  $\mu\text{m}$  and (i,j) 0.05  $\mu\text{m}$ .

For the same amount of powder, the surface area exposed to oxygen increases when the TiC particle size is reduced. Then, the conversion of TiC into TiO<sub>2</sub> is enhanced. This is evident from the heat flow signal recorded with the same heating rate, which increases for smaller particles. For example, the formation of rutile when oxidizing 5 μm TiC powder at 10 °C/min corresponds with about 45 μV of heat evolved, while under the same conditions 140 μm TiC powder results in about 28 μV of heat evolved; cf. **Figure 3.8** (a and e). Since the oxidation of TiC powder is faster when the particle size is smaller, the final temperature for full conversion of TiC powder into TiO<sub>2</sub> (rutile) during non-isothermal oxidation (at the same heating rate) decreases with particle size; see **Figure 3.8**.

A final observable trend is that the stages of oxidation are well separated from each other (in both the heat flow and the fraction converted signals) at larger particle sizes. However, as the particle size is reduced, these stages become indistinguishable in the fraction converted plots especially for the 50 nm powder.

### 3.3.3 Evaluation of the activation energy

The activation energy for oxidation of the different TiC powders is determined using **Eq. (3.8)**. As more than one peak occurs during the transformation reaction, the peak temperature ( $T_p$ ) is defined as the highest point in the differentiated mass gain signal. The results for the various TiC powders are presented in **Figure 3.9**. With decreasing particle size the lines for the maximum conversion of TiC into TiO<sub>2</sub> shifts to lower temperatures, and this defines the temperature window where a particle is activated. The slope of these lines corresponds to the activation energy of the reaction and the figure clearly shows it decreases with decreasing particle size.

The values of the activation energy  $E_A$  as a function of the TiC particle size are presented in **Table 3.2**. It is observed that  $E_A$  significantly decreases with decrease in particle size for sub-micron and nano-sized particles and is more or less constant for particle sizes  $> 5 \mu\text{m}$ . The activation energies determined here are comparable to those determined in other studies (e.g. [11, 25] ), i.e. 192 and 245 kJ/mol. The (non-significant) difference may arise from the size of the TiC particles and the limited temperature window of the isothermal experiments used in the analysis.



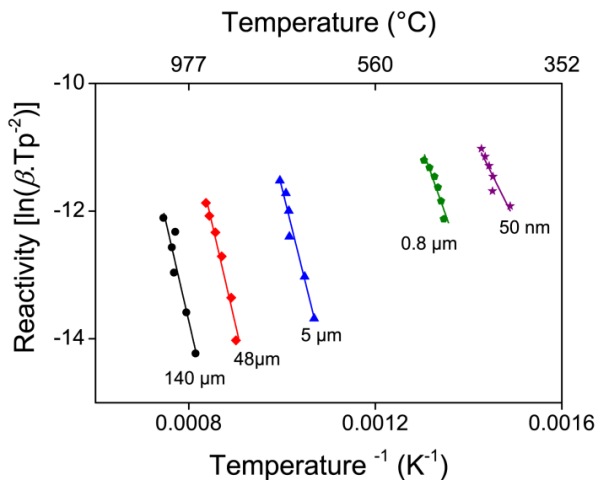


Figure 3.9: Kissinger plot for estimating the activation energies size for the oxidation of TiC powder with different particles sizes in dry synthetic air; see Eq. (8).

Effects of particle size on the activation energy have been reported for other materials as well [26, 27]. It can be conceived that when the surface to volume ratio increases the activation energy decreases, since the atoms at the surface have fewer bonds and neighbouring atoms and thus need less energy to transfer into oxide [28].

Table 3.2: Activation energies as determined for oxidation of TiC powders with different particle sizes.

Size ( $\mu\text{m}$ )	$E_A$ (kJ/mol)
140	$263 \pm 42$
48	$262 \pm 23$
5	$244 \pm 24$
0.8	$172 \pm 27$
0.05	$122 \pm 24$

Hence, the reduction of the bulk activation energy,  $E_A^{bulk}$ , can be related to the surface energy  $\sigma$  according to [29]:

$$E_A = E_A^{bulk} - \frac{6\sigma V_m}{d} \quad (3.15)$$

in which  $V_m$  is the molar volume and  $d$  the particle size. For TiC the surface energy equals  $2.73 \text{ J/m}^2$  [30] and the molar volume  $12.18 \text{ cm}^3/\text{mol}$  [31]. From **Figure 3.10**, the observed reduction in the activation energy for submicron or nano-sized particles is due to surface defects (like: dislocations, grain boundaries, steps and kinks, roughness, etc.), of which their number increases with surface area (i.e. with  $d^{-2}$ ) [32]. These surface defects promote the nucleation and growth of the oxide.

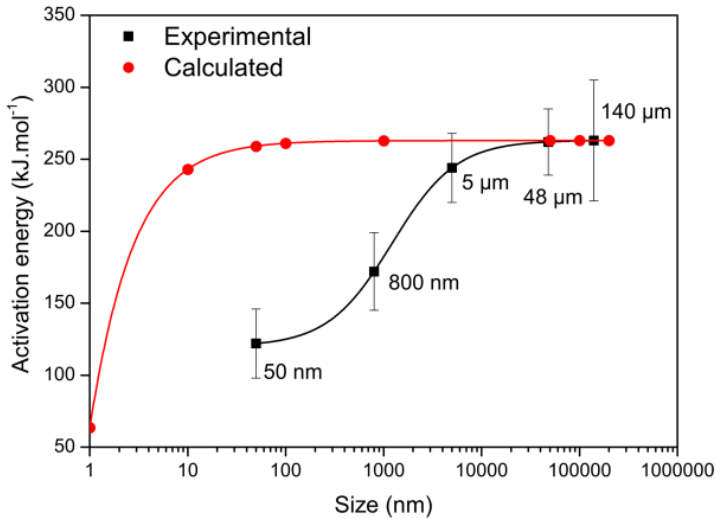


*Figure 3.10: Activation energy as a function of particle size for the oxidation of TiC powder in dry synthetic air. The calculated values pertain to the effect of surface to volume ratio; see Eq. (15).*

Hence, the activation energy as a function of particle size is presented in **Figure 3.10** and the relationship can be best described with **Eq. (3.16)**.

$$E_A = 263 + \left( \frac{120 - 263}{\left( 1 + \left( \frac{d}{1220} \right)^{1.325} \right)} \right) \quad (3.16)$$

Where  $E_A$  is the Activation energy in KJ/mol and  $d$  is the particle size in nm.

### 3.3.4 Reaction model for TiC oxidation

Out of the many reaction models [18], the non-isothermal plots of the rate of conversion with temperature pre-empt that the oxidation of TiC may be either an Avrami-Erofeyev, diffusion, or an order reaction model. Hence, the experimental data are compared with the Avrami-Erofeyev (A3), 3D diffusion-Jander (D3), Ginstling-Brounshtein (D4) and the third order (F3) reaction models using the master curve plotting method [23]; see Section 2.2. To ascertain the validity of the identified model, master plots are made for all the powders at different heating rates, see **Figure 3.11**.

It is seen that for different heating rates the experimental data closely resembles the F3 (third order reaction model) more than any other model. The integral and the differential form of the third order reaction model are respectively defined as:

$$g(\alpha) = (1/2) \left[ (1 - \alpha)^{-2} - 1 \right] \quad (3.17)$$

$$f(\alpha) = (1 - \alpha)^3 \quad (3.18)$$

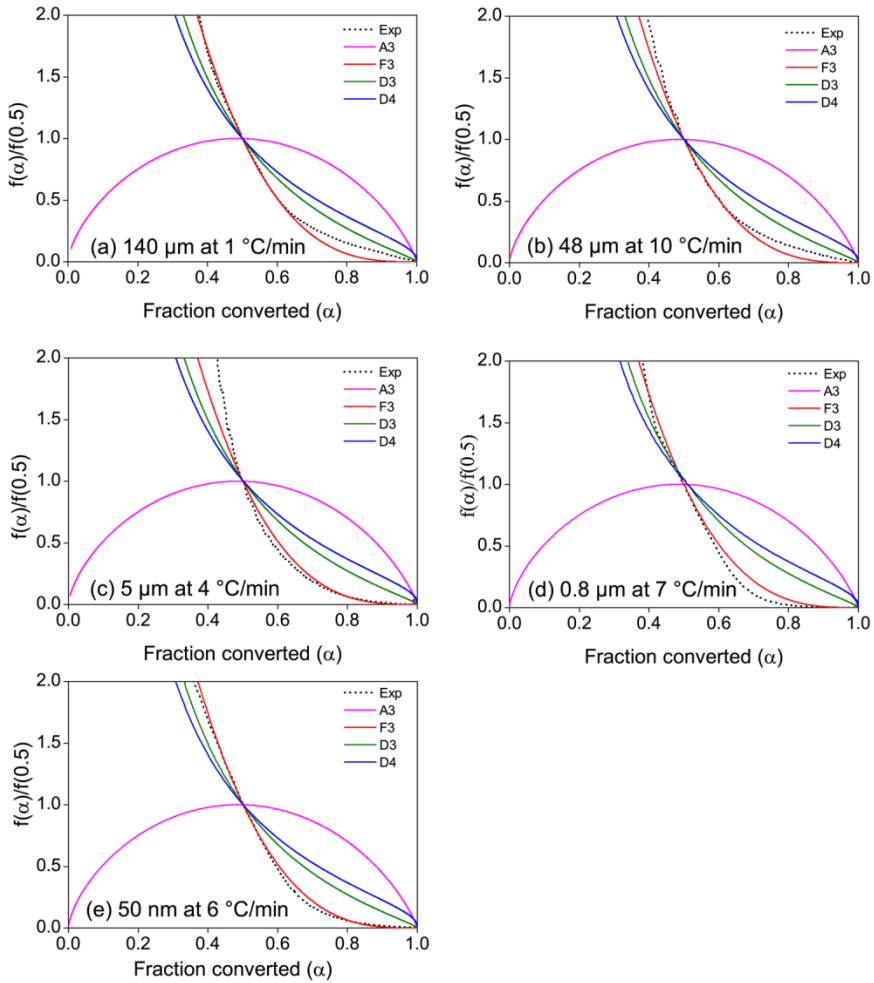


Figure 3.11: Master plots of theoretical models and experimental data of TiC powders with average size of: (a) 140  $\mu\text{m}$ , (b) 48  $\mu\text{m}$ , (c) 5  $\mu\text{m}$ , (d) 0.8  $\mu\text{m}$  and (e) 0.05  $\mu\text{m}$ .

The rate determining step in the oxidation of TiC is the diffusion of oxygen from the gaseous phase through the formed oxide layers and the opposite diffusion of titanium and carbon from the material into the scale.

### 3.3.5 The Arrhenius pre-exponential factor

The last of the kinetic triplet, i.e., the pre-exponential factor ( $A$ ) is evaluated from the integral form of the kinetic rate equation given in Eq. (3.10) combined with Eq. (3.16). The generalized time Eq. (3.8) is determined at every temperature from 25 to 1200 °C using Eq. (3.13), the applied heating rate and the estimated  $E_A$ . A linear fitting of Eq. (3.10) is made for the range of  $\alpha$  pertaining to the third oxidation stage (i.e. transformation into rutile) to find the constant  $A$ . The calculated pre-exponential factors see Table 3.3, are relatively constant with the same order of magnitude. However is significantly decreases for the nano-metre sized particles [33,34]. As the particle size decreases, the partial molar surface enthalpy and the partial molar surface entropy increases, leading to the decrease of the apparent activation energy and the pre-exponential factor [29, 35]. There is no simple explanation for the high value of the Arrhenius parameter for the 5  $\mu\text{m}$  particle, other than undetected impurities or structural defects.

*Table 3.3: The evaluated pre-exponential factors (a) for TiC powders oxidized in dry synthetic air.*

Size ( $\mu\text{m}$ )	$A$ ( $\text{s}^{-1}$ )
140	$3.3 \times 10^{10}$
48	$5 \times 10^{10}$
5	$100 \times 10^{10}$
0.8	$8.3 \times 10^{10}$
0.05	$1 \times 10^8$

Finally, the conversion  $\alpha$  of TiC into  $\text{TiO}_2$  by oxidation in air can be expressed as a function of temperature and time for each particle size by:

$$\alpha = 1 - [(2A\theta + 1)^{-1/2}] \quad (3.19)$$

with  $\theta$  calculated using Eq. (3.14). It can be seen in Figure 3.12, that at higher temperatures the calculated results fit well with the experimental results with a slight deviation at lower temperatures. This deviation is associated with initial stages of oxidation which corresponds to the formation of the oxycarbides and/or anatase.

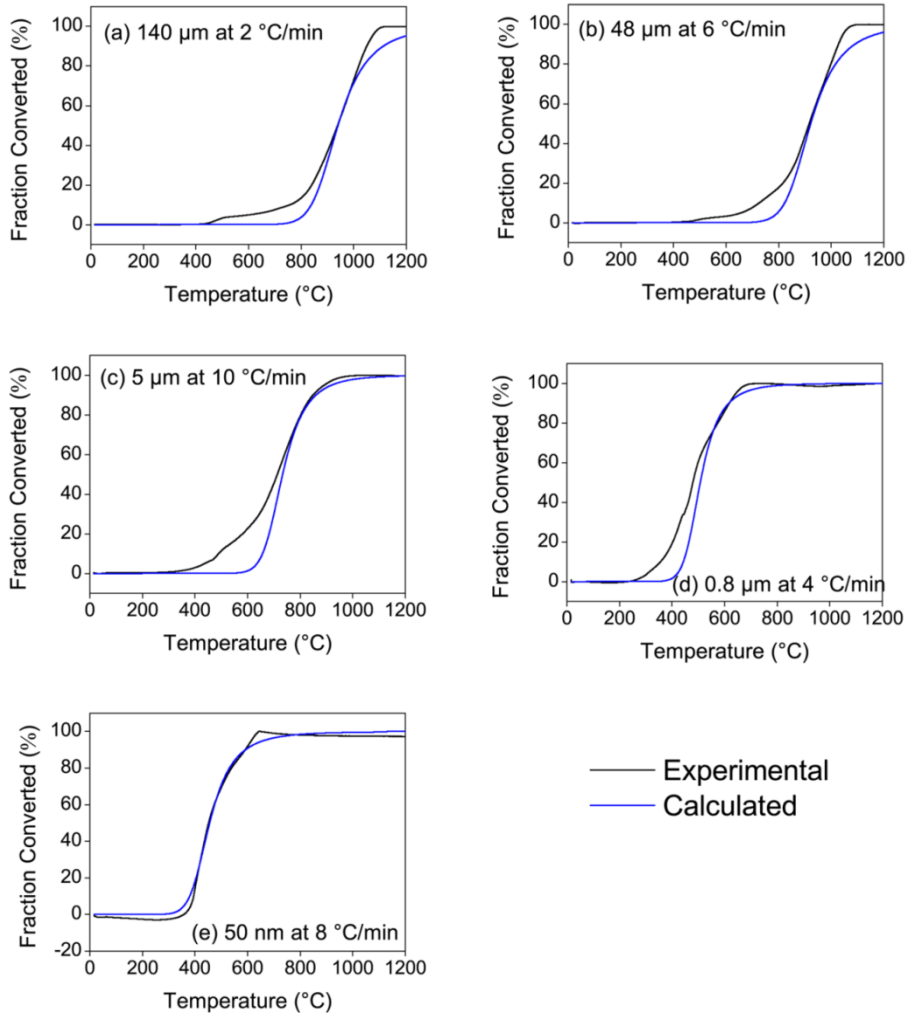


Figure 3.12: comparing the fraction converted ( $\alpha$ ) for the experimental data and the calculated results of TiC powders in dry synthetic air.

### 3.4 Conclusions

Oxidation of TiC was found to proceed via the formation of oxycarbides  $\rightarrow$  anatase / rutile  $\rightarrow$  rutile and closely follows a third order reaction path. The temperature window for activation of the oxidative decomposition of the TiC healing particles

i.e. for triggering the self-healing reaction drops from 1000 to 400 °C as particle size decreases from 140  $\mu\text{m}$  to 50 nm. As the change in optimal healing temperature does not depend on the chemical composition of the matrix material as such, the present study shows in a generic manner that extrinsic self-healing in oxide ceramic matrices can be tailored to a specific temperature range by tuning the size of the healing particle. Further, the activation energy required for oxidation decreases significantly for particles ranging between 10  $\mu\text{m}$  to 50 nm. Above 10  $\mu\text{m}$  particle size the activation energy for the thermal oxidation of TiC becomes constant.

### **Acknowledgements**

This research was sponsored by the People Program (Marie Curie ITN) of the European Union's seventh framework program, FP7, grant number 290308 (SHeMat). The authors are indebted to Ing. Ruud Hendriks for performing XRD analysis.

## References

- [1] Yoshioka, S., Boatemaa, L., van der Zwaag, S., Nakao, W., and Sloof, W.G., *On the use of TiC as high-temperature healing particles in alumina based composites*. Journal of the European Ceramic Society, 2016. 36(16): p. 4155-4162.
- [2] Boatemaa, L., Kwakernaak, C., van der Zwaag, S., and Sloof, W.G., *Selection of healing agents for autonomous healing of alumina at high temperatures*. Journal of the European Ceramic Society, 2016. 36(16): p. 4141-4145.
- [3] Ando, K., Kim, B.S., Chu, M.C., Saito, S., and Takahashi, K., *Crack-healing and mechanical behaviour of Al<sub>2</sub>O<sub>3</sub>/SiC composites at elevated temperature*. Fatigue & Fracture of Engineering Materials & Structures, 2004. 27(7): p. 533-541.
- [4] Osada, T., Nakao, W., Takahashi, K., Ando, K., and Saito, S., *Strength recovery behavior of machined Al<sub>2</sub>O<sub>3</sub>/SiC nano-composite ceramics by crack-healing*. Journal of the European Ceramic Society, 2007. 27(10): p. 3261-3267.
- [5] Ono, M., Nakao, W., Takahashi, K., Nakatani, M., and Ando, K., *A new methodology to guarantee the structural integrity of Al<sub>2</sub>O<sub>3</sub>/SiC composite using crack healing and a proof test*. Fatigue & Fracture of Engineering Materials & Structures, 2007. 30(7): p. 599-607.
- [6] Ando, K., Chu, M.C., Yao, F., and Sato, S., *Fatigue strength of crack-healed Si<sub>3</sub>N<sub>4</sub>/SiC composite ceramics*. Fatigue & Fracture of Engineering Materials & Structures, 1999. 22(10): p. 897-903.
- [7] Salas-Villaseñor, A.L., Lemus-Ruiz, J., Nanko, M., and D., M., *Crack disappearance by high-temperature oxidation of alumina toughened by Ni nanoparticles*. Advanced Materials Research, 2009. 68: p. 34-43.
- [8] Nakao, W. and Abe, S., *Enhancement of the self-healing ability in oxidation induced self-healing ceramic by modifying the healing agent*. Smart Mater. Struct. 21, 2012: p. 1-7.
- [9] Farle, A., Boatemaa, L., Shen, L., Gövert, S., Kok, J.B.W., Bosch, M., Yoshioka, S., van der Zwaag, S., and Sloof, W.G., *Demonstrating the self-healing behaviour of some selected ceramics under combustion chamber conditions*. Smart Materials and Structures, 2016. 25(8): p. 084019.



- [10] Lavrenko, V.A., Glebov, L.A., Pomitkin, A.P., Chuprina, V.G., and Protsenko, T.G., *High-temperature oxidation of titanium carbide in oxygen*. *Oxidation of Metals*, 1975. 9(2): p. 171-179.
- [11] Stewart, R.W. and Cutler, I.B., *Effect of temperature and oxygen partial pressure on the oxidation of titanium carbide*. *Journal of the American Ceramic Society*, 1967. 50(4): p. 176-181.
- [12] Shimada, S., *A thermoanalytical study of oxidation of TiC by simultaneous TGA-DTA-MS analysis*. *Journal of Material Science*, 1996. 31: p. 673-677.
- [13] Shimada, S. and Kozeki, M., *Oxidation of TiC at low temperatures*. *Journal of Materials Science*, 1992. 27(7): p. 1869-1875.
- [14] Favergeon, L., Morandini, J., Pijolat, M., and Soustelle, M., *A general approach for kinetic modeling of solid-gas reactions at reactor scale: application to kaolinite dehydroxylation*. *Oil Gas Sci. Technol. – Rev. IFP Energies nouvelles*, 2013. 68(6): p. 1039-1048.
- [15] Turkdogan, E.T., *Gas-solid reactions*, J. Szekeley, J. W. Evans and H. Y. Sohn, *Academic Press*, 1976. 400 pages. *AIChE Journal*, 1977. 23(4): p. 612-612.
- [16] Xu, Z., Sun, X., and Khaleel, M.A., *A generalized kinetic model for heterogeneous gas-solid reactions*. *The Journal of chemical physics*, 2012. 137(7): p. 074702.
- [17] Brown, E.M., *Introduction to thermal analysis: Techniques and applications*, Chapter 10. 2<sup>nd</sup> ed. 2001: Kluwer, Amsterdam.
- [18] Khawam, A. and Flanagan, D.R., *Solid-state kinetic models: basics and mathematical fundamentals*. *The Journal of Physical Chemistry B*, 2006. 110(35): p. 17315-17328.
- [19] Lyon, R.E., *An integration method of non-isothermal kinetic analysis*. 1997, Federal aviation administration: U.S. Department of transportation. p. 1996.
- [20] Senum, G.I. and Yang, R.T., *Rational approximations of the integral of the Arrhenius function*. *Journal of thermal analysis*, 1977. 11(3): p. 445-447.
- [21] Kissinger, H.E., *Reaction kinetics in differential thermal analysis*. *Analytical Chemistry*, 1957. 29(11): p. 1702-1706.
- [22] Kissinger, H.E., *Variation of peak temperature with heating rate in differential thermal analysis* *Journal of Research of the National Bureau of Standards* 1956 57(4): p. 217-221.

- [23] Gotor, F.J., Criado, J.M., Malek, J., and Koga, N., *Kinetic analysis of solid-state reactions: the universality of master plots for analyzing isothermal and nonisothermal experiments*. The Journal of Physical Chemistry A, 2000. 104(46): p. 10777-10782.
- [24] Sloof, W.G., Delhez, R., de Keijser, T.H., Schalkoord, D., Ramaekers, P.P.J., and Bastin, G.F., *Chemical constitution and microstructure of TiC x coatings chemically vapour deposited on Fe-C substrates; effects of iron and chromium*. Journal of Materials Science, 1988. 23(5): p. 1660-1672.
- [25] Voitovich, V.B., *Mechanism of the high temperature oxidation of titanium carbide, in high temperature materials and processes*. 1997. p. 243.
- [26] Kurlov, A.S. and Gusev, A.I., *Effect of particle size on the oxidation of WC powders during heating*. Inorganic Materials, 2011. 47(2): p. 133-138.
- [27] Quanli, J., Haijun, Z., Suping, L., and Xiaolin, J., *Effect of particle size on oxidation of silicon carbide powders*. Ceramics International, 2007. 33(2): p. 309-313.
- [28] Phuoc, T.X. and Chen, R.-H., *Modeling the effect of particle size on the activation energy and ignition temperature of metallic nanoparticles*. Combustion and Flame, 2012. 159(1): p. 416-419.
- [29] Fu, Q.-S., Xue, Y.-Q., Cui, Z.-X., and Wang, M.-F., *Study on the Size-Dependent Oxidation Reaction Kinetics of Nanosized Zinc Sulfide*. Journal of Nanomaterials, 2014. 2014: p. 8.
- [30] Hugosson, H.W., Eriksson, O., Jansson, U., Ruban, A.V., Souvatzis, P., and Abrikosov, I.A., *Surface energies and work functions of the transition metal carbides*. Surface Science, 2004. 557(1): p. 243-254.
- [31] Villars, P. and Cenzual, K., *Pearson's crystal data-crystal structure database for inorganic compounds*, in ASM International Materials Park. 2010.
- [32] Šesták, J., *Rationale and fallacy of thermoanalytical kinetic patterns*. Journal of Thermal Analysis and Calorimetry, 2011. 110(1): p. 5-16.
- [33] Zhang, W., Xue, Y., and Cui, Z., *Size-dependence of surface thermodynamic functions of nano-Cu by dissolution kinetics*. Colloids and Surfaces A: Physicochemical and Engineering Aspects, 2017. 533: p. 81-86.
- [34] Cui, Z., Duan, H., Xue, Y., and Li, P., *An investigation of the general regularity of size dependence of reaction kinetics of nanoparticles*. Journal of Nanoparticle Research, 2015. 17(5).

- [35] Fu, Q., Cui, Z., and Xue, Y., *Size dependence of the thermal decomposition kinetics of nano-  $\text{CaC}_2\text{O}_4$ : A theoretical and experimental study*. *European Physical Journal Plus*, 2015. 130(10).

# 4

## **Self-healing of Al<sub>2</sub>O<sub>3</sub> containing Ti microparticles**

---

This chapter is in press by Ceramics International. Authors: Boatemaa, L., van der Zwaag, S. and Sloof, W. G. [doi.org/10.1016/j.ceramint.2018.03.119](https://doi.org/10.1016/j.ceramint.2018.03.119)

*This work explores the possibility of using embedded micron-sized Ti particles to heal surface cracks in alumina and to unravel the evolution of the crack filling process in case of pure solid-state oxidation reactions. The oxidation kinetics of the Ti particles is studied and the results are applied in a simple model for crack-gap filling. An activation energy of 136 kJ/mol is determined for the oxidation of the Ti particles having an average particle size of 10  $\mu\text{m}$ . The almost fully dense alumina composite containing 10 vol. % Ti has an indentation fracture resistance of  $4.5 \pm 0.5 \text{ MPa m}^{1/2}$ . Crack healing in air is studied at 700, 800 and 900 °C for 0.5, 1, and 4 h and the strength recovered is measured by 4-point bending. The optimum healing condition for full strength recovery is 800 °C for 1 h or 900 °C for 15 min. Crack filling is observed to proceed in three steps i.e., local bonding at the site of an intersected Ti particle, lateral spreading of the oxide and global filling of the crack. It is discovered that, although significant strength recovery can be attained by local bonding of the intersected particles, full crack filling is required to prevent crack initiation from the damaged region upon reloading. The experimental results observed are in good agreement with the predictions of a simple discrete crack filling/healing model.*

## 4.1 Introduction

In recent years, material scientists have turned to the concept of ‘*damage management*’ rather than ‘*damage prevention*’ when re-designing engineering materials to make them more reliable for various applications [1]. This concept, also known as self-healing is based on the notion that the formation of damage is not problematic as long as it is autonomously and timely healed or repaired in-situ as this would ensure the continued safe operation of the component or part.

In the original field-defining studies on self-healing materials, polymeric matrices were healed by incorporating capsules containing a liquid healing agent and a catalyst within the matrix [2]. As a crack propagates through the matrix, the microcapsules are ruptured and the catalyst particles are exposed, the healing agent flows into the crack and polymerizes once it gets into contact with one of the catalyst particles. The structural integrity across the crack plane is re-instated by the (solid) polymerized healing agent [3]. This type of healing is now categorized as extrinsic healing because healing is achieved by the addition of discrete foreign entities (i.e., the healing agent and the catalyst) to the (polymeric) matrix. It is also classified as autonomous healing as no additional trigger such as the supply of heat [4] is necessary to initiate the polymerization reaction leading to healing, i.e. the healing conditions in particular the temperature are the same as those during cracking (with the exception of the load responsible for the cracking having been removed).

In later years, ceramic oxides composites such as  $\text{Al}_2\text{O}_3$ ,  $\text{ZrO}_2$  and mullite filled with discrete solid healing particles prone to undergo oxidative expansive decomposition have also been studied as promising autonomous self-healing systems for high temperature applications [5-10]. Although the initial damage is generally introduced at room temperature, healing is realized by exposure to the intended use conditions, i.e. an oxygen-containing atmosphere heated to a suitably high temperature [4, 11]. At such high temperatures, an oxidation reaction is initiated and the crack is filled with the reaction products. In case the oxide adheres well to the crack faces and the degree of filling is high enough, the load-bearing capacity of the composite is restored.

In an earlier study [12], 6 physical and chemical criteria were used to identify suitable healing particles to be used in the creation of high-temperature self-healing alumina composites. Experimentally the approach has been found to work well for alumina composites containing either 15 or 20 vol. % TiC [13] or SiC [8, 10] particles, in agreement with the predictions of the selection model. Although that selection study did identify the alumina-Ti as a potentially attractive self-healing system such composite material have not been made and tested yet. Cracks in alumina containing Ti healing particles should under the same conditions (temperature and time) heal faster than composites containing TiC as the oxidation of Ti leads to a larger volume expansion for an equal amount of Ti atoms [12]. And while not so relevant for the self-healing behaviour, the inclusion of ductile metallic particles in a brittle ceramic matrix may be beneficial from a mechanical properties perspective [14]. In addition, dilute  $\text{Al}_2\text{O}_3$ -Ti composites retain their low coefficient of thermal expansion (CTE) and have a relatively high strength to weight ratio [15].

This work, therefore, investigates the high-temperature healing behaviour of an  $\text{Al}_2\text{O}_3$  composite containing 10 vol. % Ti particles with an average size of 10  $\mu\text{m}$ . The activation energy for and the temperature window available for self-healing are studied through thermal analysis of the oxidation kinetics of the Ti particles. Another very important and unique aspect of this work is the determination of the evolution of the crack filling and the semi-quantitative description of how the solid-state formation of  $\text{TiO}_2$  leads to re-bonding of the cracked surfaces and restores the load-bearing capacity of the composite. For  $\text{Al}_2\text{O}_3$  self-healing composites containing SiC, the healing agent formed (i.e.,  $\text{SiO}_2$ ) is amorphous during the early stages of the high-temperature oxidation process [16, 17] and the amorphous character generates a viscous behaviour leading to liquid-like spreading of the reaction product into the crack. The ability of solid  $\text{TiO}_2$  to ‘spread’ into the crack gap and filling it as well as bond with the crack faces is of equal interest but has not been documented yet. Finally, the experimental observations on crack healing are compared to a simple model to predict the filling fraction as a function of time, temperature and original structure of the  $\text{Al}_2\text{O}_3$ -Ti composite.

## 4.2 Crack gap filling model

Consider a ceramic composite with randomly distributed spherical healing particles; see **Figure 4.1**. When fracture occurs, a planar crack of uniform width  $w$  is assumed to intersect the dispersed particles and at the appropriate temperature the intersected Ti particles oxidize into an oxide. The specific volume increase  $\phi$  per particle due to oxidation is given by:

$$\phi = \frac{V_{ox} - V_p}{V_p} \quad (4.1)$$

Where  $V_{ox}$  and  $V_p$  are the molar volumes of the oxide (healing oxide) and the particle (healing particle) respectively. Now consider a representative unit volume  $V_u$  of the self-healing composite containing evenly distributed spherical particles (each of diameter  $d$ ) which is crossed by a plane  $a$  of area  $A_u$  as **Figure 4.1** (the particles intersected by the plane are marked with a cross).

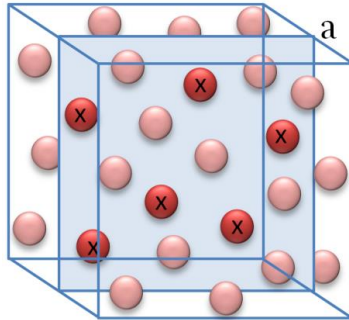


*Figure 4.1: A representative unit volume of a ceramic matrix composite containing randomly distributed spherical healing particles with plane 'a' intersecting the volume element.*

If  $p$  is the probability that a planar crack crosses a healing particle, then:

$$p = d \frac{A_u}{V_u}, \text{ with } A_u = V_u^{2/3} \text{ implies } p = \frac{d}{V_u^{1/3}} \quad (4.2)$$



This implies that the number of healing particles  $n_p$  exposed to the crack is:

$$n_p = \rho N_p \text{ with } N_p = \frac{\phi V_u}{V_p}, \text{ and } V_p = \frac{\pi d^3}{6} \quad (4.3)$$

$N_p$  is the total number of spherical capsules present inside the unit volume element and  $\phi$  is the volume fraction of healing particles added to  $V_u$ , then:

$$n_p = \frac{d}{V_u^{1/3}} \frac{6\phi V_u}{\pi d^3} = \frac{6\phi V_u^{2/3}}{\pi d^2} \quad (4.4)$$

Next, the volume of oxide filling the crack is:

$$V_f = \alpha_p \phi n_p V_p = \alpha \phi \phi d V^{2/3} \quad (4.5)$$

where  $\alpha_p$  is the fraction of the particle converted into the oxide. The volume of the gap with a width  $w$  to be filled is defined as:

$$V_g = w A_u = w V_u^{2/3} \quad (4.6)$$

Let  $\psi$  be the fraction of the crack gap filled, i.e.:

$$\psi = \frac{V_f}{V_g} \quad (4.7)$$

Eq. (4.7) can be rewritten in terms of Eqs (4.5) and (4.6) as:

$$\psi = \frac{\alpha_p \phi \phi d}{w} \quad (4.8)$$

A first order estimate of the early stages of crack filling can be made if all parameters in Eq. (4.8) are known. The volume expansion  $\phi$ , the volume fraction healing particles  $\phi$  and their size  $d$  are input parameters and are known up front, while the crack gap width  $w$ , on the other hand, can be chosen or measured once the damage is introduced into the material. Please note that in this simple model the filling fraction can be larger than 1 for small crack widths as the oxidation continues even

when the crack is fully filled. The conversion of the healing particle into the healing oxide represented by  $\alpha_p$  depends on (absolute) temperature and time:

$$\alpha_p = \alpha_p(T, t) \quad (4.9)$$

which is related to the oxidation of the healing particles.

### 4.2.1 Oxidation kinetics of the healing particles

The rate of a solid-state isothermal reaction can be expressed by the following general equation:

$$\frac{d\alpha}{dt} = A e^{\left(\frac{-E_A}{RT}\right)} f(\alpha) \quad (4.10)$$

where  $\alpha$  is the fraction converted at any time  $t$ . In case of an oxidation reaction it can be defined as:  $\alpha = (m_t - m_0)/(m_\infty - m_0)$ , in which  $m_0$ ,  $m_t$  and  $m_\infty$  denote the mass at time  $t$  is 0,  $t$  and  $\infty$ ,  $f(\alpha)$  is a differential form of the reaction model,  $E_A$  is the activation energy,  $A$  is the pre-exponential (frequency) factor of the Arrhenius relation, and  $T$  the absolute temperature [18]. Separating variables and integrating Eq. (4.10) gives the integral form of the isothermal rate law:

$$g(\alpha) = kt \quad (4.11)$$

$$\text{where } g(\alpha) = \int_0^\alpha \frac{d(\alpha)}{f(\alpha)} \quad (4.12)$$

$$\text{and } k = A e^{\left(\frac{-E_A}{RT}\right)} \quad (4.13)$$

$g(\alpha)$  is the integral reaction model and  $k$  is the rate constant. There are several reaction models which are classified based on the shape of their isothermal curves [19]. When the appropriate model for the reaction is identified, the conventional isothermal model-fitting method can be employed to determine the activation energy  $E_A$  and frequency factor  $A$ . This method involves two fits: the first determines

the rate constant  $k$  of the reaction at each temperature according to **Eq. (4.11)** and the second determines the Arrhenius constant  $A$  and the  $E_A$  from **Eq. (4.13)**. Then, an expression for  $\alpha$  can be written.

## 4.2.2 Reaction model

To determine the appropriate model to analyze the experimental data the so-called ‘master curve plotting’ method is employed. This method is based on the concept of generalized time  $\theta$ [18], which is defined for an isothermal reaction as:

$$\theta = \int_0^t e^{\left(\frac{-E_A}{RT}\right)} dt \quad \text{or} \quad \frac{d\theta}{dt} = e^{\left(\frac{-E_A}{RT}\right)} \quad (4.14)$$

$\theta$  denotes the reaction time taken to attain a particular fraction converted at infinite temperature. Now, **Eqs (4.10)** and **(4.14)** can be rewritten in terms of generalized time respectively as:

$$\frac{d\alpha}{d\theta} = Af(\alpha) \quad (4.15)$$

$$g(\alpha) = A\theta \quad (4.16)$$

As a reference point for the master-curve plotting analysis generally, the level  $\alpha=0.5$  is chosen and using **Eq. (4.15)** it can be derived that:

$$\frac{d\alpha/d\theta}{(d\alpha/d\theta)_{\alpha=0.5}} = \frac{f(\alpha)}{f(0.5)} \quad (4.17)$$

From the experimentally determined conversion rate, with respect to the generalized time, as a function of fraction converted,  $f(\alpha)/f(0.5)$  versus  $\alpha$  can be obtained, since:

$$\frac{d\alpha}{d\theta} = \frac{d\alpha}{dt} \exp\left(\frac{E_A}{RT}\right) \quad \text{OR} \quad \frac{d\alpha}{d\theta} = \beta \frac{d\alpha}{dT} \exp\left(\frac{E_A}{RT}\right) \quad (4.18)$$

Therefore, Eq. (4.17) becomes:

$$\frac{d\alpha/d\theta}{(d\alpha/d\theta)_{\alpha=0.5}} = \frac{d\alpha/dt}{(d\alpha/dt)_{0.5}} \frac{\exp(E_A/RT)}{\exp(E_A/RT)} \quad (4.19)$$

For the experimental kinetic data under isothermal conditions, the exponential terms in Eq. (4.19) cancel out since  $T_t = T_{0.5}$ . By comparing the experimental result with theoretical reaction models [18], the reaction model that best fits the measured data can be determined.

### 4.2.3 Activation energy and Arrhenius constant

The activation energy is evaluated from the slope of the plot of  $\ln k$  vs  $1/T$  using the Arrhenius relation defined by Eq. (4.13) and the intercept gives the Arrhenius constant A. First, the rate constants are evaluated at each temperature from the linear relation between the integral form of the identified reaction model and time, given by Eq. (4.11).

## 4.3 Experimental procedure

The starting materials were commercially available alumina powder (AKP-50, Sumitomo Chemical Co., Ltd, Tokyo, Japan) with an average particle size of 0.2  $\mu\text{m}$  and Ti powder (PN: TI-M-02M-MP.05UMS, American elements, USA) with an average particle size of 10  $\mu\text{m}$ . The purity of the alumina and Ti powder is 99.99 % and 99.45 %, respectively. The size distribution of the powders was measured by laser diffraction using a Microtrac 3500 (Microtrac Inc., USA). The particle size of the Ti powder was found to range from 4 to 15  $\mu\text{m}$  with an average size of 10  $\mu\text{m}$ .

The phase purity and composition of the Ti powder was analyzed by X-ray diffraction (XRD) using a Bruker D8 Advance diffractometer (Bruker, Germany) with a graphite monochromator and Co K $\alpha$  radiation. The diffractograms were processed with the accompanying software Diffrac.EVA 4.1 from Bruker. The shape of the Ti particles and the microstructure of the composite were observed with scanning electron microscopy (SEM) using a JSM 6500FD (JEOL, Japan). After healing the extent of filling was observed with SEM and the reaction products were analyzed by X-ray microanalysis (XMA) using the energy dispersive spectrometer (EDS) attached to the scanning electron microscope. This EDS is an Ultra Dry detector (30 mm<sup>2</sup>) operated with Noran System Seven software package (ThermoFisher, USA) for data acquisition and analysis.

The oxidation kinetics of the Ti particles was studied isothermally over the temperature range from 600 to 850 °C (with increments of 50 °C) by thermogravimetric analysis (TGA) using the Setsys Evolution 16 simultaneous thermal analyzer (Setaram, France). 20 $\pm$ 1 mg of the Ti powder was put into an Al<sub>2</sub>O<sub>3</sub> crucible (100  $\mu$ L) and the furnace was heated up from room temperature at 5 °C/min under pure N<sub>2</sub> (with H<sub>2</sub>O < 10 ppm) supplied at 50 sccm, when the desired temperature was reached the flow of N<sub>2</sub> was reduced by 20 vol. % and replaced by O<sub>2</sub> thereby generating synthetic air in the furnace. The mass change curves were corrected using blank measurements under similar conditions.

A composite of Al<sub>2</sub>O<sub>3</sub> containing 10 vol. % of Ti was prepared by first mixing the powders. To avoid agglomeration of the Ti particles an alkali-free organic polyelectrolyte Dolapix CE64 (Zschimmer & Schwarz, Germany) was added as a surfactant [20]. This aided in the homogenous distribution of the healing particles; see **Figure 4.2a**. in the absence of the polyelectrolyte, the Ti particles remained stuck to each other as shown in **Figure 4.2b**.

The powders were mixed using distilled water as the liquid media. The mass fractions as used for mixing were 50 % of powders, 45 % of distilled water and 5 % of the surfactant. Mixing was done using zirconia balls (of diameters 5 and 10 mm) in a planetary ball mill PM 100 (Retsch, Germany), the powder to ball mass ratio was 2:1. The suspension was mixed for 6 h at 150 rpm with an on-and-off period of 20:10 min. The slurry was left to dry overnight at 90 °C for 16 h. Then the cake was ground and passed through 200, 120 and 50  $\mu$ m sieves before sintering in a spark

plasma sintering (SPS) furnace. The evenly mixed powder was packed into a 40 mm graphite mold and heated at 20 °C/min up to 1400 °C and held for 10 min. in argon under 50 MPa for SPS in an HPD 25 SD furnace (FCT Systeme, Germany). After sintering the system was cooled naturally after lifting up the pistons. The density of the composite was measured by the Archimedes method using an analytical balance (Mettler Toledo AG-204, Switzerland) according to ASTM B 311-93.

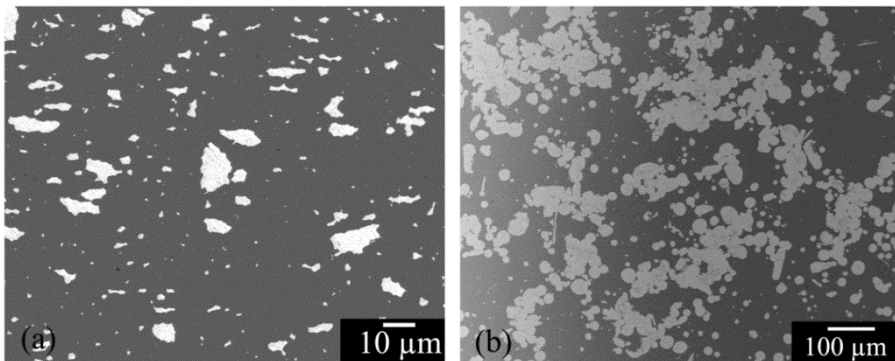


*Figure 4.2: Microstructure of the  $Al_2O_3$ -Ti composite showing the distribution of Ti (white phase) in alumina produced with (a) and without (b) adding the surfactant Dolapix.*

To study the strength recovery, the sintered composite discs were machined to 3.0 x 4.0 x 26.0 mm rectangular bars with beveled edges. The surfaces of the bars were polished to a mirror finish with 1 μm diamond suspension. Cracks were introduced at the centre of the bar by means of Vickers' indentation using a Zwick/Z2.5 hardness tester (Zwick, Germany) operated in force controlled mode of 5 N/s with a maximum load of 20 N held for 20 s at load. The cracks formed were parallel and perpendicular to the long axis of the sample.

The indentation fracture resistance of the composite was measured by making several indents at 10, 20, 50 and 100 N. The indent size  $2a$  and the crack length  $2c$  defined respectively as the average of the diagonals of the imprint made by the indent and the average of the horizontal and vertical cracks formed in addition to the indent size was measured at the various loads. The length of cracks generated was then used in calculating the composite's fracture toughness. Annealing of the

cracked samples to induce partial or full filling of the indentation cracks was carried out in a Carbolite TZF 17/600 furnace (Carbolite Gero, UK) at 700, 800 and 900 °C for 0.5, 1, and 4 h filled with natural air. The strength recovered was measured by 4-point bending tests which were performed at room temperature on a self-aligning stage [13]. This stage has a 20/10 mm span with hardened steel rollers 2 mm diameter. The stage was mounted to an Instron 5500R (Instron Corporation, USA) material testing frame with a 10 kN load cell. The cross-head was displaced at a velocity of 0.5 mm/min and the bar specimen was placed so that its centre coincides with the middle of the spans.

## 4.4 Results

### 4.4.1 Kinetics of Ti oxidation

The oxidation kinetics of the Ti particles between 600 and 850 °C was determined from the mass gain measured (cf. Section 4.2.1) and the results are presented in **Figure 4.3**. The oxidation kinetics of the collection of Ti particles between 600 to 900 °C is diffusion controlled as mentioned in [21], and the rate is mainly governed by dissolution of oxygen in the metal.

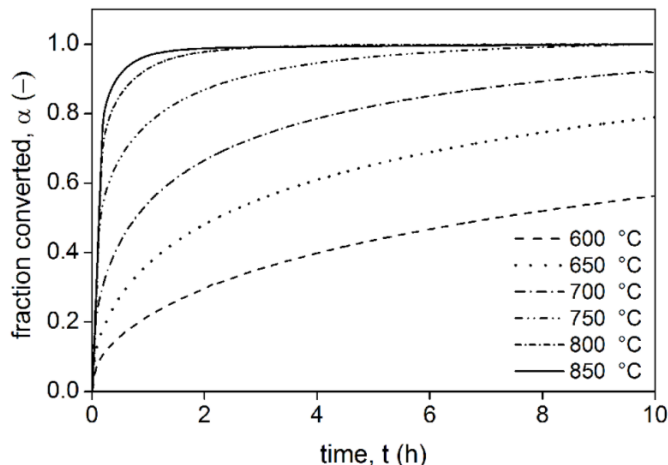


*Figure 4.3: Fraction of Ti powder converted to  $TiO_2$ ,  $\alpha$ , in dry synthetic air as a function of time for different annealing temperatures.*

The oxidation rate decreases with time due to the increasing thickness of the oxide shell which acts as a strong diffusion barrier, see **Figure 4.3.** At the applied temperatures, according to the XRD data only rutile ( $\text{TiO}_2$ ) formed. Other phases such as;  $\text{Ti}_2\text{O}$ ,  $\text{TiO}$  and  $\text{Ti}_3\text{O}_5$  only form at higher temperatures and low oxygen partial pressure levels [21]. From **Figure 4.3** and [19], it is clear that the oxidation of Ti follows a deceleratory model and the master plotting method, see **Figure 4.4** confirms that the reaction best conforms to a D3 diffusion model.

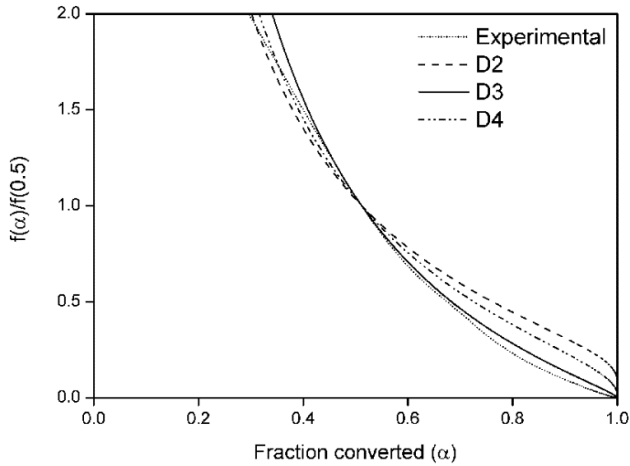


**Figure 4.4:** Master plot of theoretical models and experimental data of Ti oxidation.

The integral form of the D3 diffusion model is given by:

$$g(\alpha) = \left(1 - (1 - \alpha)^{1/3}\right) \quad (4.20)$$

Although Ginstling-Brounshtein [22] have shown that this equation is invalid for higher conversion fractions or longer reaction times, it can be used as a first order approximation for lower conversion fractions yielding with **Eq. (4.11)**:

$$\alpha = 1 - \left(1 - \sqrt{kt}\right)^3 \quad (4.21)$$

A linear fitting of the fraction converted at each temperature according to **Eq. (4.11)**, using the D3 model yielded the various  $k$  values presented in **Table 4.1**



Table 4.1: Rate constant  $k$  values found from linear fitting of Eq. (4.11) at different temperatures.

T (°C)	k (s <sup>-1</sup> )
600	0.0058
650	0.0162
700	0.0313
750	0.0722
800	0.2212
850	0.2968

The activation energy is determined from the slope of the plot in **Figure 4.5**. It is evaluated to be  $137 \pm 9$  kJ/mol. The lower value in comparison to that of bulk Ti (213 kJ/mol [23]) may be due to the much larger density of surface defects of the particles. This difference in activation energy cannot be explained by the variation of surface bonding states due to surface curvature constraints, since the particles are of micron rather than nano size [24].

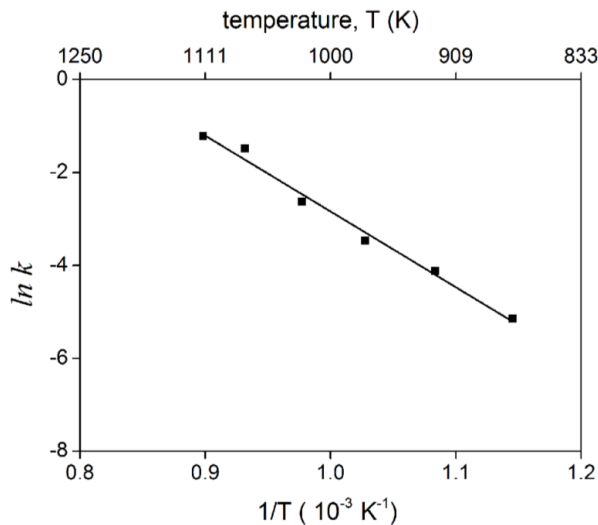
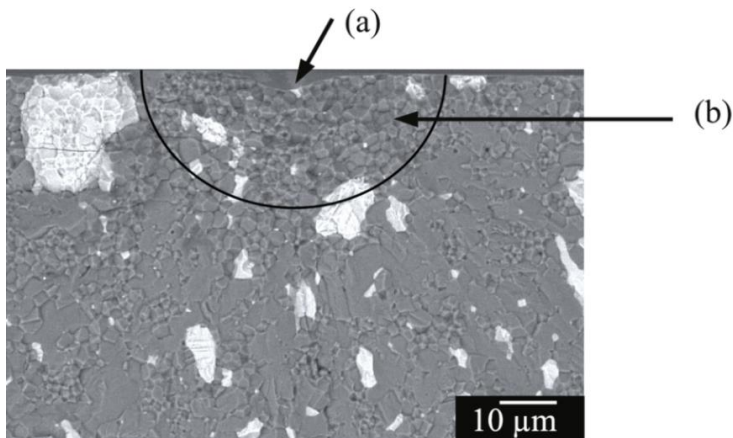


Figure 4.5: Arrhenius plot of  $\ln k$  vs  $1/T$  to determine the activation energy for oxidation of  $10 \mu\text{m}$  sized Ti powder.

#### 4.4.2 Mechanical properties of the $\text{Al}_2\text{O}_3$ -Ti composite

The sintered samples were very dense with densities between 97.7 - 99.2 % of the calculated theoretical density. A cross-sectional view of the indented surface shows that the 20 N load generated cracks had a half-penny shaped geometry of about 20  $\mu\text{m}$  in radius, see **Figure 4.6**. This is a common morphology for Vickers indentation induced cracks [25] and hence the indentation fracture resistance of the composite was evaluated according to [26].



*Figure 4.6: Cross section of indented surface: (a) Marks the imprint of the indent and (b) The half-penny crack.*

For composite materials containing well dispersed particles, cracks propagate through either the matrix, along the interface or through the particles, depending on which path is energetically most favourable. The lower modulus of Ti (110 GPa [27]) with respect to  $\text{Al}_2\text{O}_3$  (380 - 410 GPa [28]) leads to the crack being attracted to the Ti particles [29], rendering it the preferred crack path as shown in **Figure 4.7**.

The indentation fracture resistance of the composite is evaluated by making several cracks by Vickers indentation at different loads (i.e., at 10, 20, 50 and 100 N). From the indent size  $2a$  and crack length  $2c$ , the indentation fracture resistance of  $\text{Al}_2\text{O}_3$  containing 10 vol. % of Ti particles of average size 10  $\mu\text{m}$  is evaluated to be  $4.5 \pm 0.5 \text{ MPa m}^{1/2}$ . This compares well with the fracture toughness as measured for  $\text{Al}_2\text{O}_3$

composites containing either 20 vol. % TiC [13] or 20 vol. %  $\text{Ti}_2\text{AlC}$  [30],  $4.3 \pm 0.1 \text{ MPa m}^{1/2}$  and  $4.9 \pm 0.5 \text{ MPa m}^{1/2}$  respectively.

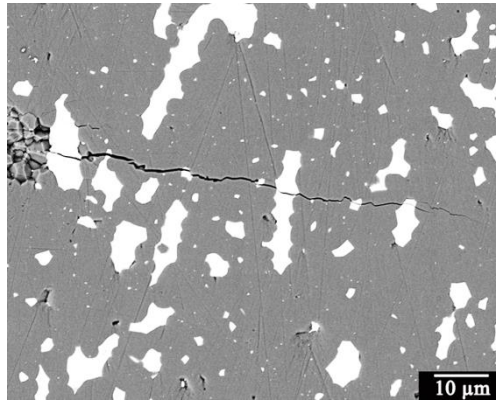


*Figure 4.7: Crack particle interaction showing cracks running through the softer Ti phase. Grey area is alumina and the white patches are Ti particles.*

### 4.4.3 Evolution of crack filling

To prove that Ti particles embedded in  $\text{Al}_2\text{O}_3$  can heal surface cracks, a crack of length  $2c$  about  $100 \mu\text{m}$  was made and healed at  $800^\circ\text{C}$  for 4 h.

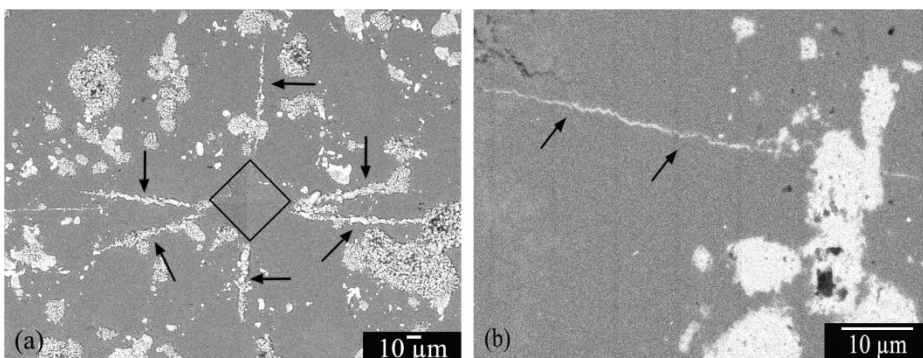


*Figure 4.8: Grey area is  $\text{Al}_2\text{O}_3$  and white area is  $\text{TiO}_2$ . (a) All cracks are fully filled with  $\text{TiO}_2$  indicated by arrows. (b) Surface oxide removed to show full filling of a crack of about  $50 \mu\text{m}$  in length. Arrows indicate a fully filled crack without Ti particles on the crack path.*

After healing, the cracks emerging from the corners of the Vickers indent were observed using SEM to be fully covered with a light coloured material confirmed by X-ray microanalysis to be  $\text{TiO}_2$ ; see **Figure 4.8a**. After removal of the surface oxides by gentle polishing, the whole length of the crack was found to be filled with  $\text{TiO}_2$  even though Ti particles were not identified everywhere along the length of the crack; see **Figure 4.8b**.

The evolution of the crack-gap filling process was investigated by annealing a sample with several indents at a fixed temperature of 700 °C for different times and observing the extent of filling after every annealing exposure. The healing temperature was selected at 700 °C as the kinetics at this temperature is relatively slow. The microscopic images for two different areas taken after 1, 2, 4 and 6 h of exposure are presented in **Figure 4.9** and **4.10**. From the observations it is concluded that the crack filling proceeds in 3 successive steps:

In the first step, 'hairy' oxides grow on crack-intersected particles. These hairy oxides on opposite sides of the crack grow into each other (i.e., intertwine) leading to the local bonding of the healing particle, see **Figure 4.9** b and c. This step is hereafter referred to as the local bonding step.

In the second step, the oxides from the intersected particles grow laterally into the crack, see **Figure 4.10**b, and c, but can still be clearly connected to the particle from which they stem. This second step is called the lateral spreading step. Finally, there are areas along the crack with no intersected particles, yet oxides are seen filling and sprouting out of the cracks; see **Figure 4.9** and **4.10**d and e. This results from oxidation of particles that are exposed in the depth of the crack. This step is called the global filling step. Local bonding and lateral spreading are thought to occur consecutively; however, global filling occurs simultaneously with steps 1 and 2, provided enough oxygen reaches the intersected Ti particles further below the surface.

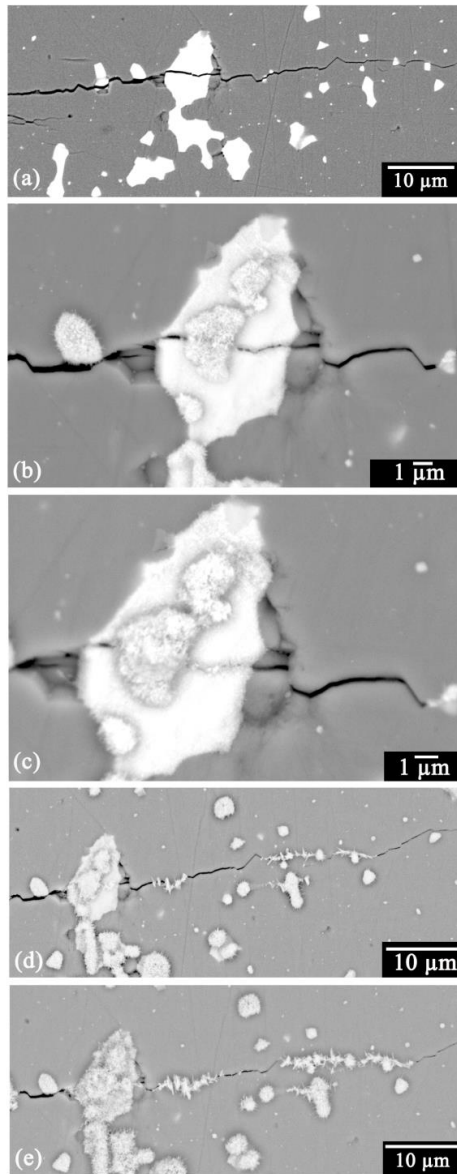


*Figure 4.9: Evolution of crack-gap filling of the  $\text{Al}_2\text{O}_3$  containing 10 vol. % of Ti by oxidation in air at 700 °C for different times. (a) Starting material, (b) Annealed after 1 h, (c) 2 h, (c) 4 h, and (e) 6 h.*

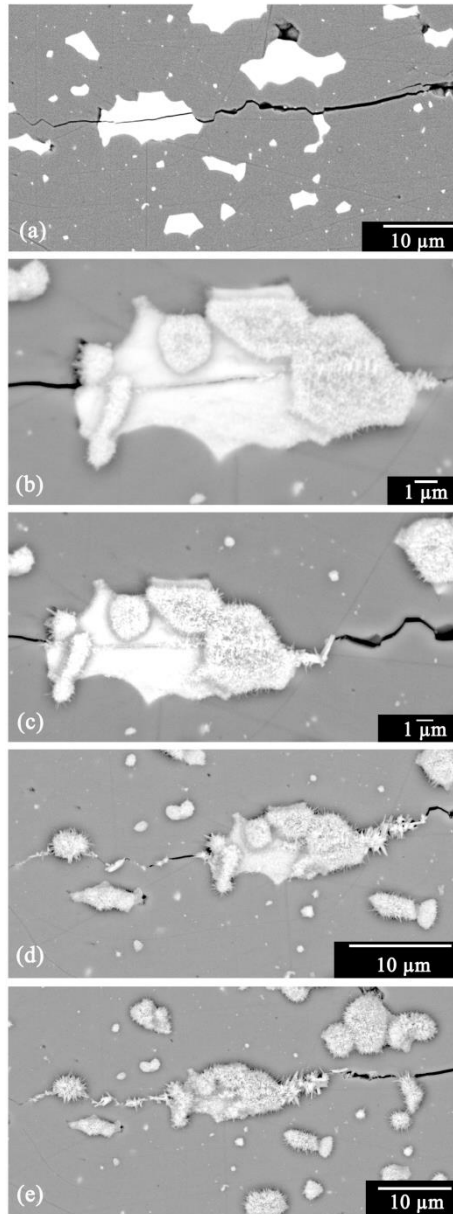
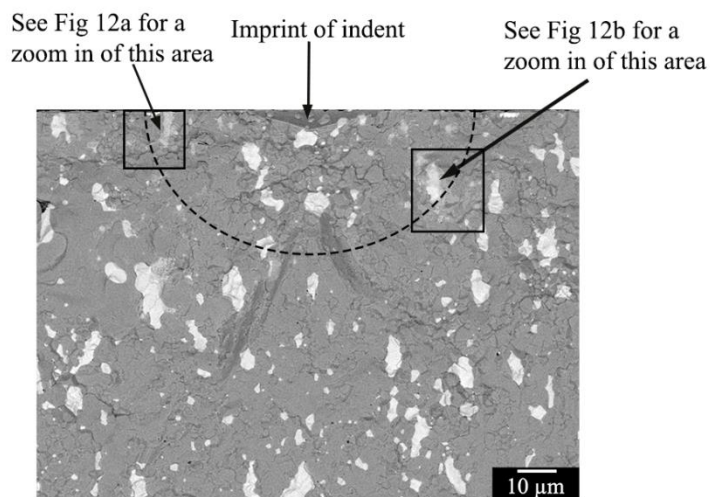


Figure 4.10: Evolution of crack-gap of crack-gap filling of another area of the same sample as in Figure 4.9. (a) Starting material, (b) Annealed after 1 h, (c) 2 h, (d) 4 h, and (e) 6 h.

The *spreading or flowing* mechanism was studied in more detail by SEM recordings of cross-sections of a sample fractured after healing and by the stepwise planar removal of material from a partially healed sample.

For the cross-sectional analysis, the sample was healed at 800 °C for 30 min. and fractured. The crack was not fully filled and so acted as a crack initiator causing the sample to break into 2 equal halves along the path of the indent. A cross section of the fractured surface showing the semi-circular crack front and the imprint of the indent is shown in **Figure 4.11**.



*Figure 4.11: Side view of a partially healed indentation induced crack after sample fracturing (see text).*

A zoom-in of two areas on the crack plane of **Figure 4.11**, is presented in **Figure 4.12**. Three different phases associated with the matrix (darker grey), healing particle (white) and healing oxide (lighter grey), respectively, can be distinguished in both micrographs.

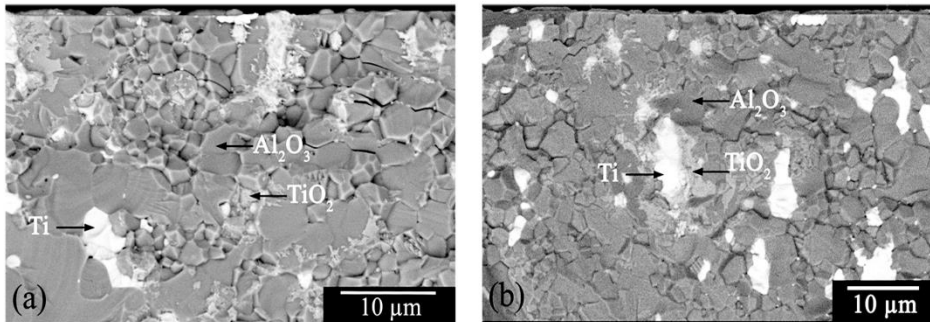


*Figure 4.12: SEM images of two different areas of the crack plane of a sample oxidized at 800 °C for 30 min. showing the matrix, healing particle and the healing oxide that has spread onto the crack plane.*

Next, X-ray mapping of **Figure 4.12b** is performed to affirm the presence of TiO<sub>2</sub> (healing oxide) on the crack surface and the results are presented below in **Figure 4.13**. In **Figure 4.13b**, oxygen is identified over the whole surface except for the Ti particles (in white). Ti is identified and mapped in blue over a larger area in **Figure 4.13c**, (in the bigger ellipse) an area larger than where only Ti was detected in **Figure 4.13b**. The overlap of Ti and O within the larger ellipse indicates the presence of TiO<sub>2</sub> on the crack surface. This is a clear evidence of crack filling by a particle in the plane of the crack. With time TiO<sub>2</sub> continues to form from such particles in the crack plane, the oxides spread over the crack surface and fill the crack outwards contributing to global filling as depicted in **Figure 4.9** and **4.10** (d and e).



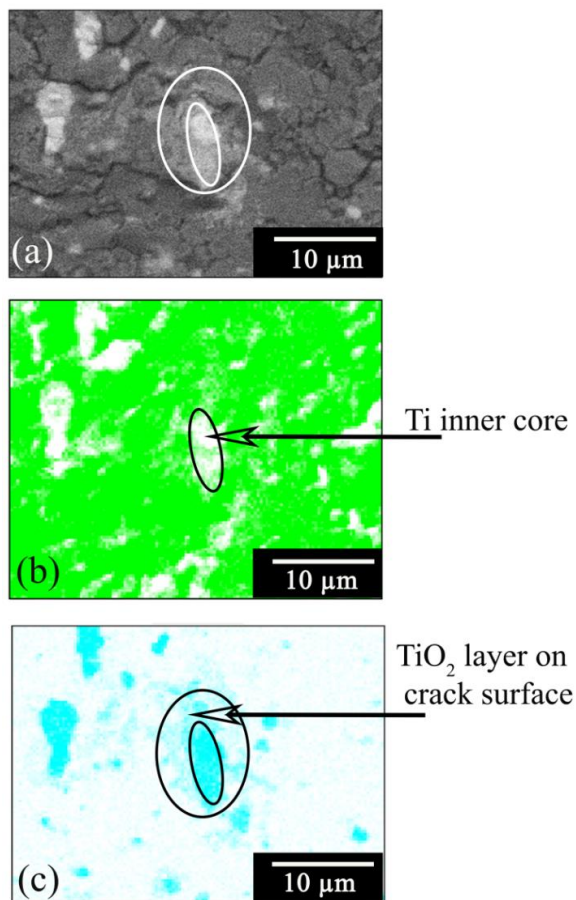


*Figure 4.13: (a) SEM image of a crack plane after annealing at 800 °C for 30 min. in air, (b) O  $k\alpha$  X-ray map and (c) Ti  $k\alpha$  X-ray map of the same area.*

Next, looking at the stepwise planar removal of material (parallel to the original sample surface) of an untested but partially healed sample which was annealed at 800 °C for 1 h to observe crack filling as a function of the depth of the crack. The results from two different cracks are presented in **Figure 4.14** and **4.15**. A crack about 40 μm long that is fully filled with lots of surface oxides is presented in **Figure 4.14a**. The surface oxides are removed in **Figure 4.14b** to clearly show the fully filled crack intersection with the original sample surface. Ti particles, which directly contribute to crack filling (by local bonding and lateral spreading), are observed along the crack path at point M, N and O. However, at point P no Ti particle is identified, although the crack in this area is fully filled.

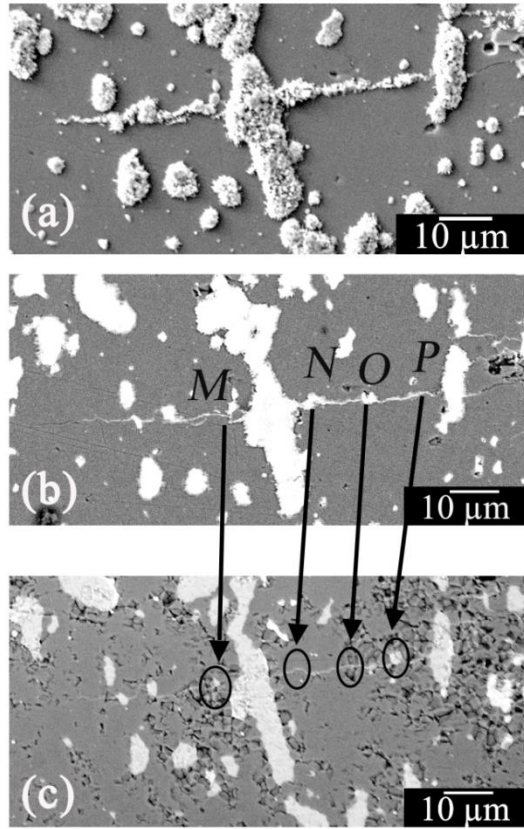


*Figure 4.14: SEM images after annealing at 800 °C for 1 h in air. (a) Fully filled crack with surface oxides. (b) Crack filling after removal of surface oxides. (c) After removal of about 3 μm thick material, particles at point M diminish, while that at N and O disappear, new particle which contributes to healing is identified at point P.*

About 3 μm of surface material was removed by gentle polishing and the new surface observations are given in **Figure 4.14c**. At this depth, part of the particle at point M still remains and the crack is filled in this area. In contrast, the particles at points N and O are no longer present, yet, the crack at these areas is still fully filled. A new particle is now intersected by the crack at point P.

Evidence presented in **Figure 4.12** suggests that global filling takes place 3 μm from the surface at point P, the oxide formed from this particle spread into the crack outwards to the surface as in **Figure 4.14b**. Particles at point N and O may have also

spread downwards into the crack and/or there may still be a particle buried deep in the crack which fills the crack upward.

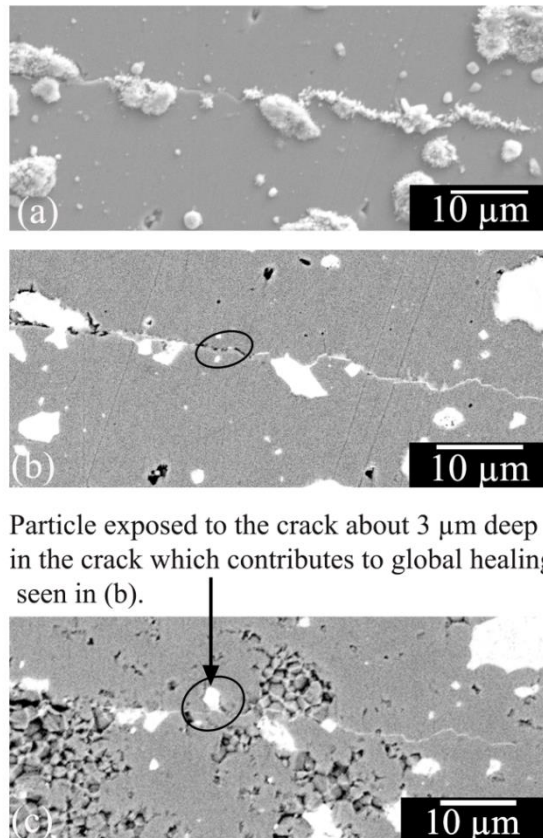


*Figure 4.15: SEM images after annealing at 800 °C for 1 h in air. (a) Filled crack with surface oxides. (b) Crack not fully filled after removal of surface oxides. (c) Particle exposed to the crack 3 μm in the depth of the crack which oxidizes and spreads into the crack contributing to global filling.*

Similarly, **Figure 4.15a** shows a partially filled crack with surface oxides. After removal of the surface oxides in **Figure 4.15b**, the area in the ellipse is not filled, although, oxides can be seen in the crack. After removal of about 3 μm thick material in **Figure 4.15c**, the crack in the ellipse is filled with oxides from a particle exposed to the crack at this depth. This clearly illustrates global filling by a particle

buried in the depth of the crack, which given enough time would have continued to fill the whole crack.

Figure 4.9 and 4.10 have clearly illustrated the local bonding and lateral spreading stages of crack filling, while Figure 4.12 to 4.15 prove the concept of global filling as particles identified along the crack path in the depth of the material significantly contribute to crack filling closer to the surface.

#### 4.4.4 Strength-recovery

The pre-cracked samples were healed at 700, 800 and 900 °C for 0.25, 0.50, 1, 2 and 4 h, and the results of the post-healing fracture strength measurements are presented in Figure 4.16.

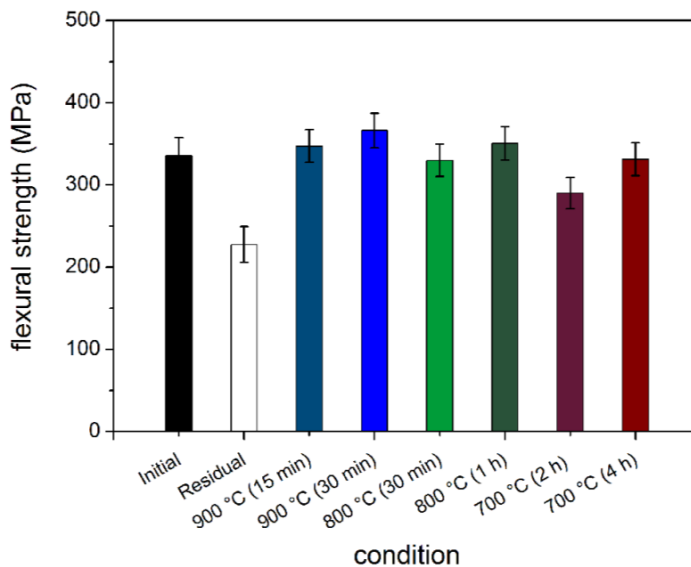


Figure 4.16: Room temperature flexural strength values of the  $Al_2O_3$ -Ti composites before, after indentation damage and after healing at the indicated temperature-time combinations.

The original and the non-healed strength values are also included; each value plotted is the average of 8 samples tested per condition. The strength of the intact specimen was  $335 \pm 23$  MPa and after indentation at 20 N a crack of length  $c$  of 35  $\mu$ m was generated which decreased the initial strength by 32 % to  $228 \pm 22$  MPa. In the reference  $Al_2O_3$ -TiC composite [13] a bending strength decrease of about 50 %

has been reported for indentation at 20 N, confirming that the current  $\text{Al}_2\text{O}_3$ -Ti composite is relatively ductile as expected.

As shown in **Figure 4.16**, the flexural strength was fully recovered after healing at 700 °C for 4 h, 800 °C for 1 h and at 900 °C for 30 min. with average flexural strengths of 331, 350 and 360 MPa, respectively. The average bending strength values after extensive healing were found to be slightly higher than that of the original samples. This may have resulted from the filling of surrounding pores left behind after sintering. The period for the first set of healing experiments was reduced by half to find an optimum healing condition (lowest temperature and shortest time) at which full strength can be recovered. At 800 and 900 °C for 30 and 15 min., respectively, full strength was recovered at 329 and 347 MPa, respectively. However, at 700 °C for 2 h only 88 % of the initial strength was recovered. The optimum healing condition for the studied composite is 800 °C for 1 h or 900 °C for 15 min.

Further analysis of the failure behaviour of samples after healing revealed that all samples kept at 800 °C for 1 h and at 900 °C for 15 and 30 min. broke at positions not connected with those of the (healed) indentation induced cracks. For those three conditions, the cracks observed were fully filled. For conditions at which the cracks were recorded to be only partially filled (such as after healing at 800 °C for 30 min.), it was observed that the crack plane was not fully covered with the healing oxide, see **Figure 4.12**, however, local bonding and lateral spreading had occurred. The (room temperature) failure load was higher than after the indentation, but sample failure still took place at the sample centre (where the indent was made). Similarly, after healing at 700 °C for 2 h, cracks were partially filled with oxides from local bonding and lateral spreading with most of the samples failing along the centre. At this condition, **Figure 4.9c** and **10c** clearly depicts that there was no global filling.

Finally, although cracks were not fully filled after 4 h at 700 °C, substantial global filling had taken place (see, **Figure 4.9d** and **4.10d**) leading to only 20 % of the samples breaking along the centre. It can therefore be concluded that local bonding, which leads to bridging of the crack, significantly increases the residual strength, however, global filling is vital in obtaining a strong healed zone.

#### 4.4.5 Application of the crack-gap filling model

An estimate of the filling fraction  $\Psi$  (i.e. the ratio of volume of oxide formed during healing with respect to the initial crack volume, cf. **Eq. (4.8)**), can be obtained from the oxidation kinetics of the healing particles, see **Eq. (4.21)**. However, as the surface area created when a particle is intersected by the crack is relatively small, more time is required for an embedded healing particle to fully transform than for a set of free particles as measured by thermogravimetric analysis; cf. Section 4.4.1. Therefore, the conversion of the healing particle into the healing oxide in **Eq. (4.4.1)** is modified to reflect the increased time required for the transformation of an embedded healing particle **Eq. (4.9)**. Thus:

$$\alpha_p = \alpha(T, t \cdot f_A) \quad (4.22)$$

The area correction factor  $f_A$  is determined by comparing the area of the intersected particle, which is exposed to the crack gap, to the surface area of the free spherical particle as:

$$f_A = \frac{2\pi \langle r \rangle^2}{4\pi r^2} \quad (4.23)$$

where  $\langle r \rangle$  is the average radius of the surface of a randomly intersected spherical healing particle with radius  $r$ . It can be shown that:

$$\langle r \rangle = \frac{\pi}{4} r \quad (4.24)$$

hence  $f_A = \pi^2/32$  and the **Eq.(4.8)** for the early stage filling fraction becomes:

$$\theta = \frac{1 - \left(1 - \sqrt{kt \cdot f_A}\right)^3}{w} \phi \varphi d \quad (4.25)$$

where all terms have the usual defined meanings,  $\phi$  is 0.8 (i.e. conversion from Ti to  $\text{TiO}_2$ ),  $\varphi$  is 0.1,  $d$  is 10  $\mu\text{m}$  and  $w$  (measured during SEM observation) is 0.5  $\mu\text{m}$ . The filling fraction computed from the model according to **Eq. (4.25)** at different temperatures is in good agreement with the experimental results; see **Figure 4.17**.

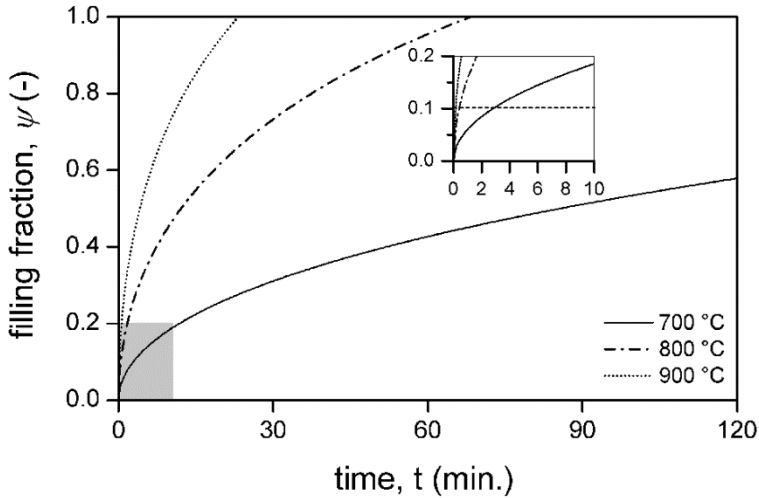


*Figure 4.17: Predicted filling fraction as function of time at different temperatures for an initial crack width of  $0.5 \mu\text{m}$  and conditions as specified in the text. the line at 1.0 indicates full filling of the crack gap.*

For example, experimentally it has been determined that samples annealed at  $900 \text{ }^\circ\text{C}$  for 15 min. were fully healed while the model predicts full healing at about 20 min. Similarly, for samples annealed at  $800 \text{ }^\circ\text{C}$  partial healing was observed after 30 min., while full healing was observed after 60 min. The model predicts that, 70 min. is required for full strength recovery at this temperature. Finally, at  $700 \text{ }^\circ\text{C}$ , all samples annealed for 120 min. broke along the original crack path in accordance with a filling fraction of about 55 % predicted by the model.

Next, the model is extended to predict the time when local bonding occurs at the studied temperatures. The intersected spherical particles will form cylindrical healing oxide bridges during local bonding across the width of the crack ( $w$ ). The filling fraction required for this can be evaluated from:

$$\psi_{local} = n_p \frac{V_{bridge}}{V_g} \quad (4.26)$$

Where  $n_p$  and  $V_g$  have been previously defined (cf. **Eq. (4.4)** and **(4.6)**, respectively) and  $V_{bridge}$  is the volume of the cylindrical oxide bridge formed between intersected particles.

$$V_{bridge} = \pi \langle r \rangle^2 w \quad (4.27)$$

in which the average radius of the surface of a randomly intersected spherical healing particle is defined in **Eq. (4.24)**. Now, the local bridging by the healing particles according to **Eq. (4.26)** becomes:

$$\psi_{local} = \frac{3\pi^2}{32} \varphi \quad (4.28)$$

and thus only depends on the volume fraction healing particles  $\varphi$ .

This minimal filling fraction required to establish the local bonding stage is evaluated to be 0.0925. This level is indicated in the insert in **Figure 4.17**, where it is seen that at the studied temperatures local bonding can be established in a relatively short time (i.e. under 1 min. at 800 and 900 °C and in about 4 min. at 700 °C).

The influence of the crack opening distance on the filling fraction is analysed using the optimum healing conditions from the experiments (i.e. 700 °C for 4 h, 800 °C for 1 h and 900 °C for 0.25 h). According to **Eq. (4.8)**, the filling fraction is inversely proportional with the width of the crack and this relation is depicted in **Figure 4.18**. It is observed that, at any temperature, doubling the crack width decreases the filling fraction by about 50 %, hence the width of the crack is identified as a sensitive parameter in strength recovery. It is also observed that the specified healing conditions local bonding is always established even at crack openings of up to 2  $\mu\text{m}$  although the cracks will not be fully filled and will fail along the damaged region.



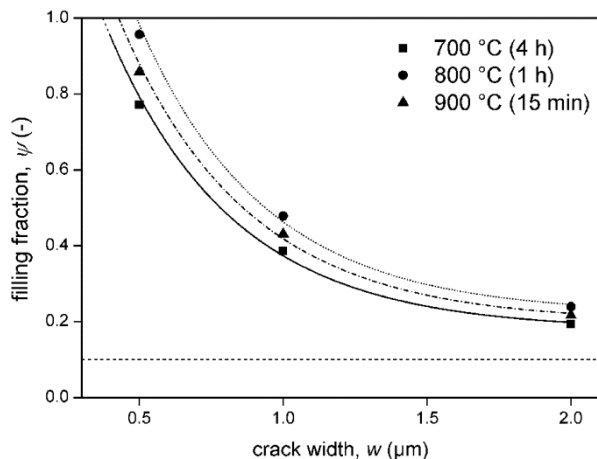


Figure 4.18: Calculated fraction of the crack filled  $\psi$  as a function of crack width for different temperatures and specified times. The dashed line at 0.1 indicates the minimum filling required for the whole crack to be bridged in the local bonding stage and the line at 1.0 indicates full filling of the crack gap.

## 4.5 Conclusions

This work affirms the capability of embedded Ti particles to heal and close up surface cracks in  $\text{Al}_2\text{O}_3$  by oxidation at high temperatures. In a dense  $\text{Al}_2\text{O}_3$  based composite containing 10 vol. % of Ti, room temperature Vickers indentation induced cracks with a radius of 20  $\mu\text{m}$  and a width of less than 1  $\mu\text{m}$  can be fully filled by annealing 800  $^\circ\text{C}$  for 1 h or 900  $^\circ\text{C}$  for 15 min. The full filling is accompanied by a full recovery of the bending strength at room temperature. The activation energy for oxidation and the indentation fracture toughness were evaluated to be 136 kJ/mol and  $4.5 \pm 0.5 \text{ MPa m}^{1/2}$ , respectively. Crack filling proceeds in three steps: local bonding and lateral spreading and finally global filling which takes place provided oxygen reaches Ti particles buried in the crack plane. The bridging of cracks by local bonding leads to significant strength recovery but full crack filling through global filling is essential in obtaining a strong healed zone. The results from the kinetic crack-gap filling model are in good agreement with the experimental results.

## **Acknowledgements**

This research was sponsored by the People Program (Marie Curie ITN) of the European Union's seventh framework program, FP7, grant number 290308 (SHeMat). The authors are indebted to Dr A.C. Riemslag for his assistance with mechanical testing.

## References

- [1] van der Zwaag, S., *An Introduction to Material Design Principles: Damage Prevention versus Damage Management*, in *Self Healing Materials: An Alternative Approach to 20 Centuries of Materials Science*, S. van der Zwaag, Editor. 2007, Springer Netherlands: Dordrecht. p. 1-18.
- [2] Brown, E.N., N.R. Sottos, and S.R. White, *Fracture testing of a self-healing polymer composite*. *Experimental Mechanics*, 2002. **42**(4): p. 372-379.
- [3] Brown, E.N., S.R. White, and N.R. Sottos, *Microcapsule induced toughening in a self-healing polymer composite*. *Journal of Materials Science*, 2004. **39**(5): p. 1703-1710.
- [4] Hager, M.D., et al., *Self-healing materials*. *Advanced Materials*, 2010. **22**(47): p. 5424-5430.
- [5] Houjou, K., K. Ando, and K. Takahashi, *Crack-healing behaviour of ZrO<sub>2</sub>/SiC composite ceramics*. *International Journal of Structural Integrity*, 2010. **Vol. 1**(1): p. 73-84.
- [6] Ono, M., et al., *A new methodology to guarantee the structural integrity of Al<sub>2</sub>O<sub>3</sub>/SiC composite using crack healing and a proof test*. *Fatigue & Fracture of Engineering Materials & Structures*, 2007. **30**(7): p. 599-607.
- [7] Takahashi, K., et al., *Threshold stress for crack healing of mullite reinforced by SiC whiskers and SiC particles and resultant fatigue strength at the healing temperature*. *Journal of the American Ceramic Society*, 2007. **90**(7): p. 2159-2164.
- [8] Takahashi, K., et al., *Crack-healing behavior of Al<sub>2</sub>O<sub>3</sub> toughened by sic whiskers*. *Journal of the American Ceramic Society*, 2003. **86**(12): p. 2143-2147.
- [9] Ando, K., et al., *Crack-healing behavior under stress of mullite/silicon carbide ceramics and the resultant fatigue strength*. *Journal of the American Ceramic Society*, 2001. **84**(9): p. 2073-2078.
- [10] Ando, K., et al., *Crack-healing and mechanical behaviour of Al<sub>2</sub>O<sub>3</sub>/SiC composites at elevated temperature*. *Fatigue & Fracture of Engineering Materials & Structures*, 2004. **27**(7): p. 533-541.

- [11] Ghosh, S.K., *Self-healing materials: Fundamentals, design strategies, and applications*, in *Self-Healing Materials*. 2009, Wiley-VCH Verlag GmbH & Co. KGaA. p. 1-28.
- [12] Boatemaa, L., et al., *Selection of healing agents for autonomous healing of alumina at high temperatures*. *Journal of the European Ceramic Society*, 2016. **36**(16): p. 4141-4145.
- [13] Yoshioka, S., et al., *On the use of TiC as high-temperature healing particles in alumina based composites*. *Journal of the European Ceramic Society*, 2016. **36**(16): p. 4155-4162.
- [14] Heffelfinger, J.R., R.R. Kieschke, and C.B. Carter, *Characterization and microanalysis of interfacial reactions in metal–matrix composite systems*. *Journal of Microscopy*, 1997. **185**(2): p. 217-224.
- [15] Wadsworth, J. and F.H. Froes, *Developments in metallic materials for aerospace applications*. *JOM*, 1989. **41**(5): p. 12-19.
- [16] Ogbuji, L.U., *Development of oxide scale microstructure on single-crystal SiC*. *Journal of Materials Science*, 1981. **16**(10): p. 2753-2759.
- [17] Schuster, P., *Formation of cristobalite from silicon carbide*. *Materials Research Bulletin*, 1969. **4**: p. 311.
- [18] Gotor, F.J., et al., *Kinetic analysis of solid-state reactions: The universality of master plots for analyzing isothermal and nonisothermal experiments*. *The Journal of Physical Chemistry A*, 2000. **104**(46): p. 10777-10782.
- [19] Khawam, A. and D.R. Flanagan, *Solid-state kinetic models: Basics and mathematical fundamentals*. *The Journal of Physical Chemistry B*, 2006. **110**(35): p. 17315-17328.
- [20] Gutierrez-Gonzalez, C.F., et al., *Processing, spark plasma sintering, and mechanical behavior of alumina/titanium composites*. *Journal of Materials Science*, 2014. **49**(10): p. 3823-3830.
- [21] Kofstad, P., *High-temperature oxidation of titanium*. *Journal of the Less Common Metals*, 1967. **12**(6): p. 449-464.

- [22] Ginstling, A.M. and V.I. Brounshtein, *Concerning the Diffusion Kinetics of Reactions in Spherical Particles*. J. Appl. ChciL USSR, 1950. **23**: p. 1327-1338.
- [23] Kofstad, P., P.B. Anderson, and O.J. Krudtaa, *Oxidation of titanium in the temperature range 800–1200°C*. Journal of the Less Common Metals, 1961. **3**(2): p. 89-97.
- [24] Šesták, J., *Rationale and fallacy of thermoanalytical kinetic patterns*. Journal of Thermal Analysis and Calorimetry, 2011. **110**(1): p. 5-16.
- [25] Cuadrado, N., et al., *Geometry of nanoindentation cube-corner cracks observed by FIB tomography: Implication for fracture resistance estimation*. Journal of the European Ceramic Society, 2015. **35**(10): p. 2949-2955.
- [26] Lawn, B.R. and E.R. Fuller, *Equilibrium penny-like cracks in indentation fracture*. Journal of Materials Science, 1975. **10**(12): p. 2016-2024.
- [27] Chen, Z., et al., *Microstructures and mechanical properties of Mn modified, Ti-Nb-based alloys*. Journal of Alloys and Compounds, 2017. **723**(Supplement C): p. 1091-1097.
- [28] Auerkari, P., *Mechanical and physical properties of engineering alumina ceramics*. 1996, Technical Research Centre of Finland, VTT Manufacturing Technology. p. 3-36.
- [29] Ponnusami, S.A., S. Turteltaub, and S. van der Zwaag, *Cohesive-zone modelling of crack nucleation and propagation in particulate composites*. Engineering Fracture Mechanics, 2015. **149**: p. 170-190.
- [30] Boatemaa, L., et al., *Autonomous high temperature healing of surface cracks in Al<sub>2</sub>O<sub>3</sub> containing Ti<sub>2</sub>AlC particles* Submitted to the Journal of the American ceramic society.

# 5

## **On the use of TiC as high-temperature healing particles in alumina based composites**

---

This chapter has been published in the Journal of the European ceramic society 36 (16) 2016 p 4155-4162. Authors: Yoshioka, S., Boatemaa, L., van der Zwaag, S., Nakao W. and Sloof, W. G.

*We report on the use of TiC particles as high temperature healing agent in alumina based composites. The selection of TiC was based on a theoretical analysis of its high temperature stability in contact with  $Al_2O_3$ , its volumetric expansion upon oxidation and the adhesion between the reaction products  $TiO_2$  with  $Al_2O_3$ . Fully dense 15 and 30 vol. percent TiC-Alumina composites were made by Spark Plasma Sintering. Initial damage was produced by Vickers' indentations. The strength recovery was determined for temperatures between 400 and 800 °C. The mechanical measurements were complemented by microstructural characterization of the base material and the healed cracks.*

## 5.1 Introduction

In recent years there has been a lot of research into the autonomous healing of surface cracks in ceramics [1-23] and metallo-ceramics (MAX phase materials) [24-32] by oxidative filling of cracks when exposed to high temperatures. In the case of metallo-ceramics the healing is of the so-called *intrinsic* self-healing type [33, 34], meaning that the metallo-ceramic itself is capable of undergoing an oxidative reaction resulting in filling of the crack and partial or complete recovery of the tensile strength. In the case of oxidic ceramics, such a reaction is impossible as the matrix is already in its oxidized state and cannot undergo any further reaction. Hence, for such materials the ability to heal surface cracks relies on the presence of intentionally embedded discrete particles called 'healing agents' which show a desirable response to high temperature exposure to oxygen containing gasses. Earlier works on such *extrinsic* healing ceramic systems focused on the oxidation of granular SiC particles embedded in several oxidic ceramic matrices. Harmer *et al.* observed that indentation induced cracks in alumina containing 5 vol. % SiC could be healed partially by means of annealing at 1300 °C for 2 h [1-2]. However, they also noted that the formed SiO<sub>2</sub> could not seal the pre-cracks fully due to the low SiC particle content. Ando *et al.* were the first to report in detail on the self-healing behaviour of SiC particles containing alumina matrix composites as a function of temperature and annealing time [3-5]. It was shown that alumina containing 15 vol. % SiC composite can attain a complete strength recovery by annealing in air at 1300 °C for 1 h or at 1200 °C for 10 h [3]. Ando *et al.* demonstrated that other structural ceramic matrix composites containing SiC particles as self-healing particles, such as mullite/SiC [6-7], Si<sub>3</sub>N<sub>4</sub>/SiC [8-9], ZrO<sub>2</sub>/SiC [10-11], also show self-healing behaviour. They demonstrated that mullite-based composites containing 20 vol. % of SiC particles could achieve complete strength recovery by various heat treatments at rather high temperatures, such as annealing for 5 h at 1200 °C or for 1 h at 1300 °C [7]. On the other hand, Si<sub>3</sub>N<sub>4</sub>/20 vol. % SiC and ZrO<sub>2</sub>/20 vol. % SiC composites recovered their room-temperature strength by annealing at relatively low temperatures e.g. at 1000 °C for 1 h in Si<sub>3</sub>N<sub>4</sub>/SiC [9] and at 800 °C for 30 h in ZrO<sub>2</sub>/SiC composite [10], respectively. However, it was also observed that Si<sub>3</sub>N<sub>4</sub>/SiC specimens annealed above 1400 °C and ZrO<sub>2</sub>/SiC specimens annealed above 1000 °C lose their mechanical properties due to excessive corrosion. In general, relatively high annealing temperatures (mostly above 1200 °C) are required for adequate



oxidation of SiC particles in order to seal the crack-gap and to recover mechanical integrity of ceramics matrix composites.

Several methodologies have been proposed with the aim of enhancing the crack-healing ability of SiC containing composites. The first attempt involved the inclusion of SiC whiskers in order to simultaneously improve the fracture toughness,  $K_{IC}$ , and self-healing ability of the composite [12-15]. Nakao et al. [12] observed that the  $K_{IC}$  value of 20 vol. % SiC-whisker containing alumina based composites ( $K_{IC}=5.6 - 5.7 \pm 0.2 \text{ MPa} \cdot \text{m}^{1/2}$ ) is considerably higher than that of monolithic alumina ( $K_{IC}=3 - 4 \text{ MPa} \cdot \text{m}^{1/2}$ ). Furthermore, it was found for alumina with 20 vol. % SiC whisker that the minimum healing temperature at which the strength of the composite can recover within 1 h is 100 °C lower than that of alumina/ granular SiC composites. The effect was attributed to the larger surface area of the SiC whiskers per unit of volume. An alternative method to enhance the healing ability is downsizing of the healing agent [16-17]. Nakao *et al.* reported that alumina composite containing 18 vol. % of nano-SiC having a diameter of 10 -30 nm can attain full strength recovery within 10 h annealing at 950 °C [17]. So, depending on the morphology and size of the SiC fraction the minimum required temperature for the complete strength recovery can be varied in range of 950 - 1300 °C.

More recently, some advanced healing agents replacing SiC have been proposed. Abe *et al.* developed alumina/ 10 vol. % NiAl composites which can heal cracks within 10 h in 1250 °C [18]. Nanko *et al.* proposed the use of nano-Ni powder as healing agents [19-21] and Maruoka *et al.* observed that alumina with 5 vol. % nano Ni composites can attain full strength recovery by annealing for 1 h at 1200 °C [21]. In order to achieve full healing at lower temperatures, Ti containing self-healing agents has been proposed. For example, mullite with 15 vol. %  $\text{TiSi}_2$  composites can achieve full strength recovery by annealing at 600 °C for 10 h [22]. The potential of Ti containing MAX phase,  $\text{Ti}_2\text{Al}_{0.5}\text{Sn}_{0.5}\text{C}$ , as healing agent has been studied by Bei *et al.* and they found that alumina with 20 vol. %  $\text{Ti}_2\text{Al}_{0.5}\text{Sn}_{0.5}\text{C}$  composites can recover their strength fully by annealing for 5 h at 900 °C [23].

A potentially interesting self-healing system not yet studied in any detail is presented by alumina composites containing TiC particles as the healing agent. The results of a theoretical analysis of the prevailing reactions and some experimental crack healing

studies are described below. The results clearly demonstrate that TiC is a potentially attractive healing agent for alumina matrices.

## 5.2 Theoretical analysis of the healing potential of TiC in an alumina matrix

In a recent publication Farle et al. [30] presented a theoretical frame work to predict the (intrinsic) healing ability of 59 metallo-ceramics on the basis of a number of fundamental physical parameters such as the thermal stability in an oxidative environment, the diffusion kinetics, the volume expansion upon oxidation, the work of adhesion between the reaction product and the matrix material and the CTE and modulus of the reaction product in relation to that of the parent phase. The first four parameters give information on the potential crack filling behaviour while the two latter parameters give information on the quality of the mechanical properties of healed cracks upon re-loading. In the present analysis we follow their analysis but focus on the properties relevant for extrinsic self-healing systems based on embedded granular healing particles.

### 5.2.1 Thermodynamic stability of TiC

The thermodynamic stability of TiC in the presence of oxygen and that of its intended reaction product  $\text{TiO}_2$  in the presence of  $\text{Al}_2\text{O}_3$  is calculated using FACTSAGE (CRCT-ThermFACT Inc. & GTT-Technologies). In **Figure 5.1** the thermodynamic stability of TiC in air as a function of temperature is shown. The figure shows that thermodynamically speaking TiC can transform into  $\text{TiO}_2$  even at room temperature.

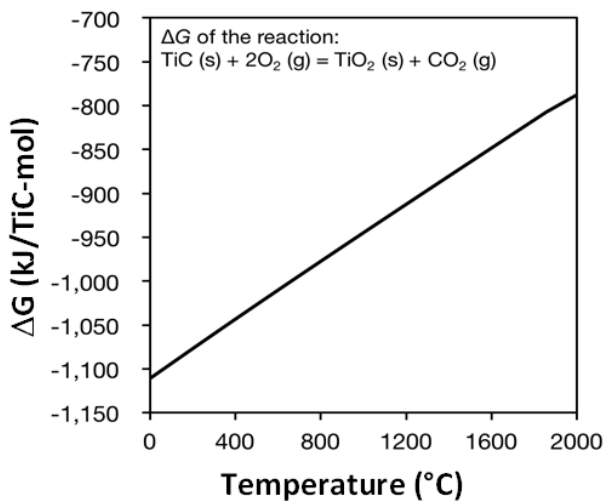


*Figure 5.1: Thermodynamic stability of TiC in air versus that of  $\text{TiO}_2$  as a function of temperature.*

For the temperature window of 1000-2000  $^\circ\text{C}$ , the calculated phase diagram for the  $\text{TiO}_2$  and  $\text{Al}_2\text{O}_3$  system is shown in **Figure 5.2**. This figure shows that there is no deep eutectic and that the lowest temperature at which a liquid phase is present is about 1700  $^\circ\text{C}$ . Hence, this temperature sets the upper healing temperature ever to be considered for this system.

According to the phase diagram, at temperatures between 1270  $^\circ\text{C}$  and 1800  $^\circ\text{C}$   $\text{TiO}_2$  can react with  $\text{Al}_2\text{O}_3$  and form the intermediate compound  $\text{Al}_2\text{TiO}_5$ . This reaction product resembles the mullite formed in the  $\text{SiO}_2 - \text{Al}_2\text{O}_3$  system. There are no reports on the reaction between  $\text{SiO}_2$  and the alumina matrix so the formation of mullite can be assumed to be quite slow or even absent. We postulate that this also applies to the  $\text{Al}_2\text{TiO}_5$  compound. So provided the healing time is not too long, the temperature window 1270-1600  $^\circ\text{C}$  could be available for self-healing reactions. Based on the pseudo phase diagram, there are no further reactions between  $\text{TiO}_2$  and  $\text{Al}_2\text{O}_3$  below 1270  $^\circ\text{C}$  and this indicates that provided all other conditions are met, the temperature domain below 1270  $^\circ\text{C}$  is suitable for self-healing reactions and prolonged material use.

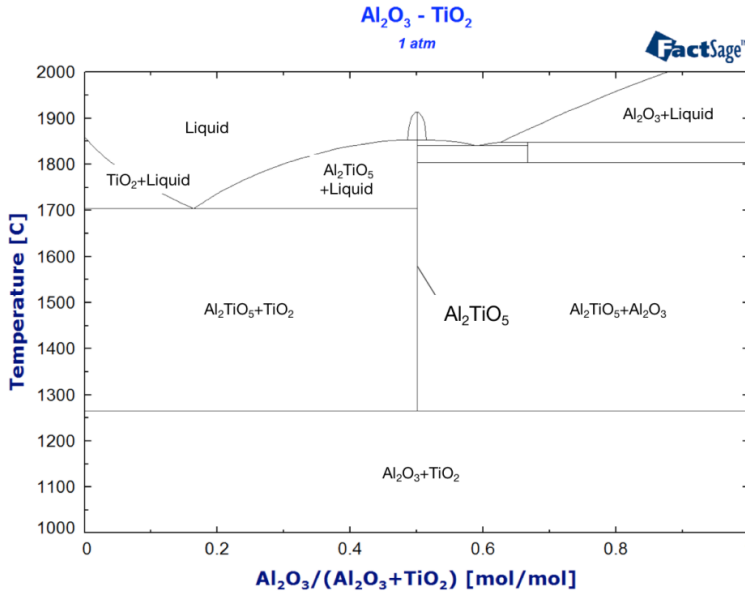


Figure 5.2:  $TiO_2$ - $Al_2O_3$  pseudo phase diagram (i.e. excluding oxides  $TiO_{2-x}$ ,  $Ti_3O_5$ ,  $Ti_2O_3$ ,  $TiO$ ).

## 5.2.2 Relative volume expansion (RVE)

Successful crack filling due to solid state chemical reactions requires that the molar volume of the reaction product is larger than that of the starting healing material in order to i) (fully or partially) fill the crack, ii) locally reconnect opposing crack faces and iii) re-establish mechanical integrity. The volumetric growth is expressed as the relative volume expansion (RVE). In this work we look at the decomposition of a carbide into a metallic oxide as presented by the following reaction:



Hence,

$$RVE(\%) = \frac{V_{MO_2} - V_{MC}}{V_{MC}} * 100 \quad (5.2)$$

Table 5.1: Reference data used for RVE calculation.

Compound	Cell volume $C (\text{\AA}^3)$	No of units ( $N$ )	Molar volume $V_x (\text{cm}^3/\text{mol})$	Reference (PDF No.)
SiC	82.77	4	12.5	01-075-0254
TiC	81.07	4	12.2	04-004-2919
SiO <sub>2</sub> (Cristobalite)	176.54	4	26.6	01-082-0512
TiO <sub>2</sub> (Rutile)	62.43	2	18.8	00-021-1276

Here,  $V_x$  is the molar volume of substance  $X$ , and is calculated from the following equation:

$$V_x (\text{cm}^3/\text{mol}) = \frac{C \left( \text{\AA}^3 \right) * 10^{-24}}{N} * N_A (\text{mol}^{-1}) \quad (5.3)$$

where,  $C$  is the cell volume of substance  $X$  and  $N$  is the number of units in each cell. The crystal data used are listed in **Table 5.1**. The calculated RVE of TiC is shown to be more than 0 % in **Table 5.2**, implying that TiC can indeed create the extra volume required for filling the crack-gap upon oxidation.

Table 5.2: Calculated RVE value of TiC and SiC.

Reaction	RVE (%)
SiC+2O <sub>2</sub> →SiO <sub>2</sub> (Cristobalite) + CO <sub>2</sub>	113.3
TiC+2O <sub>2</sub> →TiO <sub>2</sub> (Rutile) + CO <sub>2</sub>	54.0

According to previous studies [3-4], 15 vol. % fraction of SiC was sufficient for filling the surface crack with 100  $\mu\text{m}$  and attain full strength recovery of alumina/SiC composite. Assuming the local crack facing distance of the induced indentation cracks to be the same one can argue that the optimal volume fraction of TiC self-healing agent should be of the order of 30 vol. % in order to realize a comparable self-healing of TiC/ alumina composite and to compensate for the lower RVE value. Hence, our experimental studies focus on 15 and 30 vol. % TiC containing Al<sub>2</sub>O<sub>3</sub> composites.

### 5.2.3 Work of adhesion

In order to achieve complete strength recovery, the energy required to separate the crack-filling oxide from the alumina matrix should be comparable or greater than the cohesion strength of the alumina matrix. This adhesion energy of the interface between matrix and crack-filling oxide interface is defined as the ‘work of adhesion’. This work of adhesion can be expressed by [35]:

$$W_{ad} = -(\gamma_{\text{matrix}}^{\text{surf}} + \gamma_{\text{oxide}}^{\text{surf}}) + \gamma_{\text{matrix/oxide}}^{\text{interface}} \quad (5.4)$$

where,  $\gamma_{\text{matrix}}^{\text{surf}}$  and  $\gamma_{\text{oxide}}^{\text{surf}}$  is the surface energy of matrix and oxide, and  $\gamma_{\text{matrix/oxide}}^{\text{interface}}$  is the interface energy between matrix and crack-filling oxide interface. The value for the interface energy has been estimated from the interaction energies of the atoms located at each site of the interface [36, 37]. The interaction energies were calculated from solution enthalpies of an element at one site of interface dissolved in another element at the other site of the interface. Details of the calculations can be found elsewhere [38].

The calculated works of adhesions for the relevant interfaces are shown in **Figure 5.3**. As justified in Section 5.2.1, in the present analysis the formation of  $\text{Al}_2\text{TiO}_5$  is ignored. The work of adhesion for the  $\text{Al}_2\text{O}_3/\text{TiO}_2$  interface ( $4900 \text{ mJ/m}^2$ ) and that for the  $\text{TiO}_2/\text{TiO}_2$  interface ( $5630 \text{ mJ/m}^2$ ) are greater than that for the  $\text{Al}_2\text{O}_3/\text{Al}_2\text{O}_3$  interface ( $4090 \text{ mJ/m}^2$ ). The latter two values represent the cohesion of the crack filling and matrix phase, respectively. It means that the crack-healed part in alumina/TiC could be stronger than the alumina matrix itself. To put these values in perspective we also report the work of adhesion between  $\text{Al}_2\text{O}_3/\text{SiO}_2$  interface ( $4020 \text{ mJ/m}^2$ ) which is a well-known self-healing ceramic system.

From these calculations, it can be postulated that the alumina/TiC composites will attain full strength recovery once the crack is filled up adequately with the  $\text{TiO}_2$  formed.

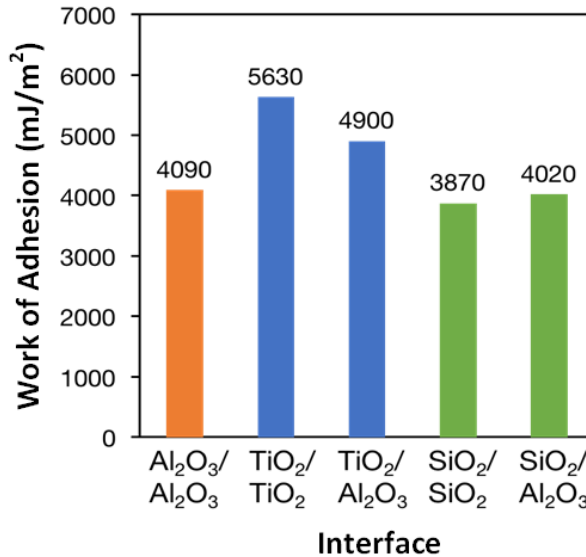


Figure 5.3: Calculated works of adhesion for relevant interfaces.

#### 5.2.4 Comparison of the thermal expansion coefficients

Even if the crack is fully filled by the formation of an oxidic phase at the healing temperature, this is no guarantee that a strong and reliable bond is formed when the sample is exposed to a wide range of temperatures. Differences in coefficient of thermal expansion (CTE) between the matrix and the material formed in the crack as a result of the healing reaction may lead to local stresses. Hence, it is important to compare the CTE's of matrix (Al<sub>2</sub>O<sub>3</sub>), healing agent (TiC) and crack-filling oxides (TiO<sub>2</sub>). Relevant average CTE values are listed together with the related values for alumina/SiC composites in **Table 5.3**. The dependence of CTE on crystal orientation was not taken into account as the material deposited in the crack is polycrystalline.

*Table 5.3: Thermal expansion coefficients of relevant compounds in alumina /TiC and alumina/ SiC composite.*

Compound	Temperature range (°C)	CTE x10 <sup>-6</sup> (°C <sup>-1</sup> )	Ref.
Al <sub>2</sub> O <sub>3</sub>	1000-1600	7.5 ± 0.4	[39]
	20-2025	7.3 - 8.3	[40]
TiC	23-848	6.99 ± 0.34 - 7.61 ± 0.20	[41]
	1000-2600	8.31 ± 0.68	[39]
SiC	25-1000	3.2 - 5.1	[42]
	1000-1600	5.68 ± 0.11	[39]
TiO <sub>2</sub> (Rutile)	30-650	7.249 - 8.816	[43]
	20-1610	8.9 -11.1	[40]
SiO <sub>2</sub> (Cristobalite)	100-500	10.9	[44]
	500-1000	1.7	[44]

From Table 5.3, the CTE values of the matrix, the unreacted healing agent and the relevant crack-filling oxides in the alumina/TiC system considered are in the range of  $6.99 \times 10^{-6}$  to  $11.1 \times 10^{-6} / ^\circ\text{C}$ . The maximum mismatch value is  $4.45 \times 10^{-6} / ^\circ\text{C}$  between TiC and TiO<sub>2</sub> at temperature region from room temperature to 500 °C. In contrast, the maximum mismatch value in the reference alumina/SiC system is  $7.7 \times 10^{-6} / ^\circ\text{C}$  between SiC and SiO<sub>2</sub> at temperature region from room temperature to 500 °C, and  $6.6 \times 10^{-6} / ^\circ\text{C}$  between alumina matrix and SiO<sub>2</sub> at above 500 °C. Considering there are no reports on the spontaneous fracture of alumina/SiC self-healing ceramics due to thermal expansion mismatch, it can be proposed that the effects of the CTE mismatch in the alumina/TiC composites on structural integrity can be ignored at this stage.

### 5.2.5 Comparison of the elastic properties

A healed crack in a ceramic compound may not only be exposed to the thermal stresses induced by temperature excursions but may also be exposed to mechanical stresses due to external loading. In this case it is important to compare the elastic moduli of the matrix, the healing agent and the decomposition product. The



Young's moduli of relevant (polycrystalline) compounds in alumina /TiC and alumina/SiC composites are listed in **Table 5.4**.

Considering that Young's modulus of  $TiC_x$  depends on the carbon level [46], it can be stated that the Young's modulus of  $TiC_x$  is more or less comparable to alumina matrix, as is the case for SiC. In contrast, the modulus of  $SiO_2$  and  $TiO_2$  is considerable lower than that of matrix. Based on the values reported and given that full strength recovery has been attained in alumina/SiC system, it is expected that the alumina/TiC can also yield comparable self-healing levels. Early cracking along the healed interface is not very likely to occur unless at higher macroscopic stress levels.

*Table 5.4: Young's modulus of related compounds in alumina /TiC and alumina/SiC composite.*

Compound	Specimen	Density (%)	Young's modulus (GPa)	Ref.
$Al_2O_3$	Sintered bulk	$\geq 99.6$	380-410	[45]
	Sintered bulk	$\geq 99.8$	380-405	[45]
	Sintered bulk	$\geq 99.5$	398-400	[45]
	Sintered bulk	$\geq 99.6$	340-380	[45]
	Sintered bulk	$\geq 99.0$	340-380	[45]
$TiC_{x(x<1)}$	Thin film	-	<460	[46]
SiC	Sintered bulk	$\geq 98.0$	415	[47]
$TiO_2$	Crystalized thin film	-	85	[48]
$SiO_2$ (Cristobalite)	Natural single crystal	-	65.2	[49]

In conclusion, based on the theoretical analysis presented above it is to be expected that autonomous high-temperature oxidative healing of the mechanical integrity of an  $Al_2O_3$  composites filled with (10-30 vol. %) TiC particles should theoretically be possible.

## 5.3 Experimental

Alumina matrix composites containing 15 vol. % TiC and 30 vol. % TiC, named Al15TiC and Al30TiC respectively, were prepared and their strength recovery at room temperature as a function of the healing temperature was studied under the conditions specified below. Furthermore, the microstructural changes responsible for the strength recovery were also determined.

### 5.3.1 Sample preparation

Alumina raw powder (AKP-50, Sumitomo Chemical Co., Ltd.) and TiC powder (STD120, H.C. Starck GmbH) were used as starting materials. The initial average sizes were 0.2 and 2  $\mu\text{m}$ , respectively. Ball-milling of TiC powder was conducted for 36 h in isopropanol with  $\varnothing 10$  mm WC ball and a WC jar, resulting in an average particle size of 0.3  $\mu\text{m}$ . Alumina powder and ball-milled TiC powder were mixed at either 15 vol. % or 30 vol. % in isopropanol using  $\varnothing 5$  mm alumina balls and a 1000 ml plastic bottle. After 12 h mixing, the mixed powder was dried in the oven for 24 h at 80 °C. The dried powder was sieved with a  $\varnothing 200$   $\mu\text{m}$  mesh sieve. The sieved powder was densified by means of spark plasma sintering (HP D 25-SD furnace, FCT Systeme GmbH) with a  $\varnothing 40$  mm carbon mould at 1500 °C for 15 min. in vacuum condition under 35 MPa. The heating rate was 10 °C/min while natural cooling was used to cool down from the maximum temperature. The typical thickness of the samples was about 5 mm. The relative density of the sintered bulk materials as measured by Archimedes' method was more than 99 %. The sintered discs were cut into rectangular samples with a dimension of 3 x 4 x 23 mm for four-point bending tests. Samples were polished in various steps with a final polish using a diamond paste with a particle size of 0.25  $\mu\text{m}$ .

### 5.3.2 Strength recovery tests

In order to study the strength recovery of Al15TiC and Al30TiC as a function of the annealing temperature, the strength values of three types of specimen (smooth specimen, pre-cracked specimen and healed specimen), were determined. Smooth

specimen refers to samples without any induced damage prior to testing. Pre-cracked specimens are samples with a standardized pre-crack at the centre of the surface introduced by Vickers' indenter. The indentation force was 20 N and the introduced crack had a surface length of about 100  $\mu\text{m}$  for both sets of samples. The surface crack opening distance of these cracks could not be established with any real accuracy but was estimated to vary between 0.1 to 0.5  $\mu\text{m}$ . The two sets of radial indentation cracks are either perpendicular or parallel to the longest dimension of the bend test samples. No strong interaction between the indentation induced radial cracks and the healing particles was observed. The healed specimens are pre-cracked and have been annealed for 1 h in air at temperatures ranging from 400 to 1000  $^{\circ}\text{C}$ .

The strength of each sample was measured by means of an auto aligning four-point bending test using the set-up shown in **Figure 5.4**. The upper and lower span between the supporting 2 mm diameter steel rollers was 20 and 10 mm, respectively. The specimen was mounted such that the maximum tensile stress was applied to the pre-crack or healed crack part. All tests were conducted at room temperature and with a cross-head displacement velocity of 0.5 mm/min.

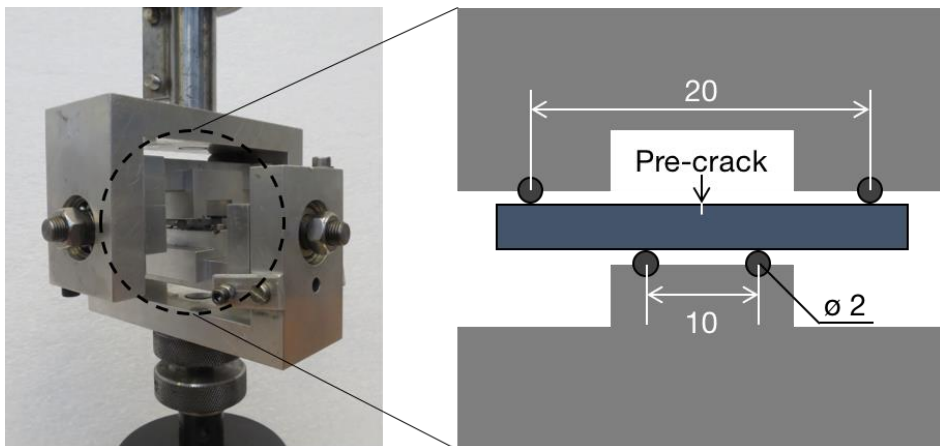


*Figure 5.4: Self-aligning four-point bending set-up used.*

### 5.3.3 Structure characterization

The external appearance of the healed cracks was recorded with a laser microscope (KEYENCE, VK-X) and analysed using image software. The chemical composition of the reaction product formed in the crack was determined using Electron Probe Micro Analysis (EPMA) using a JXA-8530F JEOL Ltd microprobe. To enable such measurements, the surface oxidation layer was removed by using a focused ion beam (JIB-4501, JEOL Ltd.). The crystal structure of the various phases in the samples prior and after thermal annealing was determined using XRD (ULTIMA IV, Rigaku Co.) operated with Cu  $K_{\alpha}$  radiation.

## 5.4 Results and discussion

### 5.4.1 Strength recovery

The results of strength recovery tests for both Al15TiC and Al30TiC are shown in Figure 5.5.

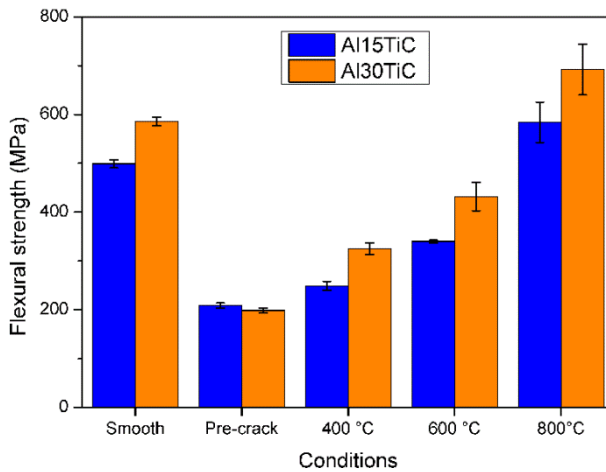
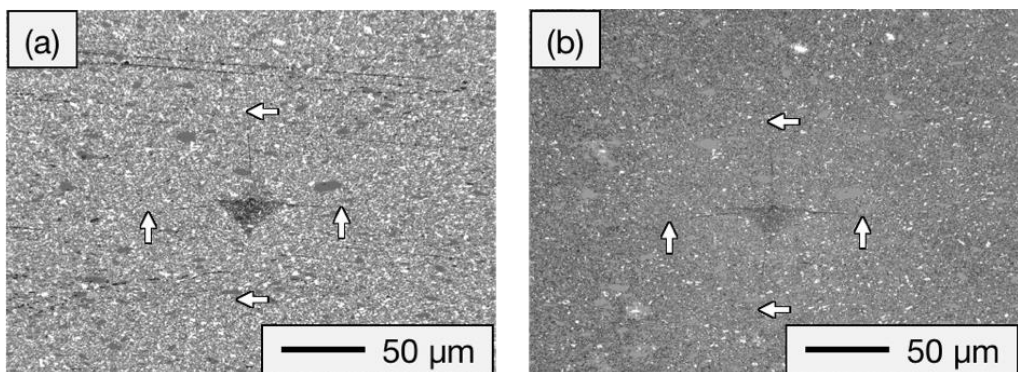


Figure 5.5: Flexural strength values of Al15TiC and Al30TiC samples after healing for 1 h in air at the reported temperature.

The averaged strength of smooth specimens at room temperature was 526 MPa for Al15TiC and 598 MPa for Al30TiC. The averaged strength of pre-cracked specimens was 208 MPa for Al15TiC and 199 MPa for Al30TiC, i.e. more or less equal and in accordance with the equal dimensions of the indentation induced cracks. **Figure 5.5** shows that annealing at 400 °C already leads to some recovery of the strength (this could be due to oxidative healing but thermal blunting of the crack tip may also play a role). This lowest temperature at which partial strength recovery is observed is considerable lower than that observed for alumina/SiC composites. Annealing at 800 °C led to a complete recovery of the strength for both sets of samples.

## 5.4.2 Microstructural observations

Laser microscope images of pre-cracked area before and after annealing at each condition are shown in **Figure 5.6 - 5.8** for annealing temperatures of 400, 600 and 800 °C respectively. **Figure 5.6** (sample annealed at 400 °C) shows no sign of surface oxidation and the cracks remain nicely visible. In contrast, **Figures 5.7** and **5.8** (annealing temperatures 600 and 800 °C, respectively) show clear signs of surface oxidation at the location of the TiC particles intercepting the external surface, and the crack is no longer discernible.



*Figure 5.6: Laser microscope image of pre-cracked area of Al30TiC (a) before annealing (b) after annealing at 400 °C for 1h. Arrows indicate the end-points of the radial cracks.*

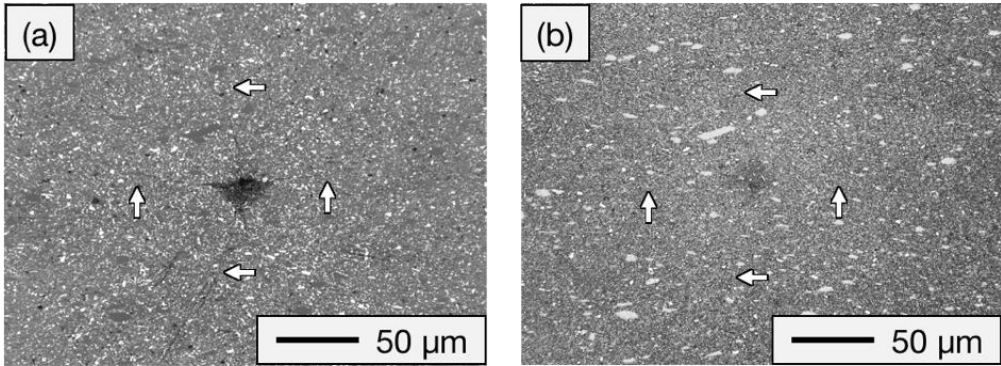


*Figure 5.7: Laser microscope image of pre-cracked area of Al<sub>30</sub>TiC (a) before annealing (b) after annealing at 600 °C for 1 h. Arrows indicate the end-points of the radial cracks.*

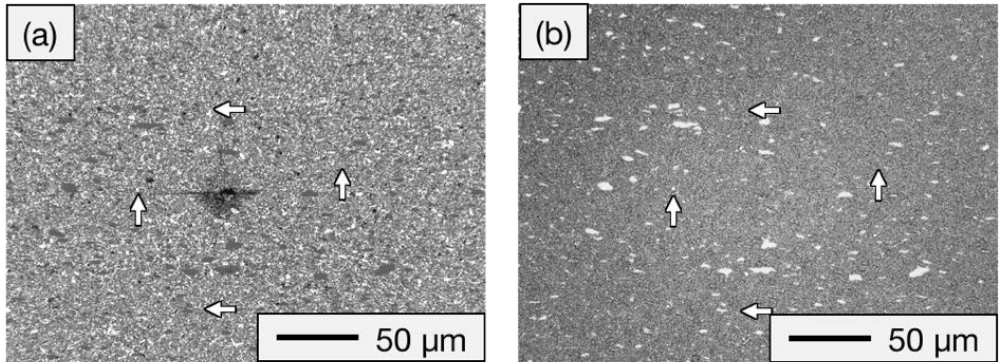


*Figure 5.8: Laser microscope image of pre-cracked area of Al<sub>30</sub>TiC (a) before annealing (b) after annealing at 800 °C for 1 h. arrows indicate the end-points of the radial cracks.*

**Figure 5.9** shows the SEM image and backscattered electron image around the healed-crack area of the healed specimen at 800 °C for 1 h after removing the surface oxidation layer by mechanical polishing using 0.25 μm diamond past. The healed crack is indicated by arrows in both figures. Taking the result of Energy Dispersive X-ray Spectrometry into account, it is clear that the crack is fully filled with the titanium oxide formed. It is interesting to note that the titanium oxide can be found also at locations in the crack well away from intersected TiC particles. This lateral spreading of the oxide along the crack is very advantageous for the healing efficiency. It also should be noticed that TiC healing-agent particles nearby the

crack surface are still intact. In conclusion: **Figure 5.9** confirm that the crack is fully filled up with titanium oxide upon 800 °C annealing for 1 h.

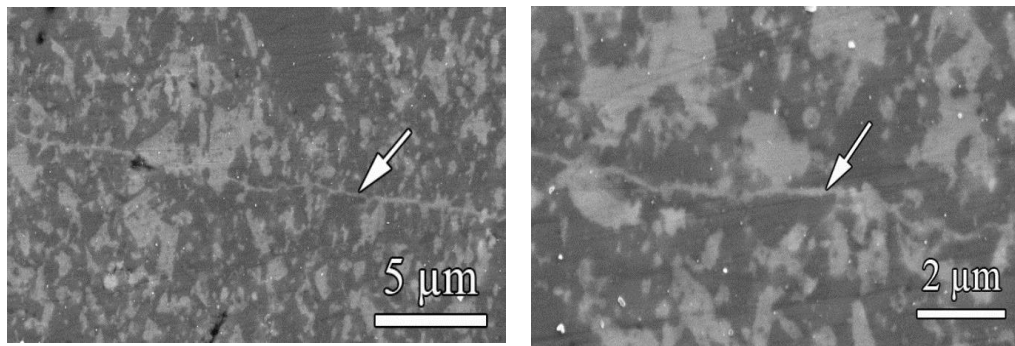


*Figure 5.9: Backscattered electron image of healed- crack area of Al<sub>30</sub>TiC annealed at 800 °C for 1h. The external oxidation layer was removed by minimal mechanical polishing.*

The results of XRD analysis of the as-synthesized and the annealed samples are shown **Figure 5.10**. Some contamination of TiC with WC was expected due to the ball milling treatment, but no traces of WC were detected. The diffractogram after 1 h annealing at 400 °C did not differ from that of the as-synthesized specimen. For higher annealing temperatures clear signs of Rutile were observed, but Anatase and Brookite were not detected. TiC was still detectable in the sample annealed at 800 °C. This indicates that the surface is not fully covered with TiO<sub>2</sub> yet and also TiC is still intact nearby the surface. Also, the formation of Al<sub>2</sub>TiO<sub>5</sub> was not detected even annealing at 800 °C. Those results correspond to the discussion on the surface observations shown above and the possibility of Al<sub>2</sub>TiO<sub>5</sub> formation during annealing at high temperatures in section 5.2.1.

Finally, it should be mentioned that at 800 °C full strength recovery was observed for both Al<sub>15</sub>TiC and Al<sub>30</sub>TiC material while it was postulated on the basis of the RVE calculations that in the case of 15 vol. % TiC (i.e. Al<sub>15</sub>TiC material) the additional volume created by the oxidation of 15 vol. % TiC might be insufficient to fully fill and heal the cracks. Clearly the critical volume concentration for full crack filling depends not only on the length of the crack but also on the average local crack facing distance (i.e. the total initial open crack volume). [50]. The full healing of the Al<sub>15</sub>TiC material may well be attributed to either more narrow indentation cracks than assumed or easier long-range transport of the Ti atoms along the crack and through the matrix. Complicated 4D nano-CT tomography measurements of the

type reported elsewhere for high temperature crack healing in MAX phase material [51] would be required to establish the degree of crack filling in this material also below the surface.

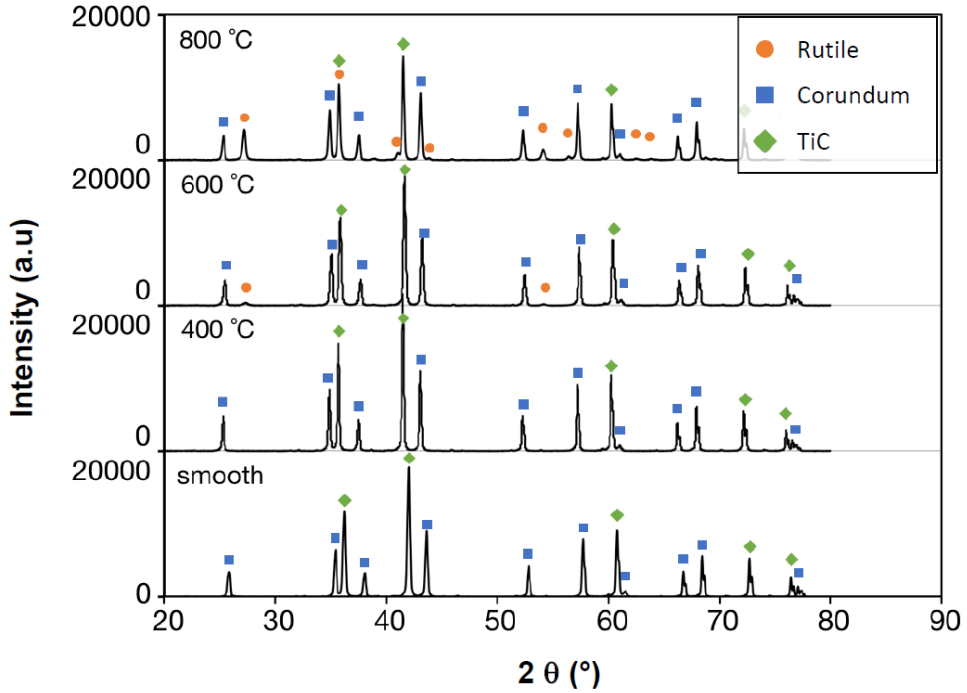


Figure 5.10: XRD patterns of Al<sub>30</sub>TiC in the pristine state (smooth) and after annealing for 1 h at the temperatures indicated.

## 5.5 Conclusions

This paper aimed to study the capability of TiO<sub>2</sub> as a crack-filling oxide for self-healing oxidic ceramics and the self-healing property of alumina/TiC composites in particular. A detailed theoretical analysis of the healing reaction and the intrinsic properties of the reaction products revealed that TiC is indeed a potentially attractive healing agent for extrinsic self-healing ceramic systems. Experimental studies on SPS sintered Al<sub>2</sub>O<sub>3</sub>-TiC composites containing 15 and 30 vol. % TiC particles with a typical diameter of 0.3-5 μm showed complete tensile strength



recovery by annealing for 1 h at 800 °C. The nature of the healing reactions was studied experimentally and found to be in accordance with the predicted complete filling of the indentation induced cracks via Rutile formation.

### **Acknowledgements**

This research was sponsored by the People Program (Marie Curie ITN) of the European Union's seventh framework program under grant no. 290308 (SHeMat) and the Strategic Young Researcher Overseas Visits Program for Accelerating Brain Circulation of Japan Society for the Promotion of Science (JSPS) under grant no. R2403, and Advanced Low Carbon Technology Research and Development Program of Japan Science and Technology Agency (JST-ALCA).

## References

- [1] Thompson, A.M., Chan, H.M., Harmer, M.P., and Cook, R.E., *Crack healing and stress relaxation in  $Al_2O_3$ /SiC "nanocomposites"*. Journal of the American Ceramic Society, 1995. 78(3): p. 567-571.
- [2] Chou, I.A., Chan, H.M., and Harmer, M.P., *Effect of annealing environment on the crack healing and mechanical behavior of silicon carbide-reinforced alumina nanocomposites*. Journal of the American Ceramic Society, 1998. 81(5): p. 1203-1208.
- [3] Ando, K., Kim, B.S., Chu, M.C., Saito, S., and Takahashi, K., *Crack-healing and mechanical behaviour of  $Al_2O_3$ /SiC composites at elevated temperature*. Fatigue and Fracture of Engineering Materials and Structures, 2004. 27(7): p. 533-541.
- [4] Ono, M., Nakao, W., Takahashi, K., Nakatani, M., and Ando, K., *A new methodology to guarantee the structural integrity of  $Al_2O_3$ /SiC composite using crack healing and a proof test*. Fatigue and Fracture of Engineering Materials and Structures, 2007. 30(7): p. 599-607.
- [5] Osada, T., Nakao, W., Takahashi, K., and Ando, K., *Kinetics of self-crack-healing of alumina/Silicon carbide composite including oxygen partial pressure effect*. Journal of the American Ceramic Society, 2009. 92(4): p. 864-869.
- [6] Chu, M.C., Sato, S., Kobayashi, Y., and Ando, K., *Damage healing and strengthening behaviour in intelligent mullite/SiC ceramics*. Fatigue & Fracture of Engineering Materials & Structures, 1995. 18(9): p. 1019-1029.
- [7] Ando, K., Chu, M.C., Tsuji, K., Hirasawa, T., Kobayashi, Y., and Sato, S., *Crack healing behaviour and high-temperature strength of mullite/SiC composite ceramics*. Journal of the European Ceramic Society, 2002. 22(8): p. 1313-1319.
- [8] Ando, K., Ikeda, T., Sato, S., Yao, F., and Kobayashi, Y., *A preliminary study on crack healing behaviour of  $Si_3N_4$ /SiC composite ceramics*. Fatigue and Fracture of Engineering Materials and Structures, 1998. 21(1): p. 119-122.
- [9] Ando, K., Chu, M.C., Yao, F., and Sato, S., *Fatigue strength of crack-healed  $Si_3N_4$ /SiC composite ceramics*. Fatigue and Fracture of Engineering Materials and Structures, 1999. 22(10): p. 897-903.
- [10] Houjou, K., Ando, K., and Takahashi, K., *Crack-healing behaviour of  $ZrO_2$ /SiC composite ceramics*. International Journal of Structural Integrity, 2010. 1(1): p. 73-84.

- [11] Houjou, K. and Takahashi, K., *Crack-healing behavior of ZrO<sub>2</sub>/SiC composite ceramics and strength properties of crack-healing specimens*. International Journal of Structural Integrity, 2012. 3(1): p. 41-52.
- [12] Takahashi, K., Yokouchi, M., Lee, S.K., and Ando, K., *Crack-healing behavior of Al<sub>2</sub>O<sub>3</sub> toughened by SiC whiskers*. Journal of the American Ceramic Society, 2003. 86(12): p. 2143-2147.
- [13] Nakao, W., Ono, M., Lee, S.K., Takahashi, K., and Ando, K., *Critical crack-healing condition for SiC whisker reinforced alumina under stress*. Journal of the European Ceramic Society, 2005. 25(16): p. 3649-3655.
- [14] Nakao, W., Mori, S., Nakamura, J., Takahashi, K., Ando, K., and Yokouchi, M., *Self-crack-healing behavior of mullite/SiC particle/SiC whisker multi-composites and potential use for ceramic springs*. Journal of the American Ceramic Society, 2006. 89(4): p. 1352-1357.
- [15] Takahashi, K., Uchiide, K., Kimura, Y., Nakao, W., Ando, K., and Yokouchi, M., *Threshold stress for crack healing of mullite reinforced by SiC whiskers and SiC particles and resultant fatigue strength at the healing temperature*. Journal of the American Ceramic Society, 2007. 90(7): p. 2159-2164.
- [16] Nakao, W., Tsutagawa, Y., and Ando, K., *Enhancement of in situ self-crack-healing efficient temperature region by SiC nanosizing*. Journal of Intelligent Material Systems and Structures, 2008. 19(3): p. 407-410.
- [17] Wataru, N. and Shihomi, A., *Enhancement of the self-healing ability in oxidation induced self-healing ceramic by modifying the healing agent*. Smart Mater. Struct., 2012. 21(2): p. 025002.
- [18] Abe, O., Ohwa, Y., and Kuranobu, Y.I., *Possibility of enhanced strength and self-recovery of surface damages of ceramics composites under oxidative conditions*. Journal of the European Ceramic Society, 2006. 26(4-5): p. 689-695.
- [19] Salas-Villaseñor, A.L., Lemus-Ruiz, J., Nanko, M., and Maruoka, D., *Crack disappearance by high-temperature oxidation of alumina toughened by Ni nanoparticles*, in *Advanced Materials Research*. 2009. p. 34-43.
- [20] Maruoka, D., Sato, Y., and Nanko, M., *Crack-healing effectiveness of nano Ni+SiC Co-dispersed alumina hybrid materials*, in *Advanced Materials Research*. 2010. p. 365-370.
- [21] Maruoka, D. and Nanko, M., *Recovery of mechanical strength by surface crack disappearance via thermal oxidation for nano-Ni/Al<sub>2</sub>O<sub>3</sub> hybrid materials*. Ceramics International, 2013. 39(3): p. 3221-3229.

- [22] Yoshioka, S. and Nakao, W., *Methodology for evaluating self-healing agent of structural ceramics*. Journal of Intelligent Material Systems and Structures, 2015. 26(11): p. 1395-1403.
- [23] Bei, G.P., Pedimonte, B.J., Pezoldt, M., Ast, J., Fey, T., Goeken, M., and Greil, P., *Crack healing in  $Ti_2Al_{0.5}Sn_{0.5}C-Al_2O_3$  composites*. Journal of the American Ceramic Society, 2015. 98(5): p. 1604-1610.
- [24] Song, G.M., Pei, Y.T., Sloof, W.G., Li, S.B., De Hosson, J.T.M., and van der Zwaag, S., *Oxidation-induced crack healing in  $Ti_3AlC_2$  ceramics*. Scripta Materialia, 2008. 58(1): p. 13-16.
- [25] Chen, G., Zhang, R., Zhang, X., Zhao, L., and Han, W., *Oxidation-induced crack healing in  $Zr_2Al_4C_5$  ceramic*. Materials and Design, 2009. 30(9): p. 3602-3607.
- [26] Li, S., Song, G., Kwakernaak, K., van der Zwaag, S., and Sloof, W.G., *Multiple crack healing of a  $Ti_2AlC$  ceramic*. Journal of the European Ceramic Society, 2012. 32(8): p. 1813-1820.
- [27] Yang, H.J., Pei, Y.T., Rao, J.C., and De Hosson, J.T.M., *Self-healing performance of  $Ti_2AlC$  ceramic*. Journal of Materials Chemistry, 2012. 22(17): p. 8304-8313.
- [28] Li, S., Xiao, L., Song, G., Wu, X., Sloof, W.G., and van der Zwaag, S., *Oxidation and crack healing behavior of a fine-grained  $Cr_2AlC$  ceramic*. Journal of the American Ceramic Society, 2013. 96(3): p. 892-899.
- [29] Yang, H.J., Pei, Y.T., and De Hosson, J.T.M., *Oxide-scale growth on  $Cr_2AlC$  ceramic and its consequence for self-healing*. Scripta Materialia, 2013. 69(2): p. 203-206.
- [30] Farle, A.S., Kwakernaak, C., van der Zwaag, S., and Sloof, W.G., *A conceptual study into the potential of  $M_{n+1}AX_n$ -phase ceramics for self-healing of crack damage*. Journal of the European Ceramic Society, 2015. 35(1): p. 37-45.
- [31] Li, S., Bei, G., Chen, X., Zhang, L., Zhou, Y., Mačković, M., Spiecker, E., and Greil, P., *Crack healing induced electrical and mechanical properties recovery in a  $Ti_2SnC$  ceramic*. Journal of the European Ceramic Society, 2016. 36(1): p. 25-32.
- [32] Li, S., Li, H., Zhou, Y., and Zhai, H., *Mechanism for abnormal thermal shock behavior of  $Cr_2AlC$* . Journal of the European Ceramic Society, 2014. 34(5): p. 1083-1088.

- [33] van der Zwaag, S., Van Dijk, N.H., Jonkers, H.M., Mookhoek, S.D., and Sloof, W.G., *Self-healing behaviour in Man-made engineering materials: Bioinspired but taking into account their intrinsic character*. Philosophical Transactions of the Royal Society A: Mathematical, Physical and Engineering Sciences, 2009. 367(1894): p. 1689-1704.
- [34] Blaiszik, B.J., Kramer, S.L.B., Olugebefola, S.C., Moore, J.S., Sottos, N.R., and White, S.R., *Self-healing polymers and composites*, in *Annual Review of Materials Research*. 2010. p. 179-211.
- [35] Howe, J.M., *Bonding, structure, and properties of metal/ceramic interfaces: Part 2 interface fracture behaviour and property measurement*. International Materials Reviews, 1993. 38(5): p. 257-271.
- [36] de Boer, F.R., Boom, R., Mattens, W.C.M., Miedema, A.R., and Niessen, A.K. *Cohesion in metals: transition metal alloys (Eds.)*. in *Cohesion and Structure*. 1989. North-Holland Publishing Co., Amsterdam, The Netherlands.
- [37] Vitos, L., Ruban, A.V., Skriver, H.L., and Kollár, J., *The surface energy of metals*. Surface Science, 1998. 411(1-2): p. 186-202.
- [38] Bennett, I.J., Kranenburg, J.M., and Sloof, W.G., *Modeling the influence of reactive elements on the work of adhesion Between oxides and metal alloys*. Journal of the American Ceramic Society, 2005. 88(8): p. 2209-2216.
- [39] Engberg, C.J. and Zehms, E.H., *Thermal expansion of Al<sub>2</sub>O<sub>3</sub>, BeO, MgO, B<sub>4</sub>C, SiC, and TiC above 1000 °C*. Journal of the American Ceramic Society, 1959. 42(6): p. 300-305.
- [40] Fei, Y., *Thermal expansion*, in *Mineral Physics and Crystallography: a Handbook of Physical Constants*, Ahrens, T.J., Editor. 1995. p. 29.
- [41] Elliott, R.O. and Kempter, C.P., *Thermal expansion of some transition metal carbides*. Journal of Physical Chemistry, 1958. 62(5): p. 630-631.
- [42] Li, Z. and Bradt, R.C., *Thermal expansion of the cubic (3C) polytype of SiC*. Journal of Materials Science, 1986. 21(12): p. 4366-4368.
- [43] Rao, K.V.K., Naidu, S.V.N., and Iyengar, L., *Thermal expansion of rutile and anatase*. Journal of the American Ceramic Society, 1970. 53(3): p. 124-126.
- [44] Aumento, F., *Stability, Lattice Parameters, and Thermal Expansion of  $\beta$ -Cristobalite*. Am. Mineral., 1966. 51(7): p. 1167-1176.
- [45] Auerkari, P., *Mechanical and physical properties of engineering alumina ceramics*. 1996: Technical Research Centre of Finland.

- [46] Török, E., Perry, A.J., Chollet, L., and Sproul, W.D., *Young's modulus of TiN, TiC, ZrN and HfN*. Thin Solid Films, 1987. 153(1-3): p. 37-43.
- [47] Munro, R.G., *Material properties of a sintered  $\alpha$ -SiC*. Journal of Physical and Chemical Reference Data, 1997. 26(5): p. 1195-1203.
- [48] Olofinjana, A.O., Bell, J.M., and Jamting, A.K., *Evaluation of the mechanical properties of sol-gel-deposited titania films using ultra-micro-indentation method*. Wear, 2000. 241(2): p. 174-179.
- [49] de Faoite, D., Browne, D.J., Chang-Díaz, F.R., and Stanton, K.T., *A review of the processing, composition, and temperature-dependent mechanical and thermal properties of dielectric technical ceramics*. Journal of Materials Science, 2012. 47(10): p. 4211-4235.
- [50] Mookhoek, S.D., Fischer, H.R., and van der Zwaag, S., *A numerical study into the effects of elongated capsules on the healing efficiency of liquid-based systems*. Computational Materials Science, 2009. 47(2): p. 506-511.
- [51] Sloof, W.G., Pei, R., McDonald, S.A., Fife, J.L., Shen, L., Boatemaa, L., Farle, A.-S., Yan, K., Zhang, X., van der Zwaag, S., Lee, P.D., and Withers, P.J., *Repeated crack healing in MAX-phase ceramics revealed by 4D in situ synchrotron X-ray tomographic microscopy*. Scientific Reports, 2016. 6: p. 23040.



# 6

## **Autonomous high temperature healing of surface cracks in $\text{Al}_2\text{O}_3$ containing $\text{Ti}_2\text{AlC}$ particles**

---

This chapter is under review by the Journal of the American Ceramic Society. Authors: Boatemaa, L., Bosch, M., Farle, A.-S., Bei, G.-P., van der Zwaag, S. and Sloof, W. G.



*In this work the oxidation induced crack healing of  $Al_2O_3$  containing 20 vol. % of  $Ti_2AlC$  MAX phase inclusions as healing particles was studied. The oxidation kinetics of the  $Ti_2AlC$  particles having an average diameter of about  $10\ \mu m$  was studied via thermogravimetry (TG) and/or differential thermal analysis (DTA). Surface cracks of about  $80\ \mu m$  long and  $0.5\ \mu m$  wide were introduced into the composite by Vickers' indentation. After annealing in air at high temperatures the cracks were filled with stable oxides of Ti and Al as a result of the decomposition of the  $Ti_2AlC$  particles. Crack healing was studied at 800, 900 and 1000 °C for 0.25, 1, 4 and 16 h and the strength recovery was measured by 4-point bending. Upon indentation, the bending strength of the samples dropped by about 50 % from  $402 \pm 35$  MPa to  $229 \pm 14$  MPa. This bending strength increased to about 90 % of the undamaged material after annealing at 1000 °C for just 15 min., while full strength was recovered after annealing for 1 h. As the healing temperature was reduced to 900 and 800 °C the time required for full strength recovery increased to 4 and 16 h, respectively. The initial bending strength and the fracture toughness of the composite material were found to be about 19 % lower and 20 % higher than monolithic alumina, respectively, making this material an attractive substitute for monolithic alumina used in high temperature applications.*

## 6.1 Introduction

Sintered alumina is an attractive material for high temperature applications due to its heat, corrosion and wear resistance [1, 2]. The strength and hardness of this material is maintained up to high temperatures [3]. However, the brittle nature of  $Al_2O_3$  results in a poor damage tolerance and hence limits its use [4]. Small cracks or defects can readily lead to abrupt fracture. Autonomous repair of small crack damage may postpone or even mitigate failure. It has been reported that crack damage in alumina can be healed by high temperature oxidation of dispersed SiC dispersed particles [5-10]. Recently, it has been shown that also dispersed TiC particles can heal cracks in alumina [11, 12], but requires much lower oxidation temperatures than SiC particles. Ideally in this case, the crack damage should be healed with alumina, but that is not feasible with oxidation of aluminium due to its low melting temperature (660 °C [13]). Hence, in this work oxidation induced repair of crack damage by dispersed  $Ti_2AlC$  MAX phase particles is explored.

MAX phase ceramics are a group of ternary carbides and nitrides which exhibit the properties of both metals and ceramics and are very promising materials for high temperature applications [14]. They exhibit a unique combination of thermal, mechanical and electrical properties [15, 16] which arises from its crystallographic structure. MAX phase materials have an atomic layered hexagonal crystal structure [17] in which ceramic layers (MX) alternate with layers of pure metals (A), where M is an early transition metal, X is either a carbon or a nitrogen and A (typically Al or Si) is usually a group IIIA or IVA element [17]. The general formula is  $MN+1AXN$ , where N equals 1, 2 or 3. The MX layer provides the material with high temperature strength and stiffness characteristic of ceramics while the relatively weakly bonded A layer provides the material with toughness, ductility, electrical and thermal conductivity values commonly found in metals [18, 19]. Dislocations in these materials glide along the basal planes and plastic deformation occurs by a combination of kink and shear band formation thereby rendering the material damage tolerant [17].

Of the ternary carbides, the  $Ti_2AlC$  phase has generated a lot of interest since its density is lower than that of other ternaries and it is the most stable phase in the Ti-Al-C system [20], making it attractive for lightweight high temperature applications.

Bulk oxidation of  $Ti_2AlC$  has been studied isothermally at high and low temperatures [19, 21]. Due to the selective diffusion of Al, a protective scale consisting of a continuous inner  $Al_2O_3$  layer and a discontinuous outer  $TiO_2$  (rutile) layer is formed [21]. The fast diffusion of Al is due to the energy barrier for migration of Al being lower than that of Ti and therefore Al diffusion is favoured during vacancy migration in  $Ti_2AlC$  [22]. To add to this, the bonding between Ti and C is strongly covalent, whereas the bonding between Ti and Al is relatively weak [23]. Hence, the mobility of Ti and C atoms by vacancy-assisted diffusion is retarded much more than that of Al atoms [24]. The combined effects results in preferential migration of Al atoms in the substrate leading to the formation of a protective  $\alpha$ - $Al_2O_3$  scale.

Cracks in bulk  $Ti_2AlC$  have been shown to self-heal when the material is annealed at high temperatures in an oxygen rich environment. Multiple crack healing has also been demonstrated [25] making  $Ti_2AlC$  a viable healing agent for the (extrinsic) healing of surface cracks in ceramics [7, 26-28]. The suitability of  $Ti_2AlC$  as a healing agent in alumina is in line with the generalised 6-point selection process for healing agents in inert oxide ceramics presented in [13]: (i)  $Ti_2AlC$  has sufficient high melting temperature of 1625 °C [29] making it sinterable, (ii) It expands with a relative volume expansion of about 57 % upon formation of its oxides and (iii) its coefficient of thermal expansion (CTE) is  $8.2 \times 10^{-6} K^{-1}$  [30], this is comparable to that of alumina which ranges between  $7.1 - 8.3 \times 10^{-6} K^{-1}$  [31], therefore only mild thermal stresses generate upon cooling from the sintering temperature. After annealing the  $Ti_2AlC$  healing particles under appropriate conditions both  $TiO_2$  and  $Al_2O_3$  are formed. The latter is the same as the matrix material and will therefore exhibit the same physical and mechanical properties, hence only the viability of  $TiO_2$  as a healing oxide is assessed hereafter. (iv)  $TiO_2$  has a melting temperature of 1857 °C, i.e. it is still a solid when the composite is operated as high as 1400 °C, (v) the work of adhesion between  $TiO_2$  and  $Al_2O_3$  is higher than that between atoms of  $Al_2O_3$  implying a strong bond of the oxide to the matrix [13]. Lastly, due to the difference in CTE tensile stresses may be generated in the  $TiO_2$  healing layer but the calculated value is well below the tensile strength of  $Al_2O_3$  [13]. Hence,  $Ti_2AlC$  passes the primary selection criteria as a suitable healing agent for  $Al_2O_3$  and this potential suitability is thus investigated experimentally in this study.

The  $Ti_2Al_{0.5}Sn_{0.5}C$  is another MAX phase which has been used as a particulate inclusion to heal surface cracks in  $Al_2O_3$  [32]. The composite contained 20 vol. % of the healing particles and complete flexural strength recovery was observed after annealing at 700 °C for 48 h or at 900 °C for 0.5 h for samples containing cracks typically 300  $\mu m$  long and 0.5  $\mu m$  wide. After annealing  $SnO_2$ ,  $TiO_2$ , and  $Al_2O_3$  were detected close to the sample surface, while  $SnO_2$  was not detected deeper inside the crack gap.

The current work concerns the synthesis of  $Ti_2AlC$  MAX phase and a study of its isothermal and non-isothermal oxidation behaviour. The recovery of the fracture strength of  $Al_2O_3$  composites containing 20 vol. % of the  $Ti_2AlC$  particles is investigated by micro indentation, subsequent high temperature annealing and finally 4-point bending at room temperature.

## 6.2 Experimental procedure

The  $Ti_2AlC$  was first synthesized from elemental powders of Ti (5  $\mu m$ , 99.5 % purity from Chempur, Germany), Al (5  $\mu m$ , 99.5 % purity from Alfa Aesar, Germany) and TiC (5  $\mu m$ , 99.5 % purity from Chempur, Germany). The powders were mixed in molar compositions of 1.15:1.1:0.85, respectively, with zirconia balls in a Planetary ball mill PM 100 (Retsch, Germany). A combination of zirconia balls with 10 and 5 mm diameter were used to attain an even mixture with a powder to ball mass ratio of 2:1. The mixing profile was 150 rpm for 4 h in argon with an on and off period of 20:10 min. The mixed powders were packed into 40 mm carbon moulds and reactively sintered by Spark Plasma Sintering (SPS) using a HP D 25 SD furnace (FCT Systeme, Germany). The samples were heated up at 60 °C/min from ambient temperature and held at 1350 °C for 2 h under vacuum. A pressure of 5 MPa was applied from the start until 20 min after 1350 °C was reached, then the pressure was increased to 50 MPa for 1 h and 40 min. The samples were cooled to room temperature at 100 °C/min.

The MAX phase tablets were fragmented using TiN coated drill bits and crushed with a heavy press. The pieces were milled in the planetary ball mill at 300 rpm in isopropanol for 10 h with an on and off period of 20:10 min. To powder the

material to submicron size range, tungsten carbide balls (with 20 and 10 mm diameter) were used. And for a narrow distribution of the particles a size separation was done by suspending the powders in isopropanol. Powders that sunk to the bottom within 1 h were re-milled until an acceptable size was achieved. The size distribution of the milled particles was measured by laser diffraction using a Microtrac 3500 (Microtrac Inc., USA). Subsequently, the composite was made using high purity (4N)  $\text{Al}_2\text{O}_3$  powder (Sumitomo Chemical Co., Ltd, Tokyo, Japan) with an average particle size of 0.2  $\mu\text{m}$  and 20 vol. % of the prepared  $\text{Ti}_2\text{AlC}$  powder. The powders were mixed with isopropanol in a Turbula mixer T2C (Willy A. Bachofen, Switzerland) for 24 h using zirconia balls (with 10 mm and 5mm diameter). After drying, the cake was ground and passed through a 200  $\mu\text{m}$  sieve before sintering. The thoroughly mixed powder was packed into a 40 mm mould and heated at 20  $^\circ\text{C}/\text{min}$  up to 1300  $^\circ\text{C}$  and held for 10 min in argon under 50 MPa in the SPS furnace. After sintering the system was cooled naturally by lifting up the pistons to avoid thermal shocking of alumina. The density of the composite was measured by the Archimedes method using an analytical balance (Mettler Toledo AG-204, Switzerland) according to ASTM B 311-93 [22].

The oxidation behaviour of the synthesized pure  $\text{Ti}_2\text{AlC}$  particles was studied isothermally and non-isothermally by thermogravimetric and/or differential thermal analysis (TGA or DTA) using a SETSYS Evolution 16/18 simultaneous thermal analyser (Setaram, France). This thermal analyser is equipped with an S-type thermocouple which is operable up to 1700  $^\circ\text{C}$ . The  $\text{Ti}_2\text{AlC}$  powder ( $20 \pm 1$  mg) was put into an  $\text{Al}_2\text{O}_3$  crucible (100  $\mu\text{L}$ ) and the furnace was heated from room temperature to 1400  $^\circ\text{C}$  with 4  $^\circ\text{C}/\text{min}$ . For the isothermal experiments, the samples were heated in the furnace from room temperature with 10  $^\circ\text{C}/\text{min}$  under pure  $\text{N}_2$  (with  $\text{H}_2\text{O} < 10$  ppm) supplied at 50 sccm, when the desired temperature was reached the volume of  $\text{N}_2$  was reduced by 20 % and replaced by  $\text{O}_2$  thereby generating synthetic air in the furnace. After the 10 h hold the sample was cooled down with 10  $^\circ\text{C}/\text{min}$  under pure  $\text{N}_2$  flowing at 50 sccm. The mass change curves were corrected for buoyance by performing a thermogravimetric measurement under the same conditions but using an empty crucible.

The oxides formed during isothermal oxidation of the  $\text{Ti}_2\text{AlC}$  particles were analysed with X-ray micro analysis (XMA) and/or X-ray diffraction. A JSM 6500F (JEOL, Japan) scanning electron microscope (SEM) equipped with an energy

dispersive spectrometer (EDS) for X-rays was used for the XMA. The EDS is an UltraDry detector (30 mm<sup>2</sup>) with Noran System Seven software package (Thermo Fisher Scientific, USA) for data acquisition and analysis. The SEM was also used for observing the shape and size of the MAX-Phase particles, the microstructure of the composite, the size of the indents and the cracks. After healing the products that filled the cracks were analysed by XMA.

The phase purity and composition of the samples were analysed by X-ray diffraction using a Bruker D8 Advance diffractometer (Bruker, Germany) equipped with a graphite monochromator. Diffractograms were recorded with Co or Cu K $\alpha$  radiation in the  $2\theta$  range of 20 to 90 ° with a step size of 0.034 ° and a dwell time of 2 s. The diffractograms were processed with the accompanying Diffrac. EVA 4.1 Bruker software.

To study the strength recovery of the alumina with Ti<sub>2</sub>AlC particles, SPS produced samples were machined to 3.0 x 4.0 x 26.0 mm rectangular bars with bevelled edges. The surfaces of the bars were polished with a 1  $\mu$ m diamond suspension in the final step. Cracks were introduced at the centre of the bar by means of Vickers' indentation using a Zwick/Z2.5 hardness tester (Zwick, Germany) under displacement control mode of 0.5  $\mu$ m/s with a maximum load of 30 N held for 20 s at load. The indenter was oriented such that the radial cracks were perpendicular to the tensile stress induced during 4-point bending. Annealing to repair the cracks was carried out in a Carbolite TZF 17/600 furnace (Carbolite Gero, UK) at temperatures ranging from 800 to 1000 °C for 0.25, 1, 4 and 16 h in air. The furnace is equipped with an S-type thermocouple close to the centre of the furnace thereby measuring the true sample temperature in the middle of the furnace.

The bending tests were performed at room temperature using a 4-point self-aligning stage with a 20/10 mm span and hardened steel rollers with 2 mm diameter [23]. The stage was mounted on Instron 5500R (Instron Corporation, USA) material testing frame. A 10 kN load cell was used and the cross-head was displaced at a velocity of 0.5 mm/min. The bar specimen was placed such that its centre coincided with the middle of the spans.

## 6.3 Results and discussion

### 6.3.1 Synthesis of $Ti_2AlC$ particles and the alumina composite

The microstructure of the synthesized  $Ti_2AlC$  is shown in **Figure 6.1**, the light grey areas are the  $Ti_2AlC$  MAX phase and the darker areas are pores and impure phases. X-ray diffraction and X-ray microanalysis of different samples showed that it was mostly high purity single phased  $Ti_2AlC$  while a few samples had small patches of either  $Ti_3AlC$ ,  $TiC$  and/or  $Ti_3AlC_2$  as impurities, see **Figure 6.2**.

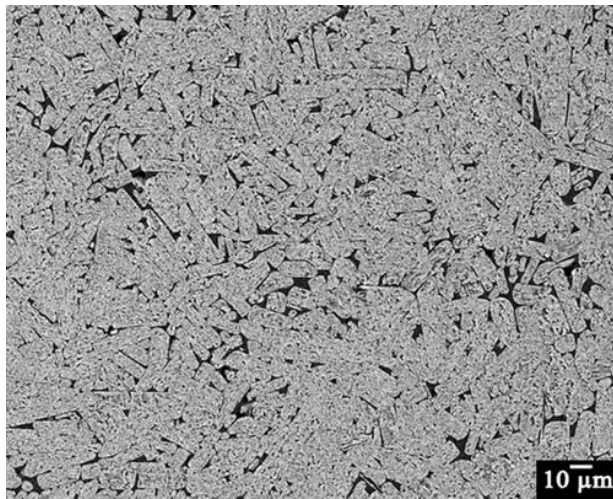


*Figure 6.1: Microstructure of the sintered  $Ti_2AlC$  pellet.*

The formation of the impurities is not fully controlled and understood at this point, but is thought to be related to the melting of the aluminium powder during the sintering process.

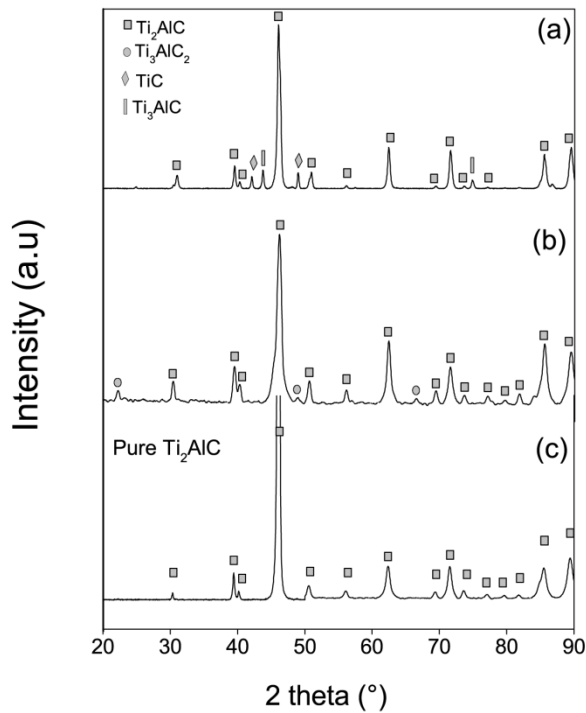


*Figure 6.2: Diffractograms showing purity levels of the sintered material (a)  $Ti_2AlC$  with  $TiC$  and  $Ti_3AlC$  impurities (b)  $Ti_2AlC$  having  $Ti_3AlC_2$  impurities and (c) pure  $Ti_2AlC$ .*

After powdering the  $Ti_2AlC$ , the particle size distribution ranged between 2 and 23  $\mu m$  with an average size of about 10  $\mu m$ . The particles as observed with SEM were irregular, platelet, cylindrical or whisker shaped depicting the underlying laminar structure of the MAX-phase.

It was observed that the elongated MAX phase particles in the composite were evenly dispersed as shown in **Figure 6.3**. At a relatively low magnification these particles appear to be aligned perpendicular to the direction of the applied pressure during sintering, however at a high magnification this alignment is not apparent. XRD and XMA analysis of the composite showed that, no chemical reaction had taken place between the healing particles and the matrix implying that the particles were intact and ready to be used for crack healing when exposed to the appropriate conditions.



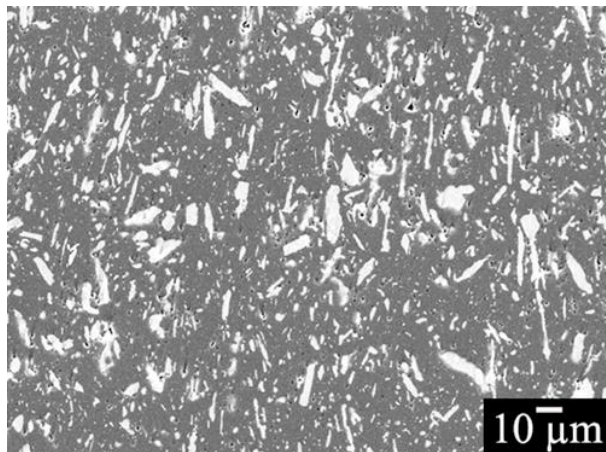


*Figure 6.3: Sintered composite showing homogenous distribution of  $Ti_2AlC$  particles (light) in alumina (dark).*

### 6.3.2 Oxidation kinetics of the $Ti_2AlC$ particles

When  $Ti_2AlC$  powder is exposed to an oxidative environment at high temperatures, Ti and Al oxidise eventually to rutile ( $TiO_2$ ) and alumina ( $Al_2O_3$ ), respectively. To identify which oxide is formed at what temperature a combined non-isothermal TGA and DTA of the  $Ti_2AlC$  powder in dry synthetic air was performed from room temperature to 1400 °C with 4 °C/min. The results presented in **Figure 6.4** show that there are two main peaks one at 580 and another at 910 °C, which are likely to be associated with the formation of  $TiO_2$  and  $Al_2O_3$ , respectively.

To identify which material is formed in the first and second peaks in **Figure 6.4**, non-isothermal oxidation experiments were executed with the  $Ti_2AlC$  powder in dry synthetic air up to 760 °C and 980 °C. X-ray diffraction of the oxidized powder heated up to 760 °C indicates that about 40 % of the starting material remains unoxidized and equal amounts of rutile and anatase ( $TiO_2$ ) were identified including a little amount of  $TiAl$ . When heating the  $Ti_2AlC$  powder up to 980 °C, it is fully converted into  $TiO_2$  and  $Al_2O_3$ . Thus, the remaining powder and any intermediary phase (e.g. anatase and  $TiAl$ ) are converted to rutile and corundum ( $\alpha$ -alumina) in the second peak; cf. **Figure 6.4**

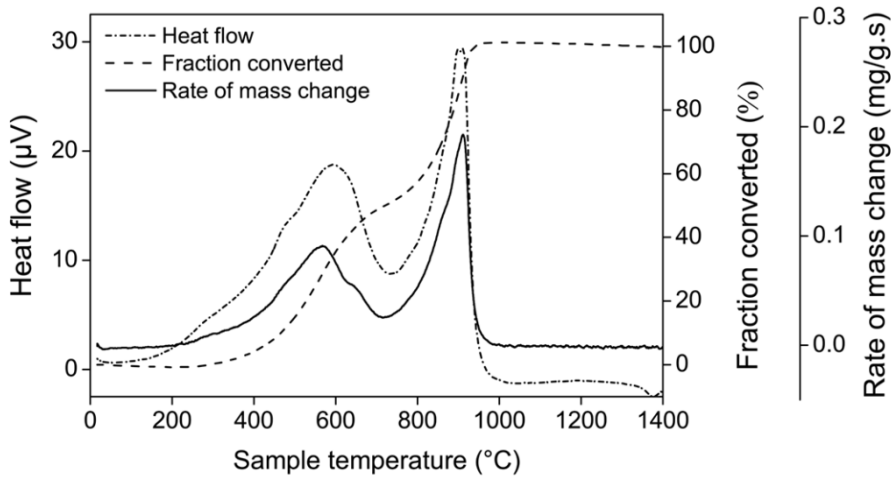


Figure 6.4: Oxidation kinetics of  $Ti_2AlC$  powder in air at  $4\text{ }^\circ\text{C}/\text{min}$ : heat flow, fraction converted and rate of mass change (recorded mass change differentiated) versus temperature.

Also, isothermal thermogravimetric oxidation experiments were performed with the  $Ti_2AlC$  powder in dry synthetic air for 10 h in the temperature range of  $560\text{ }^\circ\text{C}$  to  $1060\text{ }^\circ\text{C}$ ; see Figure 6.5. After each annealing treatment, the oxidation products were identified by XRD.

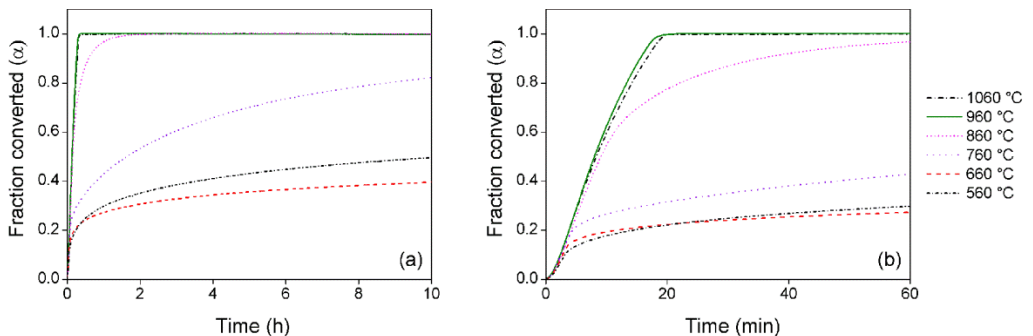
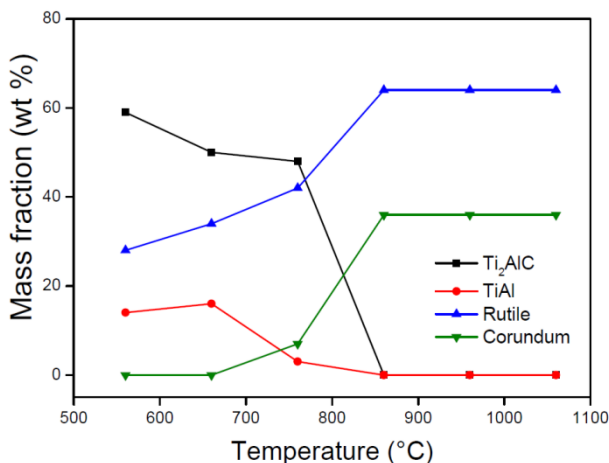


Figure 6.5: (a) Isothermal conversion of  $Ti_2AlC$  at different oxidation temperatures for 10 h in dry synthetic air as determined from thermogravimetric analysis, (b) enlargement showing the first hour.

The oxidation rate of the  $Ti_2AlC$  powder decreases with time due to the increasing thickness of the oxide shell which acts as a strong diffusion barrier as shown in

**Figure 6.5.** Above 800 °C the oxidation proceeds very fast with all  $Ti_2AlC$  being converted in 2 h at 860 °C and in 20 min at 960 and 1060 °C. However, at low temperatures the reaction proceeds at the same rate as at the high temperatures for the first few minutes before deviating to grow at a much slower rate. Thus, after 10 h 80 % of the  $Ti_2AlC$  powder kept at 760 °C had been transformed, while at 660 and 560 °C only 30 % and 40 % had been transformed, respectively.

At 560 °C and 660 °C only rutile and  $TiAl$  were detected with large amounts of the starting material; see **Figure 6.6**. At 760 °C, alumina and rutile are detected with some amount of the MAX phase. At 860 °C and above only rutile and alumina are detected. The formation of  $TiAl$  is due to simultaneous selective oxidation of carbon (transformed into  $CO_2$  as observed with mass spectrometry) and formation of  $TiO_2$ .



**Figure 6.6:** Mass fractions of the  $Ti_2AlC$  starting material and the oxidation products at different temperatures after 10 h of oxidation in dry synthetic air.

A deviation in the rate of the oxide growth at 660 °C is observed after about 20 min of exposure leading to only 30 % of the material being converted, while at 560 °C almost 40 % of the powder was transformed at the end of 10 h of oxidation period; see **Figure 6.5b**. This irregularity is likely due to the initial formation of anatase at 560 °C (according to XRD results of the non-isothermal oxidation) which grows faster [24] and is a porous and non-protective oxide [34]. At higher oxidation temperatures (660 °C and above) rutile is formed which hinders 'fast oxidation' of the underlying material [24].

### 6.3.3 Mechanical properties of the $\text{Al}_2\text{O}_3\text{-Ti}_2\text{AlC}$ composite

Surface cracks were introduced in the composite material by Vickers indentations with varying load. Application of a load of 20 N resulted in a crack of about  $80 \pm 5 \mu\text{m}$  in length ( $2c$ ), at the same load the crack registered in the alumina containing 20 vol. % of TiC composite was  $100 \pm 8 \mu\text{m}$  [11]. The relationships between load and crack length for an  $\text{Al}_2\text{O}_3$  matrix containing either  $\text{Ti}_2\text{AlC}$  or TiC are plotted in **Figure 6.7**. From these data the fracture toughness of the alumina with 20 vol. % TiC was evaluated to be  $4.3 \pm 0.1 \text{ MPa m}^{1/2}$  [11], while that of the alumina with  $\text{Ti}_2\text{AlC}$  is  $4.9 \pm 0.5 \text{ MPa m}^{1/2}$  indicating an increased resistance to fracture. This observed toughening behaviour is brought about by the mechanical behaviour and properties of both the matrix and the incorporated healing agent [35]. However, the initial average bending strength of the  $\text{Al}_2\text{O}_3$  with 20 vol.%  $\text{Ti}_2\text{AlC}$  is smaller than that of the  $\text{Al}_2\text{O}_3$  with 15 vol. % TiC composite,  $415 \pm 28$  versus  $526 \pm 90 \text{ MPa}$  [12]. The size of the TiC healing particles is on average much smaller than that of  $\text{Ti}_2\text{AlC}$ , i.e. 2 versus  $10 \mu\text{m}$ . It can be assumed that the strength of the composite decreases as the size of the healing particles increases [36].

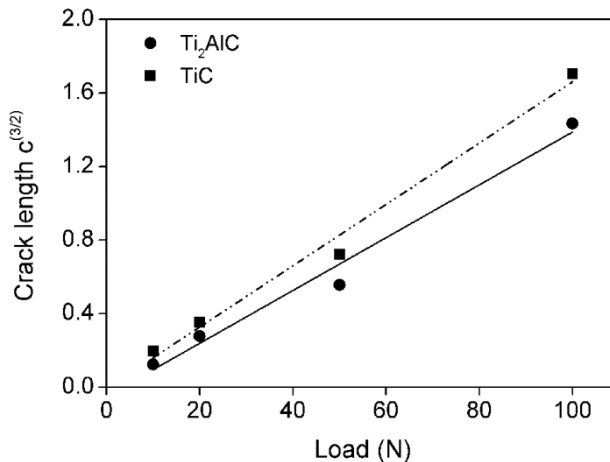


*Figure 6.7: Comparison of the length of Vickers' indentation induced cracks with length  $c$  generated in  $\text{Al}_2\text{O}_3/\text{Ti}_2\text{AlC}$  and  $\text{Al}_2\text{O}_3/\text{TiC}$  composite [23].*

Depending on the direction of a crack and the local stress intensity factors a crack may be bridged, deflected or arrested (**Figure 6.8**) as it approaches a second phase component [37]. The MAX phase exhibits some ductility leading to absorption of

energy at the tip of an approaching crack, thereby blunting the crack tip (**Figure 6.8a**). Its whisker like shape may bridge the cracks (**Figures 6.8b and 6.8c**) causing a significant shielding effect [38].

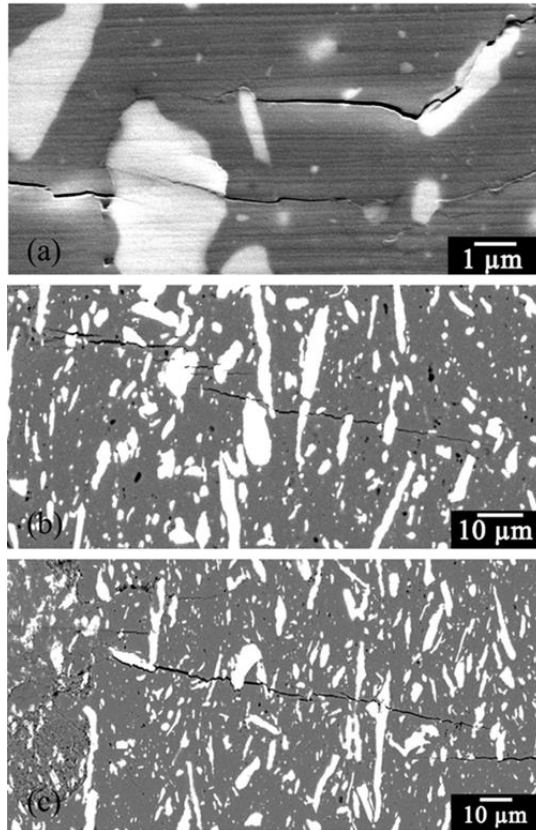


*Figure 6.8: Toughness enhancement mechanisms of  $Ti_2AlC$  in  $Al_2O_3$ . SEM images (a) Cracks blunted by particle, (b) and (c) Cracks intersecting a particle or diverted along the particle-matrix interface.*

In contrast, crack driving forces are amplified in the wake of softer particles leading to anti-shielding effects [39]. Finally, micromechanical models for crack particle interaction in brittle particulate composites [39] have shown that a crack in the matrix is attracted to the particles if the elastic modulus of the particles is lower than that of the matrix. In this case the elastic modulus of  $Ti_2AlC$  is 277 GPa [40], and it is lower than that of alumina which is between 380 - 410 GPa [41], hence cracks are

attracted to the  $\text{Ti}_2\text{AlC}$  particles. It is worth pointing out that growing of cracks through the particles or along the matrix-particle interfaces are acceptable as in both cases the particle content is exposed directly to the crack volume which is essential for the self-healing reaction to take place.

## 6.4 Strength Recovery of the $\text{Al}_2\text{O}_3\text{-Ti}_2\text{AlC}$ composite

The strength values of the virgin composite samples, the damaged samples and the healed composites as measured by 4-point bending tests are shown in **Figure 6.9**. It is noted that the long axes of the elongated  $\text{Ti}_2\text{AlC}$  healing particles are aligned perpendicular to the sample surface at which the load is applied. Each data point represents an average of 8 samples. The initial average strength of the composite was  $415 \pm 28$  MPa.

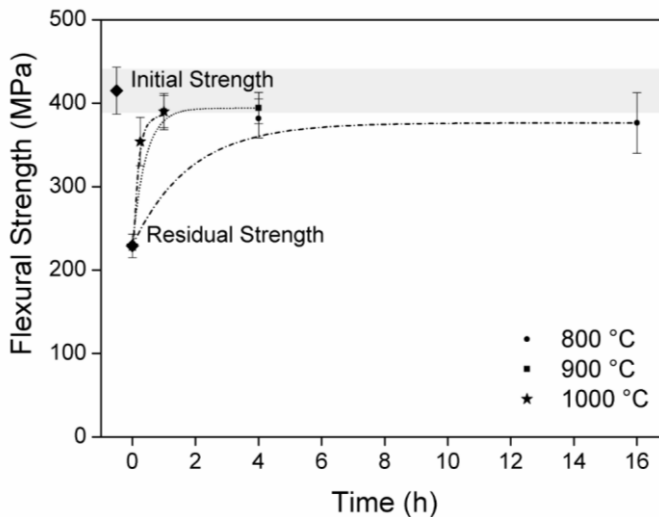


*Figure 6.9: Flexural strength of studied materials attained by 4-point bending.*

For the indented samples the strength decreased to  $229 \pm 14$  MPa which is about 50 % of the initial strength. After annealing at 1000 °C for 15 min the strength significantly increased to  $354 \pm 29$  MPa which is about 90 % of the initial strength. After 1 h at the same temperature full strength was almost regained at 97 % and after 4 h complete strength was recovered. There was no significant difference in the

strength regained for samples kept at 900 °C for 1 and 4 h as strength regain of 94 and 95 % was registered, respectively. Similarly, at 800 °C the strength recovered was 92 and 90 %, for 4 and 16 h respectively. Most healed samples fractured next to the healed crack, indicating a strong adhesion between the healing oxide and the  $\text{Al}_2\text{O}_3$  matrix. However, samples with cracks that were not fully healed fractured along the original crack path, since the unfilled parts of the crack acts as initiation sites.

Surface observations of the healed samples by SEM in the as-annealed state (**Figure 6.10a**) showed that upon annealing at 800 °C for 4 h there was significant local volume expansion at the site of some  $\text{Ti}_2\text{AlC}$  particles (as expected) but surprisingly not all particles showed this volume expansion. This may be because the basal planes which enhance outward diffusion of the elements may be aligned or tilted away from the surface of the sample. Upon polishing the sample, it is clear that crack filling starts at the particles intersected by the crack and it is also clear that the cracks are not fully filled (**Figure 6.10b**). This is somewhat remarkable given the high strength recovery of 92 %. The high strength recovery is attributed to bridging of the gaps by oxides formed locally from particles exposed to the crack. Recent work on in-situ monitoring on monolithic  $\text{Ti}_2\text{AlC}$  material [42] proved that even for reactive materials crack filling can occur well below the external surface.

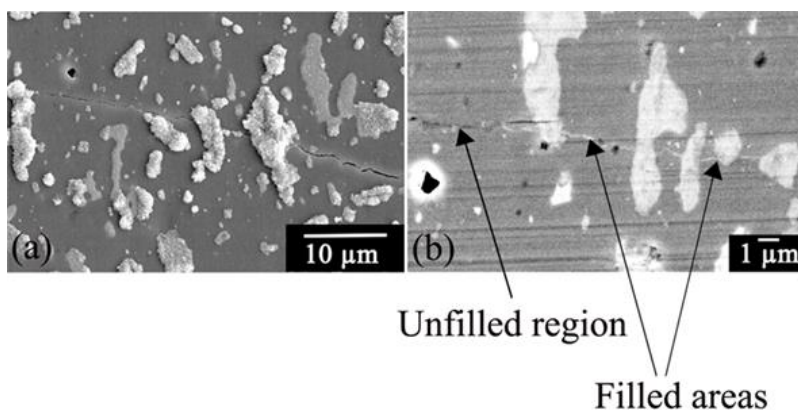


*Figure 6.10: SEM images of sample kept at 800 °C for 4 h (a) unpolished surface (b) polished surface. The crack is partially filled as indicated by the arrows.*

After annealing at  $900\text{ }^\circ\text{C}$  for 1 h cracks were found to be seemingly fully filled with  $\text{TiO}_2$  and small amounts of  $\text{Al}_2\text{O}_3$ . Upon annealing at  $1000\text{ }^\circ\text{C}$  for 1 h cracks were found to be fully filled with  $\text{Al}_2\text{O}_3$  and  $\text{TiO}_2$ . **Figure 6.11** shows the same area of a sample captured before oxidation (a), after oxidation at  $1000\text{ }^\circ\text{C}$  for 1 h (b) and after the surface is polished to show the extent of filling attained (c).

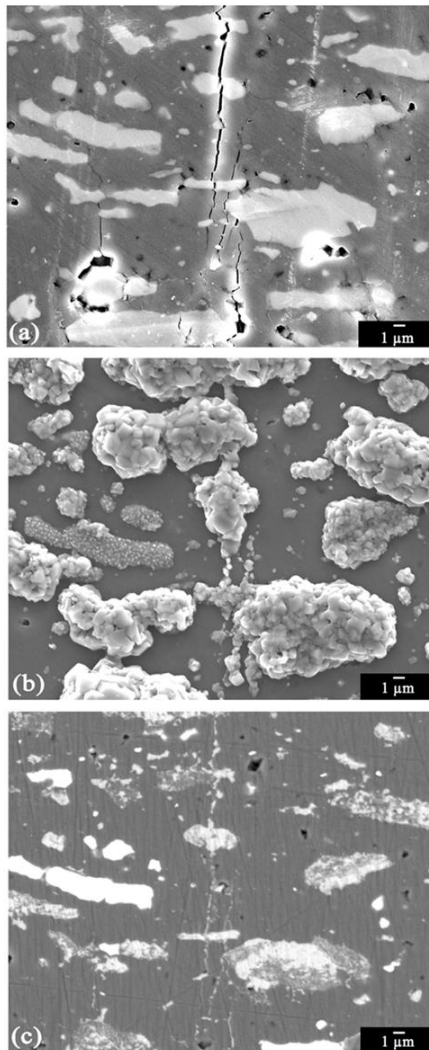


*Figure 6.11: SEM images of the same crack area before and after healing at  $1000\text{ }^\circ\text{C}$  for 1 h in air. (a) Before oxidation (b) After oxidation before polishing (c) Polished surface showing fully filled cracks.*



The completely filled crack path in the healed sample can be identified as a line filled with  $\text{TiO}_2$  (light) and interrupted by  $\text{Al}_2\text{O}_3$  (dark). The set of SEM observations clearly demonstrate the lateral expansion of the oxides formed at the healing particle into the crack which is not in direct contact with a particle. This lateral expansion of the oxides formed at the healing particles has often been assumed, but had not been demonstrated as convincingly as in this set of micrographs.

At the studied temperatures and conditions, no reaction was observed between alumina and the dispersed  $\text{Ti}_2\text{AlC}$  particles or the healing agents ( $\text{TiO}_2$  and  $\text{Al}_2\text{O}_3$ ). Therefore, the healing ability of the  $\text{Ti}_2\text{AlC}$  particles is not hindered in any way by an intermediary reaction. However, the rate of oxidation of the embedded particles will only be slower due to the reduced reaction area in comparison to the free particles.

### 6.5 Stability of the dispersed MAX-phase in the $\text{Al}_2\text{O}_3$ matrix

The success of the extrinsic healing approach as used in this research depends on the healing particle remaining unaffected by the exposure conditions of the sample and not decomposing before a crack intersected the particle. Such an unprompted reaction would not only lead to a reduction or loss of the healing potential but would also induce local stresses in the  $\text{Al}_2\text{O}_3$  matrix. This may lead to a reduction of the tensile strength and in the limit even to spontaneous crack formation. To examine the stability of the healing particles in the (non-oxygen permeable) alumina matrix cross section of undamaged samples kept at 1000 °C in ambient air for 64, 128 and 256 h have been made, **Figure 6.12a** and **b** show the microstructures of the samples kept at 64 and 256 h, respectively. The micrographs show that at the surface a dense layer of  $\text{Al}_2\text{O}_3$  formed first but also some  $\text{TiO}_2$  particles were observed on the surface.

Most importantly, the cross sections showed that even for the longest exposure time of 256 h a depletion layer of less than 20  $\mu\text{m}$  from the surface is observed. The  $\text{Ti}_2\text{AlC}$  particles within this layer do not have the stoichiometry of the starting material due to the diffusion and subsequent oxidation of Ti, Al and/or C at the

surface. Beyond this depth, XMA confirms that the MAX phase particles retain their original stoichiometry of 2:1:1 of Ti:Al:C. This depth of depletion appears to coincide with the maximum size of the MAX phase particles which is  $23\ \mu m$  and confirm that the diffusivity of oxygen in alumina is very low [43] and hence alumina acts as a strong barrier against oxidation of particles embedded in the depth of the composite. The orientation of the basal planes of a particle to the surface may also influence the rate at which Al and Ti diffuse out. While it is highly desirable that the affected zone near a free surface is restricted to the diameter of the healing particle (i.e., the particles do not react unless intersected by a crack), the combined effect of particle size and particle volume fraction determine and limit the amount of material to be deposited in the open crack. This dependence has been analysed numerically in detail for healing particles in polymeric matrices [44], but the analysis equally apply to the current case of high temperature ceramics.

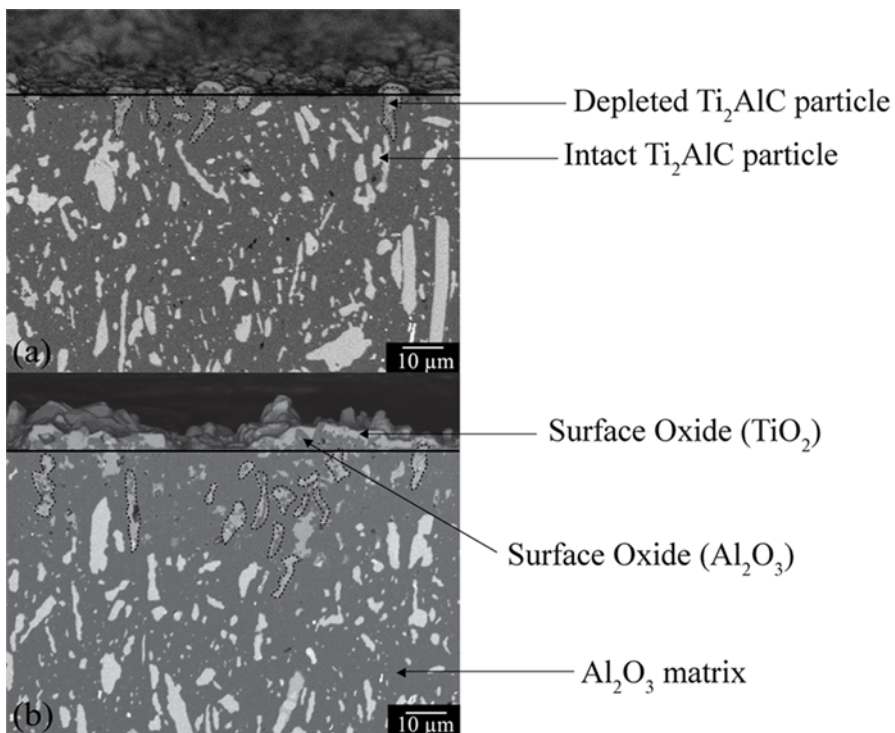


Figure 6.12: SEM cross sectional view of the composite at  $1000\ ^\circ C$  in air for (a) 64 and (b) 256 h showing the depletion of Ti and Al from the  $Ti_2AlC$  particles close to the sample surface.

## 6.6 Conclusions

The oxidation behaviour of  $Ti_2AlC$  particles and its ability to heal surface cracks in  $Al_2O_3$  containing 20 % by volume was investigated. Non-isothermal analysis revealed that oxidation starts at 600 °C, but the temperature for efficient healing is between 800 and 1000 °C. The  $Ti_2AlC$  material is a suitable healing agent for alumina and composite materials containing 20 vol. % of 10 micron sized  $Ti_2AlC$  particles as there was significant tensile strength recovery at 900 °C for 1 h or 1000 °C for 15 min. At these temperatures, the cracks are filled by both  $TiO_2$  and  $Al_2O_3$ . Healing at 800 °C required 16 h.

Most importantly, the results showed that the particles embedded in the matrix and not touching the outer sample surface did not decompose upon long term high temperature exposure and remained potentially active in the non-oxygen permeable  $Al_2O_3$  matrix unless intersected by a crack. While not explored for times longer than 256 h at 1000 °C this is a very important finding indicative that  $Al_2O_3$  ceramics filled with  $Ti_2AlC$  particles may have long term self-healing ability and can be of industrial relevance.

## Acknowledgments

This research was sponsored by the People Programme (Marie Curie ITN) of the European Union's seventh framework programme, FP7, grant number 290308 (SHeMat). The authors are indebted to Ir. Ruud Henkdricks for performing XRD analysis and to Dr. A.C. Riemslog for assistance with mechanical testing.

## References

- [1] Tzenov, N.V. and Barsoum, M.W., *Synthesis and characterization of  $Ti_3AlC_2$* . Journal of the American Ceramic Society, 2000. 83(4): p. 825-832.
- [2] Barsoum, M.W., Salama, I., El-Raghy, T., Golczewski, J., Seifert, H.J., Aldinger, F., Porter, W.D., and Wang, H., *Thermal and electrical properties of  $Nb_2AlC$ ,  $(Ti, Nb)_2AlC$  and  $Ti_2AlC$* . Metallurgical and Materials Transactions A, 2002. 33(9): p. 2775-2779.
- [3] Barsoum, M.W., *Encyclopedia of materials: Science and technology*, in Elsevier, Buschow, K.H.J., et al., Editors. 2006. p. 1-11.
- [4] Barsoum, M.W.,  *$M_{N+1}AX_N$  phases: A new class of solids; thermodynamically stable nanolaminates*. Progress in Solid State Chemistry, 2000. 28(1-4): p. 201-281.
- [5] Barsoum, M.W., *Physical Properties of the MAX Phases A2 - Buschow, K.H. Jürgen*, in *Encyclopedia of materials: Science and technology (Second Edition)*, Cahn, R.W., et al., Editors. 2006, Elsevier: Oxford. p. 1-11.
- [6] Wang, X.H. and Zhou, Y.C., *High-Temperature oxidation behavior of  $Ti_2AlC$  in Air*. Oxidation of Metals, 2003. 59(3): p. 303-320.
- [7] Pietzka, M.A. and Schuster, J.C., *Summary of constitutional data on the Aluminum-Carbon-Titanium system*. Journal of Phase Equilibria, 1994. 15(4): p. 392-400.
- [8] Song, G.M., Schnabel, V., Kwakernaak, C., van der Zwaag, S., Schneider, J.M., and Sloof, W.G., *High temperature oxidation behaviour of  $Ti_2AlC$  ceramic at 1200 °C*. Materials at High Temperatures, 2012. 29(3): p. 205-209.
- [9] Kun, L., Yuan, Q., and Ji-Zheng, D., *First-principles investigation of the vacancy effect on the electronic properties in  $M_2AlC$  ( $M = V$  and  $Nb$ )*. AIP Advances, 2014. 4(10): p. 107137.
- [10] Zhou, Y. and Sun, Z., *Electronic structure and bonding properties of layered machinable  $Ti_2AlC$  and  $Ti_2AlN$  ceramics*. Physical Review B, 2000. 61(19): p. 12570-12573.
- [11] Wang, X.H. and Zhou, Y.C., *Layered machinable and electrically conductive  $Ti_2AlC$  and  $Ti_3AlC_2$  ceramics: A review*. Journal of Materials Science & Technology, 2010. 26(5): p. 385-416.
- [12] Li, S., Song, G., Kwakernaak, K., van der Zwaag, S., and Sloof, W.G., *Multiple crack healing of a  $Ti_2AlC$  ceramic*. Journal of the European Ceramic Society, 2012. 32(8): p. 1813-1820.

- [13] Yao, F., Ando, K., Chu, M.C., and Sato, S., *Static and cyclic fatigue behaviour of crack-healed Si<sub>3</sub>N<sub>4</sub>/SiC composite ceramics*. Journal of the European Ceramic Society, 2001. 21(7): p. 991-997.
- [14] Lee, S.K., Ono, M., Nakao, W., Takahashi, K., and Ando, K., *Crack-healing behaviour of mullite/SiC/Y<sub>2</sub>O<sub>3</sub> composites and its application to the structural integrity of machined components*. Journal of the European Ceramic Society, 2005. 25(15): p. 3495-3502.
- [15] Kim, B.S., Ando, K., Chu, M.C., and Saito, S., *Crack-healing behavior of monolithic alumina and strength of crack-healed member*. Zairyo/Journal of the Society of Materials Science, Japan, 2003. 52(6): p. 667-673.
- [16] Ando, K., Ono, M., Nakao, W., Takahashi, K., and Saito, S., *Increase of structural integrity machined alumina/SiC using crack-healing*, in *Ceramic Transactions*. 2006. p. 155-162.
- [17] Boatemaa, L., Kwakernaak, C., van der Zwaag, S., and Sloof, W.G., *Selection of healing agents for autonomous healing of alumina at high temperatures*. Journal of the European Ceramic Society, 2016. 36(16): p. 4141-4145.
- [18] Potanin, A.Y., Loginov, P.A., Levashov, E.A., Pogozhev, Y.S., Patsera, E.I., and Kochetov, N.A., *Effect of mechanical activation on Ti<sub>3</sub>AlC<sub>2</sub> MAX phase formation under self-propagating high-temperature synthesis*. Eurasian Chemicotechnological Journal 2015. 17(3): p. 233-242.
- [19] Barsoum, M.W., El-Raghy, T., and Ali, M., *Processing and characterization of Ti<sub>2</sub>AlC, Ti<sub>2</sub>AlN, and Ti<sub>2</sub>AlC<sub>0.5</sub>N<sub>0.5</sub>*. Metallurgical and Materials Transactions A, 2000. 31(7): p. 1857-1865.
- [20] Martienssen, W. and Warlimont, H., *Springer handbook of condensed matter and materials data*. 2006: Springer Science & Business Media.
- [21] Bei, G.P., Pedimonte, B.J., Pezoldt, M., Ast, J., Fey, T., Goeken, M., and Greil, P., *Crack Healing in Ti<sub>2</sub>Al<sub>0.5</sub>Sn<sub>0.5</sub>C-Al<sub>2</sub>O<sub>3</sub> Composites*. Journal of the American Ceramic Society, 2015. 98(5): p. 1604-1610.
- [22] *American Society for Testing of Materials B311-93 Test method for density determination for powder metallurgy (P/M) materials containing less than two percent porosity*. 1997 (International A).
- [23] Yoshioka, S., Boatemaa, L., van der Zwaag, S., Nakao, W., and Sloof, W.G., *On the use of TiC as high-temperature healing particles in alumina based composites*. Journal of the European Ceramic Society, 2016. 36(16): p. 4155-4162.

- [24] Shimada, S. and Kozeki, M., *Oxidation of TiC at low temperatures*. Journal of Materials Science, 1992. 27(7): p. 1869-1875.
- [25] Farle, A., Boatemaa, L., Shen, L., Gövert, S., Kok, J.B.W., Bosch, M., Yoshioka, S., van der Zwaag, S. and Sloof, W.G., *Demonstrating the self-healing behaviour of some selected ceramics under combustion chamber conditions*. Smart Materials and Structures, 2016. 25(8): p. 084019.
- [26] Chin, Y.-L., Tuan, W.-H., Huang, J.-L., and Wang, C.-A., *Toughening alumina with layered Ti<sub>3</sub>SiC<sub>2</sub> inclusions*. Journal of Alloys and Compounds, 2010. 491(1-2): p. 477-482.
- [27] Chaubey, A., Konda Gokuldoss, P., Wang, Z., Scudino, S., Mukhopadhyay, N., and Eckert, J., *Effect of particle size on microstructure and mechanical properties of al-based composite reinforced with 10 vol.% mechanically alloyed Mg-7.4%Al particles*. Technologies, 2016. 4(4): p. 37.
- [28] Rattanachan, S., Miyashita, Y., and Mutoh, Y., *Microstructure and fracture toughness of a spark plasma sintered Al<sub>2</sub>O<sub>3</sub>-based composite with BaTiO<sub>3</sub> particulates*. Journal of the European Ceramic Society, 2003. 23(8): p. 1269-1276.
- [29] Withers, P.J., *Fracture mechanics by three-dimensional crack-tip synchrotron X-ray microscopy*. Philosophical transactions. Series A, Mathematical, physical, and engineering sciences, 2015. 373(2036): p. 20130157.
- [30] Ponnusami, S.A., Turteltaub, S., and van der Zwaag, S., *Cohesive-zone modelling of crack nucleation and propagation in particulate composites*. Engineering Fracture Mechanics, 2015. 149: p. 170-190.
- [31] Barsoum, M.W. and Radovic, M., *Elastic and mechanical properties of the MAX phases*. Annual Review of Materials Research, 2011. 41(1): p. 195-227.
- [32] Auerkari, P., *Mechanical and physical properties of engineering alumina ceramics*. 1996: Technical Research Centre of Finland Finland.
- [33] Sloof, W.G., Pei, R., McDonald, S.A., Fife, J.L., Shen, L., Boatemaa, L., Farle, A.-S., Yan, K., Zhang, X., van der Zwaag, S., Lee, P.D., and Withers, P.J., *Repeated crack healing in MAX-phase ceramics revealed by 4D in situ synchrotron X-ray tomographic microscopy*. Scientific Reports, 2016. 6: p. 23040.
- [34] Heuer, A.H., Hovis, D.B., Smialek, J.L., and Gleeson, B., *Alumina Scale Formation: A New Perspective*. Journal of the American Ceramic Society, 2011. 94: p. s146-s153.

- [35] Mookhoek, S.D., Fischer, H.R., and van der Zwaag, S., *A numerical study into the effects of elongated capsules on the healing efficiency of liquid-based systems*. Computational Materials Science, 2009. 47(2): p. 506-511.

# 7

## **Demonstrating the self-healing behaviour of some selected ceramics under combustion chamber conditions**

---

This chapter has been published in Smart Mater. Struct. 25 2016, 084019 p 1-10. Authors: Farle, A., Boatemaa, L., Shen, L., Goevert, S., Kok, J. B. W., Bosch, M., Yoshioka, S., van der Zwaag, S. and Sloof, W. G.



Closure of surface cracks by self-healing of conventional and MAX Phase ceramics under realistic turbulent combustion chamber conditions is presented. Three ceramics namely;  $Al_2O_3$ ,  $Ti_2AlC$  and  $Cr_2AlC$  are investigated. Healing was achieved in  $Al_2O_3$  by even dispersion of TiC particles throughout the matrix as the MAX phases,  $Ti_2AlC$  and  $Cr_2AlC$  exhibit intrinsic self-healing. Fully dense samples (> 95 %) were sintered by spark plasma sintering and damage was introduced by indentation, quenching and low perpendicular velocity impact methods. The samples were exposed to the oxidizing atmosphere in the post flame zone of a turbulent flame in a combustion chamber to heal at temperatures of approx. 1000 °C at low  $pO_2$  levels for 4 h. Full crack-gap closure was observed for cracks up to 20 mm in length and more than 10  $\mu m$  in width. The reaction products (healing agents) were analysed by SEM, XMA and XRD. A semi-quantification of the healing showed that cracks in  $Al_2O_3/TiC$  composite (width 1  $\mu m$  and length 100  $\mu m$ ) were fully filled with  $TiO_2$ . In  $Ti_2AlC$  large cracks were fully filled with a mixture of  $TiO_2$  and  $Al_2O_3$ . And in the  $Cr_2AlC$ , cracks of up to 1.0  $\mu m$  in width and more than 100  $\mu m$  in length were also completely filled with  $Al_2O_3$ .

## 7.1 Introduction

In recent years the possibility to oxidatively heal surface cracks in high temperature ceramics and metallo-ceramics and to restore mechanical strength at least once has been demonstrated in quite a number of laboratory studies [1-3]. In these laboratory studies relatively high oxygen potentials (comparable to those in heated air) and stagnant air were imposed and the samples were not exposed to any mechanical vibration during the healing treatment. These conditions differ significantly from the prevailing conditions (low partial pressure, very high gas flow velocities and extensive mechanical vibrations) in combustion chambers, where such self-healing ceramics are supposed to be used [4]. The work presented here describes the self-healing behaviour of three grades of self-healing ceramics under realistic combustion chamber conditions. The materials to be tested are an extrinsic self-healing system (alumina containing TiC particles as healing agent) and two intrinsic self-healing metallo-ceramics ( $\text{Cr}_2\text{AlC}$  and  $\text{Ti}_2\text{AlC}$ ), for which attractive self-healing behaviour under laboratory conditions had been demonstrated previously.

The early research on self-healing high temperature ceramics focussed on so-called *extrinsic* self-healing concepts, in which the crack filling reaction is due to the presences of discrete reactive particles homogeneously distributed in an inert ceramic matrix [4-6]. When a crack is formed in the matrix, the reactive particles in the path of the crack are dissected and oxygen from the environment flowing through the crack can react with the healing particle. In case the reaction product has a larger specific volume than the original particle the excess volume can fill the crack and restore mechanical contact between both opposing crack faces. In case the reaction product adheres relatively well to the matrix material, the filling of the crack not only leads to its sealing but also to the restoration of the tensile strength of the once broken sample. The early work focused on the use of SiC particles or fibres to heal  $\text{Si}_3\text{N}_4$ , mullite and alumina matrices [5, 7, 8] as SiC has a desirable oxidation behaviour leading to the formation of  $\text{SiO}_2$  which has a good bond strength to many ceramic matrices. By using SiC particles with a size of about  $0.3\ \mu\text{m}$  the bending strength of  $\text{Si}_3\text{N}_4/\text{SiC}$  composites could be recovered more or less completely by healing between  $900\text{--}1400\ \text{°C}$  for 1 h in air. For the optimum healing temperature of  $1300\ \text{°C}$  the specimen fractured even outside the healed zone [5]. Similarly, surface cracks of diameter  $100\text{--}200\ \mu\text{m}$  in mullite were completely healed after heat

treatment at 1300 °C for 1 h in air. The crack-healed zone even had a bending strength  $150 \pm 30$  MPa higher than that of the as received material [7].

The optimal volume fraction of granular healing particles was found to be between 15 and 30 % [9-11]. In recent work it has been shown that SiC whiskers rather than granular SiC particles can improve the healing capabilities even further [8] and restore not only strength but also fracture toughness. It was shown that surface cracks with a length of 100  $\mu\text{m}$  could be healed in a composite containing 20 vol. % of 30 -100  $\mu\text{m}$  long SiC whiskers. The fracture toughness increased from 3-4 MPa  $\text{m}^{1/2}$  for monolithic alumina to 5.6 MPa  $\text{m}^{1/2}$ , and it was reported that the average bending strength after healing is 970 MPa as compared to 1000 MPa for the virgin material. Since then, systematic studies have been done on the effect of crack healing conditions on the mechanical behavior of the crack healed zone [4, 12] the maximum crack size which can completely be healed [13] and the crack healing behavior under static or cyclic loading and crack healing potential [5, 14].

While SiC additions work rather well, the temperature to induce optimal healing is rather high (1300 °C) and there is a need for lower healing temperatures. TiC has recently been identified and an attractive alternative [15]. The potential of TiC in healing alumina was assessed based on detailed theoretical analysis of the healing reaction and the intrinsic properties of the reaction products  $\text{TiO}_2$  (rutile). A systematic analysis of its thermodynamic stability, relative volume expansion, work of adhesion between the healing agent and the matrix, and a comparison of the coefficient of thermal expansion between the matrix and the healing oxide revealed TiC is indeed a potentially attractive healing particle for extrinsic self-healing ceramic systems. Experimentally this was proven when surface cracks of length 100  $\mu\text{m}$  in  $\text{Al}_2\text{O}_3$ -TiC composites containing 30 vol. % TiC particles showed complete tensile strength recovery by annealing for 1 h at 800 °C in air.

The alternative approach to *extrinsic* self-healing systems in which the healing reaction is due to the intentional addition of a sacrificial phase is that of *intrinsic* self-healing systems in which the material itself can locally undergo healing reactions. In 2008 metallo-ceramic MAX phases, in particular  $\text{Ti}_3\text{AlC}_2$ , were shown to demonstrate significant self-healing when exposed to high temperatures in oxygen containing atmospheres [16, 17]. The underlying mechanism in the healing reaction is the selective oxidation of the A element in the MAX phases, such as  $\text{Ti}_3\text{AlC}_2$  and

Ti<sub>2</sub>AlC as well as Cr<sub>2</sub>AlC [16, 18, 19]. Cracks in Ti<sub>2</sub>AlC MAX phase ceramics of up to some millimetres in length and about 5 µm in width can be healed by oxidation at 1100 °C in air within 2 h [17, 20] leading to full strength recovery. Also cracks running along the same path as previously healed cracks can be restored several times [17]. The healing is due to the extensive formation of Al<sub>2</sub>O<sub>3</sub> in the crack with minor amounts of TiO<sub>2</sub> phase. Cr<sub>2</sub>AlC MAX phase also shows good self-healing behaviour but the reaction rates are a bit slower. Yet the guaranteed absence of the weak TiO<sub>2</sub> in the healed cracks may lead to higher strength values for the healed material [21]. Hence Ti<sub>2</sub>AlC and Cr<sub>2</sub>AlC were selected for testing under combustion chamber conditions as both materials meet all requirements postulated for successful healing of crack damage [22], e.g. preferential oxidation and fast diffusion of the A-element, volume expansion upon oxidation and adhesion of the healing product to the matrix. As earlier studies [19, 23] on the MAX phase materials have shown that the healing kinetics and the mode of filling of the cracks depends on the grain size, Cr<sub>2</sub>AlC samples were produced having two different average grain sizes. The influence of commonly present impurities, such as TiC and Ti<sub>x</sub>Al<sub>y</sub> in Ti<sub>2</sub>AlC are considered by producing MAX phases of different purity grades.

Apart from their self-healing potential MAX phases have interesting mechanical and physical properties, which make them interesting materials for combustion chambers: They are stable up to high temperatures and corrosion resistant [1-3, 24]. Their high thermal conductivity makes them thermal shock resistant [25] and their static strength is maintained up to high temperatures, above which creep will become the limiting factor [26, 27].

In the present work we will demonstrate the self-healing behaviour of three promising self-healing ceramics (alumina with TiC as healing agent, phase pure and impure Ti<sub>2</sub>AlC and fine and coarse grained Cr<sub>2</sub>AlC) under real combustion chamber conditions. First the synthesis of these ceramics will be outlined. Then their microstructure and oxidation behaviour will be discussed. Next, different methods to create crack damage are presented. Finally, the results of testing the self-healing ceramics with crack damage under real combustion conditions are evaluated.

## 7.2 Materials and methods

### 7.2.1 Synthesis

Discs of the self-healing ceramics  $\text{Al}_2\text{O}_3/\text{TiC}$ ,  $\text{Ti}_2\text{AlC}$  and  $\text{Cr}_2\text{AlC}$  with a diameter of 20 mm and a thickness of about 5 mm were prepared by spark plasma sintering (SPS). The powders used to sinter the materials are listed in **Table 7.1**. These powders were mixed with the molar ratios specified in **Table 7.2** using a Turbula T2C Mixer (Willy A. Bachofen, Switzerland), and 5 mm alumina balls for 24 to 48 h. The ball to powder weight ratio was about 3:1. The powder mixtures for  $\text{Ti}_2\text{AlC}$  and  $\text{Al}_2\text{O}_3/\text{TiC}$  were sintered directly in the SPS furnace (HP D 25 SD, FCT Systeme GmbH, Germany) using a graphite mould with an inner diameter of 20 mm under Argon atmosphere or in vacuum.

*Table 7.1: Starting powders for synthesis and sintering.*

Powder	Purity (%)	Particle size ( $\mu\text{m}$ )	Supplier
$\text{Al}_2\text{O}_3$	$\geq 99.99$	0.2	Sumitomo Chemicals, Japan
TiC	98	4.5	Alfa Easer, UK
Ti	$> 99.5$	100	TLS Technik GmbH & CO., Germany
Al	99.8	45	TLS Technik GmbH & Co., Germany
Cr	99.2	100	TLS Technik GmbH & Co., Germany
C Graphite)	$> 99.5$	6	Graphit Kropfmühl AG, Germany

The  $\text{Al}_2\text{O}_3/\text{TiC}$  composite was sintered at 1400 °C in Ar and cooled naturally to avoid cracking due to thermal shock.  $\text{Ti}_2\text{AlC}$  samples were directly synthesised by spark plasma sintering using the settings specified in **Table 7.2**, and a heating rate of 80 °C/min. The experiments were performed in vacuum.  $\text{Cr}_2\text{AlC}$  was prepared by a two-step sintering process described elsewhere [28]. The coarse grained material was densified directly from pulverized pressureless sintered powder and fine grained

sample was sintered from ball milled powders, details can be found in **Table 7.2**. Finally the surfaces of the sample were ground using emery paper up to grit 4000, ultrasonically cleaned in ethanol and dried by blowing with pure and dry nitrogen gas.

*Table 7.2: Powder composition and sintering conditions for preparing the self-healing ceramics.*

Sample	Powder			Ratio	Temp (°C)	Pressure (MPa)	Time (min)
Al <sub>2</sub> O <sub>3</sub> /TiC	Al <sub>2</sub> O <sub>3</sub>	TiC		0.8 : 0.2 mass % Al <sub>2</sub> O <sub>3</sub> : TiC	1400	50	10
Ti <sub>2</sub> AlC-P	Ti	Al	TiC	0.85 : 1.05 : 1.15	1400	50	30
Ti <sub>2</sub> AlC-LP	Ti	Al	TiC	0.85 : 1.05 : 1.15	1400	50	60
Cr <sub>2</sub> AlC_FG	Cr	Al	C	2 : 1.15 : 1	1250	50	60
Cr <sub>2</sub> AlC_CG							

## 7.2.2 Characterization

The density of the sintered materials was measured with the Archimedes method using an analytical balance (Mettler Toledo AG-204, Switzerland) according to ASTM B 311-93 [29]. The Vickers' hardness was determined by averaging the results from 10 - 50 N indents using a hardness tester (Zwick/Z2.5, Germany). The indents were created by loading the indenter with 5 N/s and a holding time of 20 s.

The Al<sub>2</sub>O<sub>3</sub>/TiC composite was characterized using the X-ray diffractometer with a Lynxeye position sensitive detector and Cu K $\alpha$  radiation. The phase purity of the MAX-phase samples was determined via X-ray diffraction using a Bruker D8 Advance diffractometer (Bruker, Germany) in the Bragg-Brentano geometry with graphite monochromator and Co and Cu K $\alpha$  radiation. The recorded X-ray diffractograms were processed with Bruker software Diffrac.EVA 4.1 software.

Microstructure, crack morphology and crack filling were investigated using a scanning electron microscope (SEM), type JSM 6500F (JEOL Ltd., Tokyo, Japan) equipped with an energy dispersive spectrometer (EDS, type: ThermoFisher UltraDry 30mm<sup>2</sup> detector) for X-ray microanalysis (XMA) and with Noran System Seven software package for data acquisition and analysis. The oxidation kinetics of powders of the healing materials (TiC, Ti<sub>2</sub>AlC and Cr<sub>2</sub>AlC) were investigated with combined thermogravimetry and differential thermal analysis (TGA/DTA) using a SETSYS Evolution 1750 (Setaram, France). To this end 20 ±1 mg powder is put into 250 µL alumina crucible and heated to 1400 °C at different heating rates (1, 2, 5, 10 and 15 °C/min) in a flow of pure and dry synthetic air, i.e. 40 ml/min of N<sub>2</sub> (> 5N) and 10 ml/min of O<sub>2</sub> (> 5N). The relation between the heating rate β and the measured peak temperature (T<sub>p</sub>) is given by the Kissinger-Sunose-Akahira equation [30]:

$$\ln\left(\frac{\beta}{T_p^2}\right) + \frac{E_A}{RT_p} = \text{constant} \quad (7.1)$$

where  $E_A$  is the activation energy and  $R$  is the gas constant. The slope of a straight line fitted to the data points for  $\ln(\beta/T_p^2)$  versus  $(1/T_p)$  yields the activation energy of the oxidation reaction. This relation is based on first order reaction kinetics, hence:

$$k = A \exp\left(\frac{-E_A}{RT}\right) \quad (7.2)$$

where  $k$  is the reaction rate and  $A$  the frequency factor. Earlier studies [31] have shown that a reaction rate,  $\ln k$ , corresponding to -13 generally leads to full healing of cracks of micron sized width within a time span of 1 h, whereas a value of -15 requires 10 h.

### 7.2.3 Initiation of local crack damage

As a result of the large differences in hardness and toughness different methods had to be applied to the three materials selected to induce local cracks whose healing

behaviour could be studied under the combustion chamber conditions. In the case of the alumina-TiC composite material Vickers' indentation (Zwick/Z2.5, Germany) at a load of 20 N were used to induce penny-shaped cracks. The relationship between the applied load and the length of crack generated was investigated; see **Figure 7.1**. The indent size (2a) is defined by the average of the diagonals of the imprint made, while the crack length (2c) is defined as the average of the horizontal and vertical cracks formed in addition to the indent size.

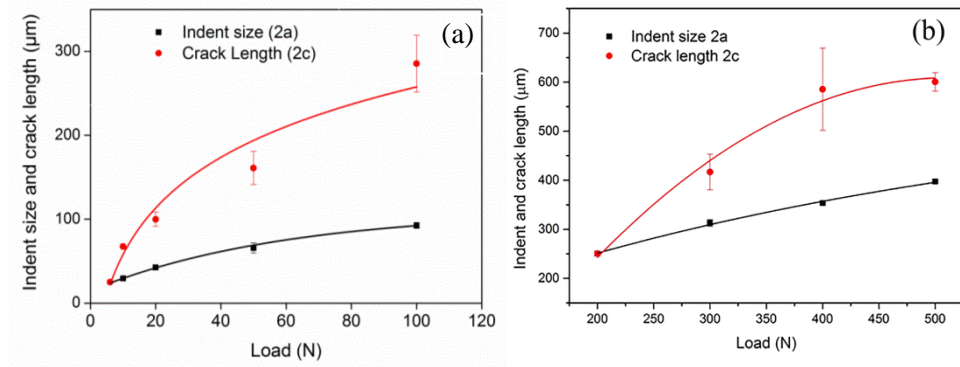


*Figure 7.1: Vicker's indent size and crack length versus applied load of (a)  $Al_2O_3$  with 20 vol. % TiC composite and (b) Fine grained  $Cr_2AlC$ .*

The fracture toughness was calculated to be  $4.3 \pm 0.1 \text{ MPa m}^{1/2}$  [32]. This is slightly higher than the reported values for the constituents, i.e.,  $4.0 \pm 0.1 \text{ MPa m}^{1/2}$  for monolithic  $Al_2O_3$  [33] and  $3.8 \text{ MPa m}^{1/2}$  for TiC [34]. When applying a load of less than 5 N the Vickers' indenter did not generate any crack. However, at 20 N an appreciable surface crack of length 100 μm forms. The cracks opened up to a width of about 1 μm, see **Figure 7.5** (a) and (b).

In the case of  $Ti_2AlC$  samples neither indentation nor an impact method resulted in finite cracks within the samples. In this case thermal shock treatments were applied. Crack formation due to thermal shock first occurred at a temperature difference between heating and cooling of 450 °C. Micro-cracks of less than 2 μm in width were formed. For maximum temperatures between 450 and 950 °C cracks between 5 and 20 mm in length were formed by quenching in water. Based on 16 experiments the results were reproducible. Crack widths remained between 1 and 15 μm in this temperature range.



The  $Ti_2AlC$  samples used in the combustion study were quenched from 850 °C. This led to a large crack of 10  $\mu m$  width and 20 mm length in the pure  $Ti_2AlC$  disk through the sample thickness. The second  $Ti_2AlC$  sample, containing  $TiC$ ,  $Ti_3AlC$  and  $Ti_3Al$  impurities formed a crack of 5  $\mu m$  in width and of approx. 0.5 mm in depth.

In the fine grained  $Cr_2AlC$  samples microcracks could be created with the Vickers' indenter by applying a load of 300 N for 12 s. Cracks of about 140  $\mu m$ , having a width of less than 1  $\mu m$  were obtained. Per disc 10 of such cracks were produced in the samples to be tested in the combustion chamber. The fracture toughness value was estimated to be 8.7  $MPa m^{-1/2}$  using the load dependence of the indentation crack length.

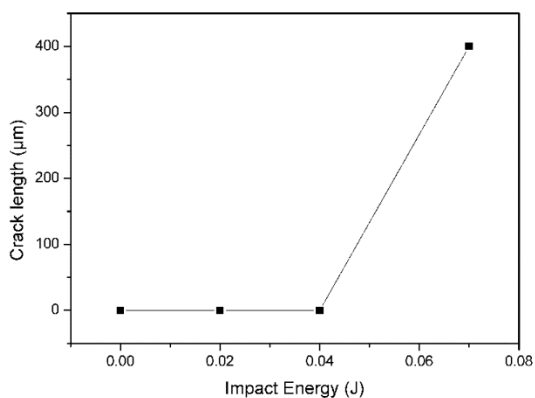


*Figure 7.2: Crack length versus impact energy for cracks created in coarse grained  $Cr_2AlC$  by impact of WC balls.*

In the case of the coarse grained material indentation loading did not result in radial cracks and only caused local plastic deformation. To induce local cracks of finite dimensions, coarse grained  $Cr_2AlC$  discs were clamped to a steel plate and subjected to low velocity perpendicular impact using 10 mm tungsten carbide balls. Beyond a critical impact energy, cracks were initiated at the crater edge and then propagated in the radial direction [35-37]. The correlation between impact energy and inducing cracks is depicted in **Figure 7.2**. The threshold impact energy for  $Cr_2AlC$  is about 50 mJ. A crack with a length of 700  $\mu m$  and a maximum crack opening of 2.5  $\mu m$  is observed in the coarse grained sample tested in the combustion chamber.

Samples tested in the combustion chamber contained cracks initiated by methods described above.  $\text{Al}_2\text{O}_3/\text{TiC}$  composites and both the fine and coarse grained  $\text{Cr}_2\text{AlC}$  had more than 5 cracks with lengths up to 1 mm and an average width of less than  $2\ \mu\text{m}$ . The through crack produced by thermal shock in the high purity  $\text{Ti}_2\text{AlC}$  sample was  $10\ \mu\text{m}$  wide and 20 mm in length, while the impurities of the second  $\text{Ti}_2\text{AlC}$  sample resulted in a thinner  $5\ \mu\text{m}$  crack with of approx. depth of 0.5 mm, while comparable in length.

## 7.2.4 Crack healing in combustion chamber

To investigate healing of crack damage at conditions encountered in a real combustion chamber, samples were placed in a combustor setup (Limousine Combustor, UTwente, The Netherlands [38]); see **Figure 7.3**. The flow in the combustor is turbulent, as the Reynolds number is well above 4000 for all conditions. The combustor is operated at atmospheric pressure and the gases are injected at room temperature. The fuel used is 100 % methane at room temperature. The air and fuel flow are controlled from a PC with control software and mass flow controller valves. The air and fuel mass flow are about  $24.62\ \text{g/s}$  and  $0.8\ \text{g/s}$ , respectively resulting in an average gas flow speed of  $16\ \text{m/s}$  at the location of the samples. The combustor is operated at an operating point with a thermal power of 40 kW and an air excess factor of 1.8. The air factor is the ratio of the actual fuel-to-air flow rate ratio to the fuel-to-air flow rate ratio necessary for stoichiometric combustion and indicates the excess of air in the chemical reaction.

The combustor can operate in a stable or unstable regime. In the unstable regime pressure oscillations are amplified by the combustion process and they grow in a limit cycle to amplitudes of 160 dB Sound Pressure Level. This phenomenon can happen in gas turbine engines but is to be avoided with a view to fatigue damage. Under the conditions mentioned before, the combustor is running stable and the observed pressure oscillations are lower (about 100 dB) and representative for normal operation of a gas turbine engine. The adiabatic flame temperature and oxygen concentration at equilibrium conditions can be estimated using Chemkin Equil [39] assuming constant pressure and enthalpy. Using the GRI-Mech 3.0 reaction mechanism [40] and an initial temperature of 295 K the adiabatic flame

temperature at these operating conditions is estimated to be about 1581 K. Under the above mentioned assumptions of adiabatic, isobaric conditions and assuming that the reacting mixture has already reached the equilibrium state, the oxygen mole fraction at the sample holder location is computed to be about 0.0876. Assuming a mixture of ideal gases, the volume fraction of oxygen then becomes 8.76 vol. %.

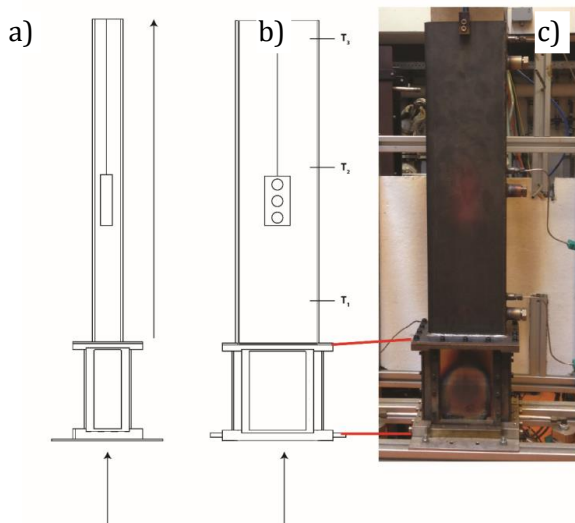


*Figure 7.3: Combustion setup: (a) schematic side view with arrows indicating gas flow direction, (b) front view showing the position of the sample holder and thermocouples and (c) actual experimental setup.*

The 6 samples (3 sets of 2) were mounted in an Inconel 800 holder suspended midway in the exhaust of the combustor; see **Figure 7.3**. Samples are arranged back to back so both samples of one material are exposed to the same conditions; see **Figure 7.3b**. After exposure to the chamber conditions for 4.5 h, the samples were removed after switching off the fuel supply and allowing the chamber to cool down in approximately 45 minutes. The temperature at the sample holder was approx. 1000 °C. Temperature fluctuations during the course of the experiment were of the order of  $\pm 2$  °C.

After exposure and subsequent cooling down the samples were examined using SEM and XMA. Both the surface and cross-sections prepared by cutting with a diamond blade were investigated regarding the oxides formed and crack gap volume filled.

## 7.3 Results

### 7.3.1 Materials characterization

All sintered materials were found to have a density above 95 %; see **Table 7.3**. The ceramic composite samples ( $\text{Al}_2\text{O}_3/\text{TiC}$ ) showed traces of WC, an impurity of the TiC powder. Impurities in the MAX phase ceramics stem from incomplete reactions during synthesis.  $\text{Cr}_2\text{AlC}$  was prepared with a fine and coarse grained microstructure resulting in a different hardness, viz. 6.0 and 3.2 GPa, respectively. The average grain sizes are reported in **Table 7.3**.

*Table 7.3: Properties of sintered materials and impurities as detected by x-ray diffraction.*

Sample	Impurities	Average grain size ( $\mu\text{m}$ )	Density (%)	Hardness (GPa)
$\text{Al}_2\text{O}_3/\text{TiC}_{01}$	WC	4.5	95 %	18.7
$\text{Al}_2\text{O}_3/\text{TiC}_{02}$	WC	4.5	99 %	19.3
$\text{Ti}_2\text{AlC-P}$	none	15-40	95.8 %	3.9
$\text{Ti}_2\text{AlC-LP}$	TiC, $\text{Ti}_3\text{AlC}_2$ , TiAl	15-40	95.1 %	3.5
$\text{Cr}_2\text{AlC}_{\text{FG}}$	Cr	2	99.1%	6.0
$\text{Cr}_2\text{AlC}_{\text{CG}}$	$\text{Cr}_7\text{C}_3$	20-30	98.7%	3.2

### 7.3.2 Oxidation of TiC, $\text{Ti}_2\text{AlC}$ and $\text{Cr}_2\text{AlC}$ in air and combustion environments

Differential thermal analysis of the powdered healing agents TiC,  $\text{Ti}_2\text{AlC}$  and  $\text{Cr}_2\text{AlC}$  determined oxidation reaction peaks for all materials below 1300 °C. In **Figure 7.4**, the reaction rates are plotted as a function of the inverse temperature for the three powders investigated.

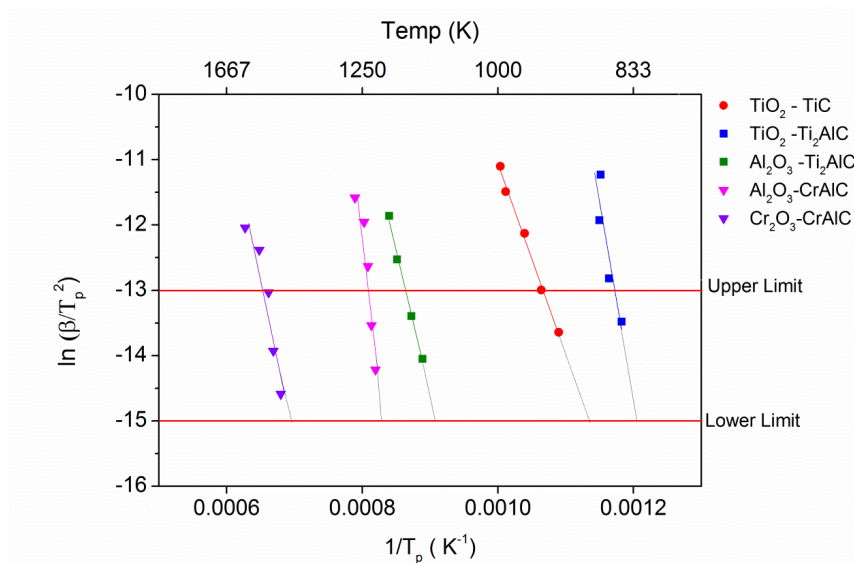


*Figure 7.4: Evaluating the activation energy for the different reactions occurring during oxidation of all healing materials considered (plot of reactivity versus peak temperature).*

Taking the values of -15 and -13 for the natural logarithm of the reaction rate as the lower and upper value for optimal healing [31] (cf. Section 7.2.2), we find the following optimal annealing temperatures, 600 - 660 °C for the formation of TiO<sub>2</sub> from TiC. For Ti<sub>2</sub>AlC the temperature range is 556 - 580 °C and 826-885 °C for the formation to TiO<sub>2</sub> and Al<sub>2</sub>O<sub>3</sub> respectively. And for Cr<sub>2</sub>AlC it is 929 - 963 °C and 1170 - 1257 °C for the formation of Al<sub>2</sub>O<sub>3</sub>, and Cr<sub>2</sub>O<sub>3</sub> respectively.

After exposure in the combustion chamber for 4 h where the temperature at sample location was measured to be between 940 and 1110 °C the colour of the Al<sub>2</sub>O<sub>3</sub>/TiC samples had changed from very dark grey to light grey, indicating full oxidation. Observations at higher resolution in the SEM showed that islands of TiO<sub>2</sub> formed all over the surface on top of the TiC particles. The activation energy of the complete transformation of TiC to rutile amounts to 242 ± 11 kJ/mol according to DTA.

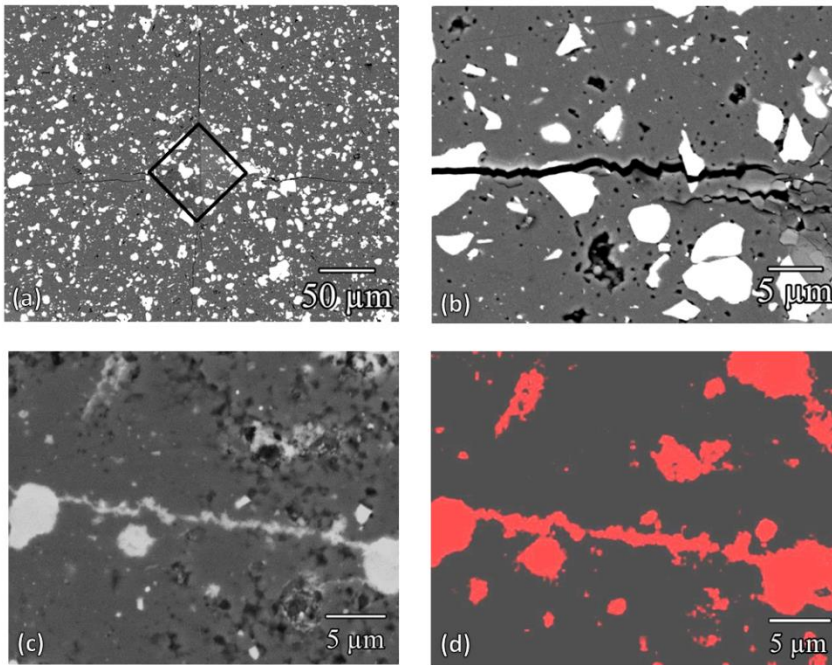


*Figure 7.5: SEM micrographs of  $\text{Al}_2\text{O}_3/\text{TiC}$  composite. (a) Cracks created by Vickers' indentation: (b) Close-up showing crack-particle interaction, (c) Healed crack after exposure to combustion environment for 4 h, (d) Ti X-ray mapping showing the filling of the healed crack.*

After removing the surface oxides by diamond polishing complete filling of the cracks with oxide was observed; see **Figure 7.5c** and **d**. Even, after removing a layer of about 10 μm by diamond polishing, the indentation induced cracks appeared to be fully filled with oxides. This suggests that the cracks running from the surface inside the composite are healed. Moreover, it seems that the oxides grew laterally from the TiC particles along the crack gap, while the oxides on the surface grew locally.

Observation of the tested Ti<sub>2</sub>AlC samples showed dark discoloration on the surface exposed to the combustion environment. Both Ti<sub>2</sub>AlC samples showed significant oxide growth after being exposed to the combustion environment for 4 h. Grains of less than 5 μm cover the complete surface and all cracks smaller than 10 μm in width within the indents; see **Figure 7.6**.

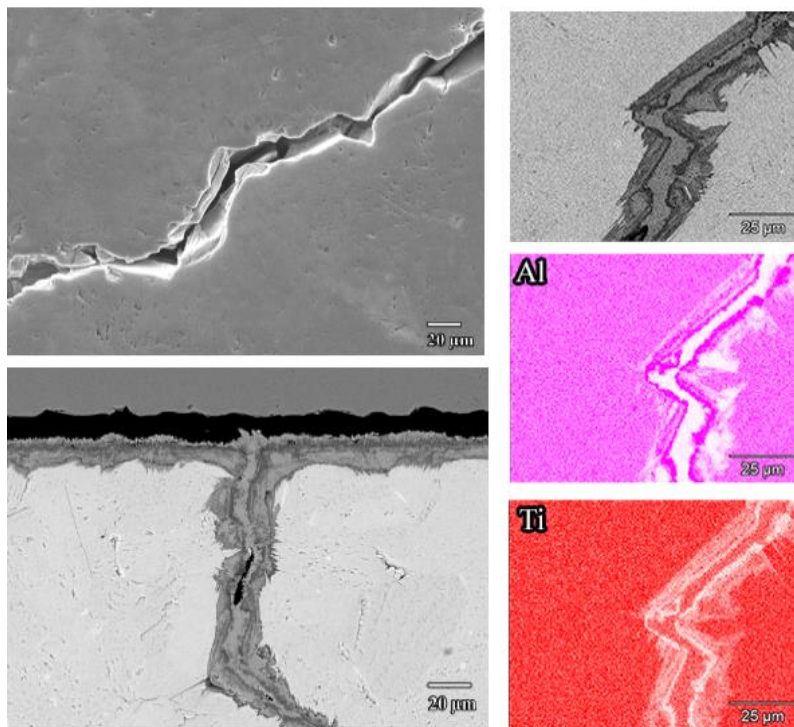


*Figure 7.6: (a) Cracks in  $Ti_2AlC$ -a after quenching in water from 850 °C; (b) Cross-section of healed crack after exposure to combustion conditions for 4 h; (c) Close up of healed crack; (d) Al X-ray map; (e) Ti X-ray map.*

The outer layer of the oxide was identified as  $TiO_2$  by SEM-XMA and XRD. A uniform and dense mixed oxide layer with a thickness of about 13  $\mu m$  developed on the high purity  $Ti_2AlC$  material. According to DTA analysis small amounts of  $TiO_2$  are expected to form around 570 °C while full rutile transformation is achieved at 700 °C, followed by  $Al_2O_3$  formation around 800 °C.

The thermally induced crack in pure  $Ti_2AlC$  was fully filled with  $TiO_2$  and  $Al_2O_3$  up to a depth of 1.2 mm; see **Figure 7.6**. Beyond this depth, oxides were formed at the opposing fracture surfaces, however not fully bridging the crack gap. The  $Ti_2AlC$  material containing impurities of  $TiC$ ,  $Ti_3AlC$  and  $Ti_3Al$  formed a 15  $\mu m$  thick mixed oxide scale with an outer layer of  $TiO_2$  of approx. 3  $\mu m$  thickness. The crack, having a jagged path and a width of only 1  $\mu m$  was fully filled up to its crack tip at a

depth of 0.5 mm. The oxide within the crack gap is  $\text{Al}_2\text{O}_3$ . Given that oxidation still occurs at oxygen potentials lower than in atmospheric air (0.088 vs 0.2 atm), the fact that cracks 1.2 mm below the surface were not fully closed was attributed to regions of the crack being sealed by surrounding oxide bridges or to the lower rate of oxidation.

The oxidation of  $\text{Cr}_2\text{AlC}$  requires higher temperatures and is slower compared to  $\text{Ti}_2\text{AlC}$ . Formation of  $\text{Al}_2\text{O}_3$  begins around 900 to 1000 °C. A second peak in the heat flow signal of the DTA analysis at 1170 - 1275 ° corresponds to the formation of an  $\text{Al}_2\text{O}_3$  and  $(\text{Cr}, \text{Al})_2\text{O}_3$  solid solution according to XRD. The oxide grown on the surface after 4 h of oxidation in the combustion chamber was about 0.24  $\mu\text{m}$  and 0.19  $\mu\text{m}$  thick on the fine and coarse grained sample, respectively. These oxide layers are thinner than the oxide layers formed in synthetic air for corresponding temperature and time, namely: 0.6  $\mu\text{m}$  and 0.5  $\mu\text{m}$ , respectively. Apparently the lower oxygen partial pressure in the combustion ambient as compared with that of air resulted in low oxide nucleation density (i.e. larger oxide grain size) and consequently slower oxidation kinetics. Hence, cracks with a width of less than 0.5  $\mu\text{m}$  were fully healed with oxide and those with larger crack opening were only partially healed; see **Figure 7.7**.

The significant difference in oxygen partial pressure from standard self-healing investigations performed in synthetic or atmospheric air (0.2 atm) to the conditions found in the combustion setup (0.088 atm) show no significant impairment of the healing ability in the case of the three tested materials. The lower  $p\text{O}_2$  resulted in thinner oxide scales for  $\text{Cr}_2\text{AlC}$  than those found in thermal gravimetric analysis, 0.2 to 0.5  $\mu\text{m}$  for fine grained  $\text{Cr}_2\text{AlC}$ . Healing in  $\text{Ti}_2\text{AlC}$  and  $\text{Al}_2\text{O}_3/\text{TiC}$  was not affected by the reduced oxygen partial pressure. Surprisingly other compositional changes to the atmosphere due to combustions, e.g. higher  $\text{NO}_x$  content, showed no effect on sample composition.



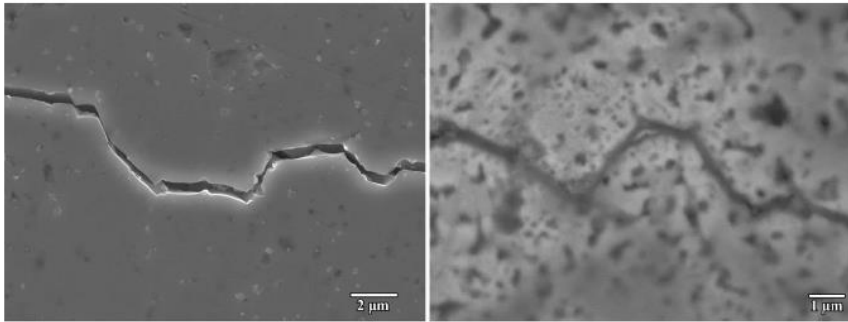


*Figure 7.7: (a) Crack damage in fine grained  $\text{Cr}_2\text{AlC}$  generated by vickers' indentation; (b) Crack healed by  $\text{Al}_2\text{O}_3$  formed in combustion environment for 4 h.*

## 7.4 Conclusions

Three high temperature ceramic systems,  $\text{Al}_2\text{O}_3/\text{TiC}$ ,  $\text{Ti}_2\text{AlC}$  and  $\text{Cr}_2\text{AlC}$  were investigated concerning their fracture, oxidation and self-healing behaviour under real combustion conditions. All tested materials showed full crack-gap filling for 0.5 to more than 10  $\mu\text{m}$  wide cracks of up to 20 mm length, after exposure to the high velocity exhaust gas mixture at approx. 1000 °C for 4 h. Although the oxygen partial pressure in the combustion chamber is much lower than in air (0.088 versus 0.2 atm), the conditions are sufficient to realize full healing of crack damage. The high gas flow rate (16 m/s) and thermal load did not impair the healing process.

## Acknowledgements

This research was sponsored in part by the People Program (Marie Curie ITN) of the European Union's seventh framework program, FP7, grant number 290308 (SHeMat) and the German Research Foundation (Deutsche Forschungsgemeinschaft, DFG, SPP 1568 'Design and Generic Principles of Self-Healing Materials', under contract SL184/1-2).

## References

- [1] Song, G.M., Schnabel, V., Kwakernaak, C., van der Zwaag, S., Schneider, J.M., and Sloof, W.G., *High temperature oxidation behaviour of Ti<sub>2</sub>AlC ceramic at 1200°C*. *Materials at High Temperatures*, 2012. 29(3): p. 205-209.
- [2] Ganguly, A., Barsoum, M.W., and Doherty, R.D., *Interdiffusion between Ti<sub>3</sub>SiC<sub>2</sub>-Ti<sub>3</sub>GeC<sub>2</sub> and Ti<sub>2</sub>AlC-Nb<sub>2</sub>AlC diffusion couples*. *Journal of the American Ceramic Society*, 2007. 90(7): p. 2200-2204.
- [3] Li, S., Song, G., Kwakernaak, K., van der Zwaag, S., and Sloof, W.G., *Multiple crack healing of a Ti<sub>2</sub>AlC ceramic*. *Journal of the European Ceramic Society*, 2012. 32(8): p. 1813-1820.
- [4] Ando, K., Ikeda, T., Sato, S., Yao, F., and Kobayasi, Y., *A preliminary study on crack healing behaviour of Si<sub>3</sub>N<sub>4</sub>/SiC composite ceramics*. *Fatigue & Fracture of Engineering Materials & Structures*, 1998. 21(1): p. 119-122.
- [5] Ando, K., Chu, M.C., Yao, F., and Sato, S., *Fatigue strength of crack-healed Si<sub>3</sub>N<sub>4</sub>/SiC composite ceramics*. *Fatigue & Fracture of Engineering Materials & Structures*, 1999. 22(10): p. 897-903.
- [6] Kim, B.S., Ando, K., Chu, M.C., and Sato, S., *Crack-healing behavior of monolithic alumina and strength of crack-healed member*. *Zairyo*, 2003. 52: p. 667-73.
- [7] Ando, K., Chu, M.C., Tsuji, K., Hirasawa, T., Kobayashi, Y., and Sato, S., *Crack healing behaviour and high-temperature strength of mullite/SiC composite ceramics*. *Journal of the European Ceramic Society*, 2002. 22(8): p. 1313-1319.
- [8] Takahashi, K., Yokouchi, M., Lee, S.-K., and Ando, K., *Crack-healing behavior of Al<sub>2</sub>O<sub>3</sub> toughened by SiC whiskers*. *Journal of the American Ceramic Society*, 2003. 86(12): p. 2143-2147.
- [9] Osada, T., Nakao, W., Takahashi, K., Ando, K., and Saito, S., *Strength recovery behavior of machined Al<sub>2</sub>O<sub>3</sub>/SiC nano-composite ceramics by crack-healing*. *Journal of the European Ceramic Society*, 2007. 27(10): p. 3261-3267.
- [10] Sugiyama, R., Yamane, K., Nakao, W., Takahashi, K., and Ando, K., *Effect of difference in crack-healing ability on fatigue behavior of alumina/silicon carbide composites*. *Journal of Intelligent Material Systems and Structures*, 2008. 19(3): p. 411-415.

- [11] Yao, F., Ando, K., Chu, M.C., and Sato, S., *Crack-healing behavior, high temperature and fatigue strength of SiC-reinforced silicon nitride composite*. Journal of Materials Science Letters, 2000. 19(12): p. 1081-1083.
- [12] Korouš, J., Chu, M.C., Nakatani, M., and Ando, K., *Crack healing behavior of silicon carbide ceramics*. Journal of the American Ceramic Society, 2000. 83(11): p. 2788-2792.
- [13] Yao, F., Ando, K., Chu, M.C., and Sato, S., *Static and cyclic fatigue behaviour of crack-healed Si<sub>3</sub>N<sub>4</sub>/SiC composite ceramics*. Journal of the European Ceramic Society, 2001. 21(7): p. 991-997.
- [14] Ando, K., Tuji, K., Furusawa, K., Hanagata, T., Chu, M.C., and Sato, S., *Effect of pre-crack size and testing temperature on fatigue strength properties of crack healed mullite Zairyo*, 2001. 50 p. 920-5.
- [15] Yoshioka, S., Boatemaa, L., van der Zwaag, S., Nakao, W., and Sloof, W.G., *On the use of TiC as high-temperature healing particles in alumina based composites*. Journal of the European Ceramic Society, 2016. 36(16): p. 4155-4162.
- [16] Song, G.M., Pei, Y.T., Sloof, W.G., Li, S.B., De Hosson, J.T.M., and van der Zwaag, S., *Oxidation-induced crack healing in Ti<sub>3</sub>AlC<sub>2</sub> ceramics*. Scripta Materialia, 2008. 58(1): p. 13-16.
- [17] Sloof, W.G., Li, S., Song, G., Kwakernaak, C., Wu, X., and van der Zwaag, S. *Multiple crack-healing and strenght recovery in MAX phase ceramics*. in *3rd Int. Conf. on Self-Healing Materials*. 2011. Bath, UK.
- [18] Yang, H.J., Pei, Y.T., Rao, J.C., De Hosson, J.T.M., Li, S.B., and Song, G.M., *High temperature healing of Ti<sub>2</sub>AlC: On the origin of inhomogeneous oxide scale*. Scripta Materialia, 2011. 65(2): p. 135-138.
- [19] Li, S., Xiao, L., Song, G., Wu, X., Sloof, W.G., and van der Zwaag, S., *Oxidation and crack healing behavior of a fine-grained Cr<sub>2</sub>AlC ceramic*. Journal of the American Ceramic Society, 2013. 96(3): p. 892-899.
- [20] Song, G.M., *Advances in science and technology of M<sub>n+1</sub>AX<sub>n</sub>*, ed. Low, I.M. 2012 Cambridge: Woodhead Publishing.
- [21] Tallman, D.J., Anasori, B., and Barsoum, M.W., *A critical review of the oxidation of Ti<sub>2</sub>AlC, Ti<sub>3</sub>AlC<sub>2</sub> and Cr<sub>2</sub>AlC in air*. Materials Research Letters, 2013. 1(3): p. 115-125.
- [22] Farle, A.-S., Kwakernaak, C., van der Zwaag, S., and Sloof, W.G., *A conceptual study into the potential of M<sub>n+1</sub>AX<sub>n</sub>-phase ceramics for self-healing of*

- crack damage*. Journal of the European Ceramic Society, 2015. 35(1): p. 37-45.
- [23] Li, S., Chen, X., Zhou, Y., and Song, G., *Influence of grain size on high temperature oxidation behavior of Cr<sub>2</sub>AlC ceramics*. Ceramics International, 2013. 39(3): p. 2715-2721.
- [24] Wang, J., Zhou, Y., Liao, T., Zhang, J., and Lin, Z., *A first-principles investigation of the phase stability of Ti<sub>2</sub>AlC with Al vacancies*. Scripta Materialia, 2008. 58(3): p. 227-230.
- [25] Liao, T., Wang, J., Li, M., and Zhou, Y., *First-principles study of oxygen incorporation and migration mechanisms in Ti<sub>2</sub>AlC*. Journal of Materials Research, 2011. 24(10): p. 3190-3196.
- [26] Barsoum, M.W. and Radovic, M., *Annual review of materials research*. Palo Alto: Annual Reviews, ed. Clarke, D.R. and Fratzl, P. Vol. 41. 2011.
- [27] Sun, Z.M., *Progress in research and development on MAX phases: a family of layered ternary compounds*. International Materials Reviews, 2011. 56(3): p. 143-166.
- [28] Duan, X., Shen, L., Jia, D., Zhou, Y., van der Zwaag, S., and Sloof, W.G., *Synthesis of high-purity, isotropic or textured Cr<sub>2</sub>AlC bulk ceramics by spark plasma sintering of pressure-less sintered powders*. Journal of the European Ceramic Society, 2015. 35(5): p. 1393-1400.
- [29] ASTM B311-93 *Test method for density determination for powder metallurgy (p/m) materials containing less than two percent porosity*, in (International A). 1997
- [30] Kissinger, H.E., *Variation of peak temperature with heating rate in differential thermal analysis* J. Res. Natl Bur. Stand. , 1956 57(217-21).
- [31] Yoshioka, S. and Nakao, W., *Methodology for evaluating self-healing agent of structural ceramics*. Journal of Intelligent Material Systems and Structures, 2015. 26(11): p. 1395-1403.
- [32] Evans, A.G. and Charles, E.A., *Fracture toughness determinations by indentation*. Journal of the American Ceramic Society, 1976. 59(7-8): p. 371-372.
- [33] Sglavo, V.M., Trentini, E., and Boniecki, M., *Fracture toughness of high-purity alumina at room and elevated temperature*. Journal of Materials Science Letters, 1999. 18(14): p. 1127-1130.

- [34] Chermant, J.L., Deschanvres, A., and Osterstock, F., *Toughness and fractography of TiC and WC*. *Fract. Mech. Ceram.*, 1978 4: p. 891-901.
- [35] Duó, P., Liu, J., Dini, D., Golshan, M., and Korsunsky, A.M., *Evaluation and analysis of residual stresses due to foreign object damage*. *Mechanics of Materials*, 2007. 39(3): p. 199-211.
- [36] Evans, A.G., *Impact damage in brittle materials in the elastic-plastic response régime*. *Proceedings of the royal society of London. A Mathematical and physical sciences*, 1978. 361(1706): p. 343-365.
- [37] Peters, J.O. and Ritchie, R.O., *Influence of foreign-object damage on crack initiation and early crack growth during high-cycle fatigue of Ti-6Al-4V*. *Engineering Fracture Mechanics*, 2000. 67(3): p. 193-207.
- [38] Roman Casado, J.C., *Nonlinear behavior of the thermoacoustic instabilities in the limousine combustor* 2013, University of Twente. p. 156
- [39] Kee, R., Rupley, F., Miller, J., Coltrin, M., Grcar, J., Meeks, E., Moffat, H., Lutz, A., Dixon-Lewis, G., and Smooke, M., *CHEMKIN Collection*, in *Release 3.6* : . 2000 Reaction Design Inc.: San Diego, CA.
- [40] Smith, G.P., *GRI-Mech 3.0*. 1999 University of California, Stanford Univerisity and SRI International p. 55. Available from: URL: [http://www.me.berkeley.edu/gri\\_mech](http://www.me.berkeley.edu/gri_mech) 51 p 55

# Summary

Alumina ( $\text{Al}_2\text{O}_3$ ) is an attractive ceramic for engineering applications operating at elevated or high temperatures because of its good thermal and chemical resistance. It also maintains high strength and hardness at high temperatures. These desirable properties are due to the strong covalent and ionic bonds existing between its atoms.

However, these same strong and directional bonds are the origins of its inherent brittleness. Over the last decade, material scientists have adopted self-healing as a means of restoring the load bearing capability of such materials after damage from micro-sized surface cracks. In this methodology, the material is restored to a status comparable to the original one by the 'healing' of such surface cracks at high temperatures. Healing is achieved by the addition of 'healing agents' to the base ceramic material which upon the occurrence of a crack oxidise into a healing oxide which fills and seals of the crack. There are some gaps in the build-up of the knowledge ladder of self-healing ceramics to an application ready level. This thesis addresses some design questions and tests the capability of newly identified healing particles under laboratory and application conditions.

An introduction to extrinsic self-healing as applied to ceramic oxides is presented in Chapter 1. A short analysis of the research done so far and the objectives of the thesis are also presented here.

Chapter 2 presents an unbiased selection procedure to determine viable healing agents to efficiently heal surface cracks in alumina at high temperatures. The selection was made from a database of transition metals, carbides and nitrides and proceeded according to 6 identified primary criteria. The healing oxide which eventually fills the crack was selected by its melting point, ability to adhere to alumina and thermal mismatch with alumina. The healing agent on the other hand was selected by its melting point, volume expansion upon oxidation and thermal mismatch with alumina. Application of all selection criteria resulted in identifying granular Ti, Cr, Zr, Nb, Hf, TiC, TiN,  $\text{Cr}_3\text{C}_2$ ,  $\text{Cr}_2\text{N}$ , ZrN, NbC and NbN as promising agents for the autonomous healing of alumina at high temperatures.

The effect of particle size on the oxidation kinetics of TiC powders is studied in Chapter 3. Different sizes of TiC powder ranging from nanometer to sub-millimetre sizes were studied by thermal analysis. The kinetic triplet:  $E_A$ ,  $f(\alpha)$  and  $A$  were derived for all the powders using the Kissinger, the master curve plotting and the Senum & Yang methods, respectively. The oxidation of TiC proceeds via the formation of oxycarbides, anatase and then rutile. Activation energy is found to be a strong function of the particle size between 50 nm and 11  $\mu\text{m}$  and becomes constant at larger particle sizes. The temperature for efficient healing was between 400 and 1000 °C. Hence, extrinsic self-healing in oxidic ceramic matrices can be tailored to a specific temperature range by tuning the size of the healing particle.

In Chapter 4, the ability of  $\text{Al}_2\text{O}_3$  containing 10 vol. % of Ti particles to self-heal is investigated at different times and temperatures. The evolution of the crack filling process via the solid-state formation of  $\text{TiO}_2$  is also studied. The fracture strength of the composites was measured by 4-point bending and the optimum healing conditions for full strength recovery is 800 °C for 1 h or 900 °C for 15 min. Crack filling was observed to proceed in three steps i.e., local bonding at the site of the intersected Ti particle, lateral spreading and global filling. It was discovered that although significant strength recovery was attained by local bonding of the intersected particles, full crack filling is required to prevent an unfilled crack region acting as a crack initiator. The results of Ti oxidation results were applied in a simple model for crack-gap filling and the experimental results observed were in good agreement with the model predictions.

Chapter 5 reports on the use of TiC particles as high temperature healing agents in alumina based composites. Fully dense alumina containing 15 and 30 vol. % TiC composites was made by Spark Plasma Sintering. Strength recovery was studied between 400 and 800 °C after damage was introduced by indentation. Complete tensile strength recovery was attained in both composites by annealing at 800 °C for 1 h in air.

In Chapter 6, the oxidation induced crack healing of  $\text{Al}_2\text{O}_3$  containing 20 vol. % of  $\text{Ti}_2\text{AlC}$  MAX phase healing particles is studied. From the oxidation kinetics of the  $\text{Ti}_2\text{AlC}$  particles, oxidation starts at 600 °C, but, the temperature for efficient healing is between 800 and 1000 °C. Crack healing was studied at 800, 900 and 1000 °C for

0.25, 1, 4 and 16 h and the strength recovery was measured by 4-point bending. The  $\text{Ti}_2\text{AlC}$  material was found to be a suitable healing agent for alumina containing 20 vol. % of 10 micron sized  $\text{Ti}_2\text{AlC}$  particles. The optimum healing conditions recorded was 900 °C for 1 h or 1000 °C for 15 min.  $\text{Ti}_2\text{AlC}$  particles embedded in the matrix (more than 20  $\mu\text{m}$  from the surface) did not decompose upon long-term high-temperature exposure and remained potentially active in the non-oxygen permeable  $\text{Al}_2\text{O}_3$  matrix until intersected by a crack.

In the last chapter of this thesis, self-healing of conventional ( $\text{Al}_2\text{O}_3/\text{TiC}$ ) and MAX Phase ( $\text{Ti}_2\text{AlC}$  and  $\text{Cr}_2\text{AlC}$ ) ceramics were tested in a combustion engine. Circular samples (20 mm in diameter and 5 mm thick) were sintered by spark plasma sintering and cracks were introduced by either, indentation, quenching and low perpendicular velocity impact method. The samples were exposed in the post-flame zone of a turbulent flame in a combustion chamber to heal at temperatures of approximately 1000 °C at low  $\text{pO}_2$  levels for 4 h. All cracks in the  $\text{Al}_2\text{O}_3/\text{TiC}$  composite (width 1  $\mu\text{m}$  and length 100  $\mu\text{m}$ ) were fully filled with  $\text{TiO}_2$ . Large cracks in the  $\text{Ti}_2\text{AlC}$  material were also fully filled with  $\text{TiO}_2$  and  $\text{Al}_2\text{O}_3$ . And in the  $\text{Cr}_2\text{AlC}$ , cracks of up to 1.0  $\mu\text{m}$  in width and more than 100  $\mu\text{m}$  in length were completely filled with  $\text{Al}_2\text{O}_3$ . Oxidation of the healing agents and hence its healing ability was not affected by the very low  $\text{pO}_2$  levels in the combusting chamber as the results were similar to those of samples studied under static laboratory conditions.





# Samenvatting

Aluminiumoxide is door zijn goede thermische en chemische resistentie een aantrekkelijk keramisch materiaal voor hoge-temperatuur toepassing. Het is niet alleen stabiel maar heeft ook een uitstekende sterkte en hardheid bij die temperaturen. Al deze eigenschappen zijn het gevolg van de sterke covalente en ionische bindingen tussen de atomen. Dezelfde sterke en gerichte bindingen zijn echter ook de verklaring voor de intrinsieke brosheid van het materiaal welke resulteert in hoge gevoeligheid voor beschadigingen aan het oppervlak. In het afgelopen decennium hebben materiaalkundigen gezocht naar routes om dit sterkteverlies via een spontaan optredende ‘self-healing’ reactie tijdens gebruik in op hoge temperatuur in-situ te neutraliseren. Dit kan bereikt worden door toevoeging van discrete ‘healing’ deeltjes tijdens de materiaalsynthese. Bij het optreden van een scheur komen de doorsneden deeltjes in direct contact met de zuurstof in de lucht en ondergaan een oxidatieve reactie die leidt tot het opvullen van de scheur met een goed hechtend reactieproduct, resulterend in een herstel van de sterkte. Doel van het onderzoek als beschreven in dit proefschrift is om meer inzicht te krijgen in dit herstelproces en om het gedrag van twee nieuwe, op basis van het betere inzicht ontworpen, aluminiumoxide-composieten onder laboratorium en turbine-relevante condities te bepalen.

Hoofdstuk 1 geeft een korte inleiding in het thema van zelfherstellend oxidisch keramiek op basis van ingebouwde discrete ‘healing’ deeltjes, de zogenaamde “extrinsic self-healing” benadering. Op basis van een analyse van wat hierover al in de literatuur bekend is, zijn de doelstelling voor dit onderzoek geformuleerd.

In Hoofdstuk 2 wordt een nieuwe objectieve procedure beschreven voor de identificatie van geschikte materialen om te dienen als ‘healing agent’ in aluminiumoxide bedoeld voor hoge-temperatuur toepassingen. De keuze uit de materialen in een grote database van overgangsmetalen, carbiden en nitriden wordt gemaakt op basis van 6 criteria. Het te vormen oxide moet een geschikt smeltpunt hebben, een goede hechting aan aluminiumoxide en een vergelijkbare thermische uitzettingscoëfficiënt. Het uitgangsmateriaal moet een passend smeltpunt hebben,

expanderen bij oxidatie en eveneens een passende thermische uitzettingscoëfficiënt hebben. Na toepassing van de selectiecriteria bleven Ti, Cr, Zr, Nb, Hf, TiC, TiN, Cr<sub>3</sub>C<sub>2</sub>, Cr<sub>2</sub>N, ZrN, NbC en NbN over als mogelijke ‘healing agent’ materialen.

Het effect van de deeltjesgrootte op de oxidatiekinetiek van één van de kandidaatmaterialen, TiC, wordt beschreven in Hoofdstuk 3. Verschillende TiC poeders met deeltjesgroottes variërend van nanometer tot sub-millimeter werden onderzocht. De kinetische parameters  $E_A$ ,  $f(\alpha)$  en  $A$  werden op basis van een uitgebreide Kissinger methode bepaald. De oxidatie verloopt via de vorming van oxycarbides, anatase en uiteindelijk rutiel. De activeringsenergie bleek een sterke functie van de deeltjesgrootte te zijn voor deeltjes kleiner dan 11  $\mu\text{m}$ . Via deze deeltjesgrootteafhankelijkheid kan de optimale temperatuur voor ‘self-healing’ gestuurd worden van 400 tot 1000 °C.

In Hoofdstuk 4 wordt het zelfherstellend gedrag van een aluminiumoxide composiet met daarin 10 volume % titanium deeltjes als een functie van de temperatuur en de tijd onderzocht. Tevens werd het vulproces van de scheur door het gevormde titaanoxide bestudeerd. Het herstel van de sterkte werd gemeten m.b.v. 4-puntsbuigproeven en de minimale condities voor volledige terugkeer van de sterkte werden bepaald op gloeien gedurende 60 minuten bij 800 °C of 15 minuten bij 900 °C. Het vullen van de scheur verliep in drie stappen: lokale overbrugging van de scheur ter plaatse van het doorsneden deeltje, laterale opvulling uitgaande van een deeltje en tot slot complete opvulling van de scheur. Alhoewel al behoorlijk herstel van de sterkte verkregen wordt bij beperkte vulgraden, is volledige vulling van de scheur nodig om deze niet in een later stadium als scheurinitiator te laten dienen. De kinetiek van het gemeten scheur-vullend proces kan redelijk goed met een nieuw-ontwikkeld model beschreven worden.

Hoofdstuk 5 beschrijft het gedrag van aluminiumoxide composieten met daarin 10 of 30 volume % TiC deeltjes. De onderzochte composieten werden door middel van Spark Plasma Sintering vervaardigd. Het herstel van de schade als gevolg van lokale puntbelasting met een Vickers’ diamant werd gemeten over het temperatuurgebied van 400 tot 800 °C. Bij de hoogste gloeitemperatuur werd compleet herstel van de sterkte bereikt na 1 uur.

In Hoofdstuk 6 wordt het herstel van aluminiumoxide composieten met daarin 20 volume %  $Ti_2AlC$  MAX deeltjes beschreven. De oxidatie van de  $Ti_2AlC$  deeltjes begint al bij 600 °C, maar wordt pas echt effectief tussen 800 en 1000 °C zoals blijkt uit 4-punts buigproefmetingen na 0.25, 1, 4 en 16 h gloeien.  $Ti_2AlC$  deeltjes met een diameter van ongeveer 10  $\mu m$  bleken als geschikte ‘healing agents’ te functioneren. Deeltjes op meer dan 20  $\mu m$  van het preparaatoppervlak bleken ook na lange tijd gloeien op hoge temperatuur nog intact te zijn en hun nuttige taak in een later stadium te kunnen vervullen.

Het laatste hoofdstuk van dit proefschrift beschrijft het gedrag van 3 zelfherstellende keramiek varianten (1 extrinsiek  $Al_2O_3/TiC$  zelfherstellend composiet en 2 intrinsiek zelfherstellende metallo-keramieksoorten  $Ti_2AlC$  and  $Cr_2AlC$ ) in een simulator voor de verbrandingskamer van een turbine motor. Alle preparaten waren met behulp van Spark Plasma Sintering vervaardigd. Scheuren in het  $Al_2O_3/TiC$  composiet met initiële lengtes van 100  $\mu m$  en een breedte van 1  $\mu m$  waren volledig gevuld met  $TiO_2$ , terwijl de grotere scheuren in het  $Ti_2AlC$  proefstuk gevuld waren met een mengsel van  $TiO_2$  en  $Al_2O_3$ . De scheuren in het  $Cr_2AlC$  proefstuk bleken gevuld met  $Al_2O_3$ . De resultaten laten zien dat het zelfherstellend gedrag van de onderzochte proefstukken bij de lage zuurstof-partiaaldruk in de turbineverbrandingskamer niet wezenlijk verschilt van dat gemeten na gloeien onder de statische condities van een laboratoriumoven.



# Acknowledgements

It is with great pleasure that I write this section to express my heartfelt gratitude to all who in diverse ways have made this dream a reality!

First and foremost, I would like to express my outmost gratitude to my promotors dr. ir. Willem Sloof and prof. dr. ir. Sybrand van der Zwaag for giving me the chance, exuding a lot in me and supporting me through every step of the way. As my daily supervisor, Wim's endearing patience, eye for details and thoroughness continually nurtured this work until completion. On the other side, Sybrand's ingenuity and speed propelled this research to the touchline. I could not have had a better combination of supervisors. Thank you!

I gratefully acknowledge the financial support from the FP7 Marie Curie ITN (SHeMat) and the Delft Centre for Materials (DCMat) towards this research.

Special thanks go to our very skilled technicians: Ing. Cees Kwakernaak and Ing. Hans C. Brouwer, who trained me on the use of the various equipment used in this work, am very grateful. I would like to thank Ing. Ruud Hendriks and Dr. A. C. Riemslog for their immense help in the XRD and the mechanical testing laboratories, respectively. Sander van Asperen is also acknowledged for his help in the microscopy laboratory.

Next, I would like to thank the SIE group members (both past and present); Lucia, Lu, Ann-Sophie, Zeynep, Neha, Vahid, Myrthe, Julia, Georgina and Yulia. Life was easier with you around. Again, I would like to thank the professors and members of the other groups on the 4<sup>th</sup> floor and also the past secretary Anke Kerklaan-Koene. Thank you very much for your help in diverse ways! Special thanks to Astrid with her help with Dutch translations. I would also like to thank the head of department, Prof. Ian Richardson, professors, members of the other groups and secretaries of the department for their warmth.

I would also like to thank the members of the Mount Zion Int. Church in Delft for their support and encouragement especially Pastor & Mrs Nwosu. I want to specially thank Frank and Evelyn Ohene-Annor for their selflessness, am very grateful!

## Acknowledgments

---

Finally, I would like to express my deepest gratitude to my dear husband who 'sacrificed' his career in order for me to attain this height! I would also like to thank my young son who sometimes missed playing outside because I was working. Next, I would like to thank my mother who realised my academic merits at a young age and went extra miles to give me private education. Old soldier! as we affectionately called my dad, would have been very proud, but alas! Your words; Aim high, strike hard and go forward will forever be with me. Last but not the least; I want to thank my beloved sister for listening to my complaints and always encouraging me.

Onyankropon nhyira obibiara! (God bless you all!)

# List of publications

## Journal Publications

1. **Boatema, L.**, Kwakernaak, C., van der Zwaag, S. and Sloof, W. G. “*Selection of healing agents for autonomous healing of alumina at high temperatures*”. Journal of the European Ceramic Society 36 (2016) 4141–4145. doi:10.1016/j.jeurceramsoc.2016.05.038.
2. Yoshioka, S., **Boatema, L.**, van der Zwaag, S., Nakao, W., Sloof, W. G. “*On the use of TiC as high-temperature healing particles in alumina based composites*”. Journal of the European Ceramic Society 36 (2016) 4155–4162. doi:10.1016/j.jeurceramsoc.2016.06.008.
3. Farle, A., **Boatema, L.**, Shen, L., Govert, S., Kok, J. B. W., Bosch, M., Yoshioka, S., van der Zwaag, S. and Sloof, W. G. “*Demonstrating the self-healing behaviour of some selected ceramics under combustion chamber conditions*”. Smart Mater. Struct. 25 (2016) 084019 (10pp). doi:10.1088/0964-1726/25/8/084019.
4. Sloof, W.G., Pei, R., McDonald, S.A., Fife, J.L., Shen, L., **Boatema, L.**, Farle, A.-S., Yan, K., Zhang, X., van der Zwaag, S., Lee, P.D., and Withers, P.J., *Repeated crack healing in MAX-phase ceramics revealed by 4D in situ synchrotron X-ray tomographic microscopy*. Scientific Reports, 2016. 6: p. 23040.
5. **Boatema, L.**, Brouwer, J. C., van der Zwaag, S. and Sloof, W.G. “*The effect of the TiC particle size on the preferred oxidation temperature for self-healing of oxide ceramic matrix materials*”. Journal of Materials Science, 53 (8) 2018 p 5973–5986. <https://doi.org/10.1007/s10853-017-1973-x>
6. **Boatema, L.**, Bosch, M., Farle, A.-S., Bei, G.-P., van der Zwaag, S. and Sloof, W.G. “*Autonomous high temperature healing of surface cracks in Al<sub>2</sub>O<sub>3</sub> containing Ti<sub>2</sub>AlC particles*”. –**Under review**.
7. **Boatema, L.**, van der Zwaag, S. and Sloof, W.G. “*Self-healing of Al<sub>2</sub>O<sub>3</sub> containing 10 vol. % of Ti microparticles*”. In press: Ceramics International. doi.org/10.1016/j.ceramint.2018.03.119



## Conference proceedings

1. **Boatema, L.**, Zhou, van der Zwaag, S. and Sloof, W. G. “*The effect of SiC particle size on the healing Efficiency of alumina at high temperatures*” in ICSHM 2013: Proceedings of the 4th international conference on self-healing materials. Magnel laboratory for concrete research.

# Curriculum Vitae

## **Linda Boatemaa**

Born on February 15, 1984 in Accra, Ghana

- 1998-2000      Senior Secondary School, Science major  
Aggrey Memorial Zion Secondary School, Cape-Coast, Ghana
- 2004-2008      B.Sc. in Physics (Honours)  
University of Cape-Coast, Cape-Coast, Ghana
- 2009-2010      M.Sc. in Advanced functional materials  
University of Augsburg, Augsburg, Germany
- 2010-2011      M.Sc. in Advanced functional materials  
Grenoble INP, Grenoble, France
- 2012-2017      PhD candidate at Delft University of Technology  
Department of Materials Science and Engineering  
Delft University of Technology, Delft, The Netherlands